

# **Conformational Plasticity of HIV-1 Env and Implications for Vaccine Design**

Thesis by  
Zhi Yang

In Partial Fulfillment of the Requirements for the Degree of  
Doctor of Philosophy

The logo for the California Institute of Technology (Caltech), featuring the word "Caltech" in a bold, orange, sans-serif font.

CALIFORNIA INSTITUTE OF TECHNOLOGY  
Pasadena, California

2022  
(Defended December 10, 2021)

© 2022

Zhi Yang

ORCID: 0000-0001-8680-3784

## ACKNOWLEDGEMENTS

I would like to thank my thesis advisor, Dr. Pamela J. Bjorkman, for her mentorship and support for the past six years. Her dedication and high standards set a great example for me to be a scientist. I appreciate the freedom and flexibility she gave me during my graduate student career which allowed me to go after some exciting yet difficult scientific problems.

I would like to thank my thesis committee including Dr. Douglas C. Rees, Dr. Rebecca M. Voorhees, and Dr. David C. Chan for their support, as well as academic and career advice.

I also want to thank the members of the Bjorkman lab. Dr. Haoqing Wang and Dr. Harry B. Gristick mentored me on learning electron microscopy and X-ray crystallography. My publication co-authors, including Kim-Marie A. Dam and Dr. Magnus A. G. Hoffmann, who provided tremendous help on the experiments and made contributions to my publications, I would like to thank Dr. Jennifer R. Keefe, Dr. Anthony P. West, Dr. Christopher O. Barnes for the helpful discussions, Dr. Jens Kaiser from the Caltech Molecular Observatory for help of X-ray crystallography data collection, Drs. Songye Chen, Andrey Malyutin, Stephen Carter, and Alasdair McDowall for their help on single particle EM and electron tomography data collection and processing, Giovanni Pinton Tomaleri from the Voorhees lab for his help on membrane protein expression and purification, Andrew T. DeLaitsch and Dr. Chengcheng Fan for their help on protein crystallography, the Caltech Protein Expression Center led by Dr. Jost Vielmetter for help on protein expression, Dr. Michael D. Bridges (UCLA) for DEER data collection and processing, Dr. Mona Shahgholi for help in mass spectrometry data collection and processing, and Welison Floriano for assistance on IT support. In addition, I would like to thank our collaborators from the Nussenzweig lab (Rockefeller), the Hubbell lab (UCLA), and the Martin lab (NIH).

Lastly, I would like to thank my parents as well as my partner, Qingli Zhu, for their support, to whom I dedicate this work.

## ABSTRACT

The human immunodeficiency virus (HIV) envelope glycoprotein (Env), a (gp120/gp41)<sub>3</sub> trimer, is present on the surface of the viral envelope membrane. Env binding to the host cell receptor, CD4, and the co-receptor, CCR5 or CXCR4, triggers a cascade of Env conformational changes and structural rearrangements which ultimately leads to the viral and host cell membrane fusion, marking the initiation of a viral infection. In this work, we present findings of the conformational changes of an Env trimer from a closed, pre-fusion state to an asymmetrically open state when bound to receptor CD4 and a co-receptor mimicking antibody, E51. We showed the importance of tyrosine sulfation in gp120 binding. The EM structures also indicate the existence of Env's multiple conformational states. Based on the structural information, we modeled the order of conformations on the path to co-receptor binding and viral-host cell membrane fusion.

As the sole viral protein present on the virion surface, the Env acts as the target for anti-HIV antibodies. Using various types of engineered Env as the immunogen, researchers made attempts to elicit anti-HIV neutralizing antibodies in animals. In this work, we identified and analyzed two neutralizing antibodies, Ab1303 and Ab1573, that target the Env CD4 binding site (CD4bs), one of the conserved epitopes on the Env gp120 surface. Using biophysical and structural methods, we described a novel recognition mechanism of these antibodies and proposed a model about the unique behavior of Env under physiological conditions. This study proved that CD4bs Abs that recognize an "occluded open" Env can be raised by sequential animal immunizations, thereby guiding the future immunogen design and therapeutic applications.

## PUBLISHED CONTENT AND CONTRIBUTIONS

- (1) **Yang, Z.**; Dam, K-M. A.; Bridges, M. D.; Hoffmann, M. A. G.; DeLaitsch, A. T.; Gristick, H. B.; Escolano, A.; Gautam, R.; Martin, M. A.; Nussenzweig, M. C.; Hubbell, W. L.; Bjorkman, P. J. Neutralizing Antibodies Induced in Immunized Macaques Recognize the CD4-Binding Site on an Occluded-open HIV-1 Envelope Trimer. *Nat. Commun., in press.* **2021.**

Z.Y. designed research, performed experiments, analyzed data, and wrote the manuscript with inputs from co-authors.

- (2) Escolano, A.\*; Gristick, H. B.\*; Gautam, R.\*; DeLaitsch, A. T.\*; Abernathy, M. E.; **Yang, Z.**; Wang, H.; Hoffmann, M. A. G.; Nishimura, Y.; Wang, Z.; Koranda, N.; Kakutani, L. M.; Gao, H.; Gnanapragasam, P. N. P.; Raina, H.; Gazumyan, A.; Cipolla, M.; Oliveira, T. Y.; Ramos, V.; Irvine, D. J.; Silva, M.; West, A. P.; Keeffe, J. R.; Barnes, C. O.; Seaman, M. S.; Nussenzweig, M. C.; Martin, M. A.; Bjorkman, P. J. Sequential Immunization of Macaques Elicits Heterologous Neutralizing Antibodies Targeting the V3-Glycan Patch of HIV-1 Env. *Sci. Transl. Med.* **2021**, 13 (621), eabk1533.

<https://doi.org/10.1126/scitranslmed.abk1533>.

Z.Y. performed structural studies.

- (3) Wang, Z.; Schmidt, F.; Weisblum, Y.; Muecksch, F.; Barnes, C. O.; Finkin, S.; Schaefer-Babajew, D.; Cipolla, M.; Gaebler, C.; Lieberman, J. A.; Oliveira, T. Y.; **Yang, Z.**; Abernathy, M. E.; Huey-Tubman, K. E.; Hurley, A.; Turroja, M.; West, K. A.; Gordon, K.; Millard, K. G.; Ramos, V.; Da Silva, J.; Xu, J.; Colbert, R. A.; Patel, R.; Dizon, J.; Unson-O'Brien, C.; Shimeliovich, I.; Gazumyan, A.; Caskey, M.; Bjorkman, P. J.; Casellas, R.; Hatziioannou, T.; Bieniasz, P. D.; Nussenzweig, M. C. mRNA Vaccine-Elicited Antibodies to SARS-CoV-2 and Circulating Variants. *Nature* **2021**, 592 (7855), 616–622.

<https://doi.org/10.1038/s41586-021-03324-6>.

Z.Y. performed structural studies and data analysis.

- (4) West, A. P.; Wertheim, J. O.; Wang, J. C.; Vasylyeva, T. I.; Havens, J. L.; Chowdhury, M. A.; Gonzalez, E.; Fang, C. E.; Di Lonardo, S. S.; Hughes, S.; Rakeman, J. L.; Lee, H. H.; Barnes, C. O.; Gnanapragasam, P. N. P.; **Yang, Z.**; Gaebler, C.; Caskey, M.; Nussenzweig, M. C.; Keeffe, J. R.; Bjorkman, P. J. Detection and Characterization of the

SARS-CoV-2 Lineage B.1.526 in New York. *Nat. Commun.* **2021**, *12* (1), 4886.

<https://doi.org/10.1038/s41467-021-25168-4>.

Z.Y. participated in figure preparation.

- (5) Hoffmann, M. A. G.; Bar-On, Y.; **Yang, Z.**; Gristick, H. B.; Gnanapragasam, P. N. P.; Vielmetter, J.; Nussenzweig, M. C.; Bjorkman, P. J. Nanoparticles Presenting Clusters of CD4 Expose a Universal Vulnerability of HIV-1 by Mimicking Target Cells. *Proc. Natl. Acad. Sci.* **2020**, *117* (31), 18719–18728.

<https://doi.org/10.1073/pnas.2010320117>.

Z.Y. participated in designing research, performing experiments, and analyzing data.

- (6) Ladinsky, M. S.; Gnanapragasam, P. N.; **Yang, Z.**; West, A. P.; Kay, M. S.; Bjorkman, P. J. Electron Tomography Visualization of HIV-1 Fusion with Target Cells Using Fusion Inhibitors to Trap the Pre-Hairpin Intermediate. *eLife* **2020**, *9*, e58411.

<https://doi.org/10.7554/eLife.58411>.

Z.Y. participated in data curation, figure preparation, and manuscript writing.

- (7) Cohen, A. A.; **Yang, Z.**; Gnanapragasam, P. N. P.; Ou, S.; Dam, K.-M. A.; Wang, H.; Bjorkman, P. J. Construction, Characterization, and Immunization of Nanoparticles That Display a Diverse Array of Influenza HA Trimers. *PLOS ONE* **2021**, *16* (3), e0247963.

<https://doi.org/10.1371/journal.pone.0247963>.

Z.Y. participated in research conceptualization, data analyses, and figure preparation.

- (8) **Yang, Z.**; Wang, H.; Liu, A. Z.; Gristick, H. B.; Bjorkman, P. J. Asymmetric Opening of HIV-1 Env Bound to CD4 and a Coreceptor-Mimicking Antibody. *Nat. Struct. Mol. Biol.* **2019**, *26* (12), 1167–1175.

<https://doi.org/10.1038/s41594-019-0344-5>.

Z.Y. designed research, performed experiments, analyzed data, and wrote the manuscript with inputs from co-authors.

- (9) Wang, H.\*; Barnes, C. O.\*; **Yang, Z.**; Nussenzweig, M. C.; Bjorkman, P. J. Partially Open HIV-1 Envelope Structures Exhibit Conformational Changes Relevant for Coreceptor Binding and Fusion. *Cell Host & Microbe* **2018**, *24* (4), 579-592.e4.

<https://doi.org/10.1016/j.chom.2018.09.003> PMID - 30308160.

Z.Y. participated in data analysis.

\* Authors contributed equally to the work

## TABLE OF CONTENTS

Acknowledgements .....	iii
Abstract.....	iv
Publications .....	v
Table of Contents .....	vii
Chapter 1: Introduction	
HIV-1 Env in Membrane Fusion .....	1
Structure of Env and anti-HIV Neutralizing Antibody .....	5
CD4-induced Antibodies.....	8
References .....	9
Chapter 2: Asymmetric opening of HIV-1 Env bound to CD4 and a coreceptor-mimicking antibody	
Abstract.....	14
Introduction .....	15
Results .....	17
Discussion .....	23
Acknowledgements .....	27
Methods .....	28
Figures and Tables .....	32
Extended Data .....	43
Supplementary Information .....	51
References .....	55
Chapter 3: Neutralizing Antibodies Induced in Immunized macaques Recognize the CD4 Binding Site on an Occluded-open HIV-1 Envelope Trimer	
Abstract.....	59
Introduction .....	60
Results .....	63
Discussion .....	74
Acknowledgements .....	77
Methods .....	78
Figures and Tables .....	84
Supplementary Information .....	96
References .....	104

*Chapter 1***INTRODUCTION****HIV-1 Env in membrane fusion**

Human immunodeficiency virus-1 (HIV-1), an enveloped single-stranded, positive sense RNA virus, is the causative agent behind the ongoing AIDS (acquired immunodeficiency syndrome) pandemic. As the sole viral protein on the surface of the virus lipid membrane envelope, the HIV-1 envelope glycoprotein (HIV-1 Env) is responsible for targeting the human CD4+ T cells and facilitating the membrane fusion between the virus and host cell, thereby initiating the infection<sup>1</sup>.

After the Env-mediated membrane fusion, the capsid core is released into the infected cell. The cone-shaped core is then transported into the nucleus and disassembled<sup>2</sup>. The enclosed viral genome is then released, reverse transcribed into DNA, and integrated into the host cell genome. The integrated viral DNA could remain silent without propagating for a period, a stage referred to as latency. Once the integrated viral genes are activated for transcription, RNA genome along with other viral proteins are produced and packaged into capsids. Finally, enveloped viral particles are formed with capsids and other membrane-associated protein components, including the Env, budding out from the host cell membrane<sup>2</sup> (Fig. 1).

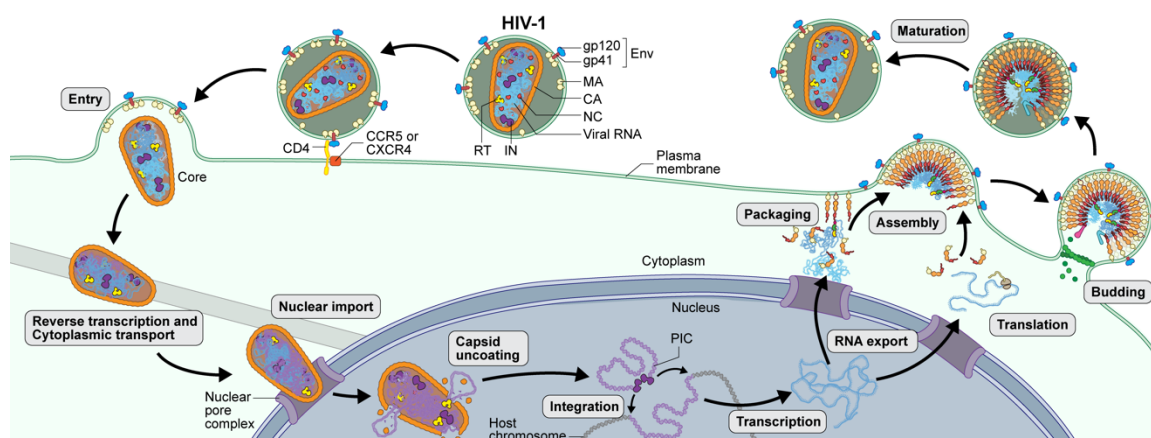


**Figure 1. A schematic view of the HIV life cycle.** (Source: *scienceofhiv.org*)

Despite various origins, for many enveloped viruses, the protein machineries responsible for target cell attachment and membrane fusion share certain similar structural characteristics and employ analogous generic membrane fusion mechanisms<sup>1</sup>. The fusion machineries generally contain a receptor binding domain and a membrane fusion domain. The receptor binding segment can recognize its receptor present on the target cell membrane, whereas the membrane fusion segment facilitates the membrane fusion process. In order to fulfill its catalytic function of membrane fusion, the protein needs to be activated, often through proteolytic cleavage between the two domains<sup>1</sup>.

The HIV-1 Env is composed of three copies gp120/gp41 heterodimers. The trimeric Env initiates the membrane fusion process through gp120 subunits binding to its receptor CD4, a molecule that can be found on the surface of CD4+ T cells. Such binding reveals the binding site for a co-receptor, the CCR5 or CXCR4 chemokine receptor<sup>3,4</sup>. Co-receptor binding further leads to the fusogenic conformational transition of gp41, who would place its hydrophobic fusion peptide into the host cell membrane. Followed by the dissociation of the gp120 subunits, trimeric gp41 forms a putative “pre-hairpin” intermediate with trimeric coiled-coil structure<sup>5</sup>. This intermediate structure would then collapse on itself to form a more stable “six helix bundle”, spatially bringing the viral and host cell membranes in proximity and eventually leads to membrane fusion<sup>6</sup> (Fig. 2).

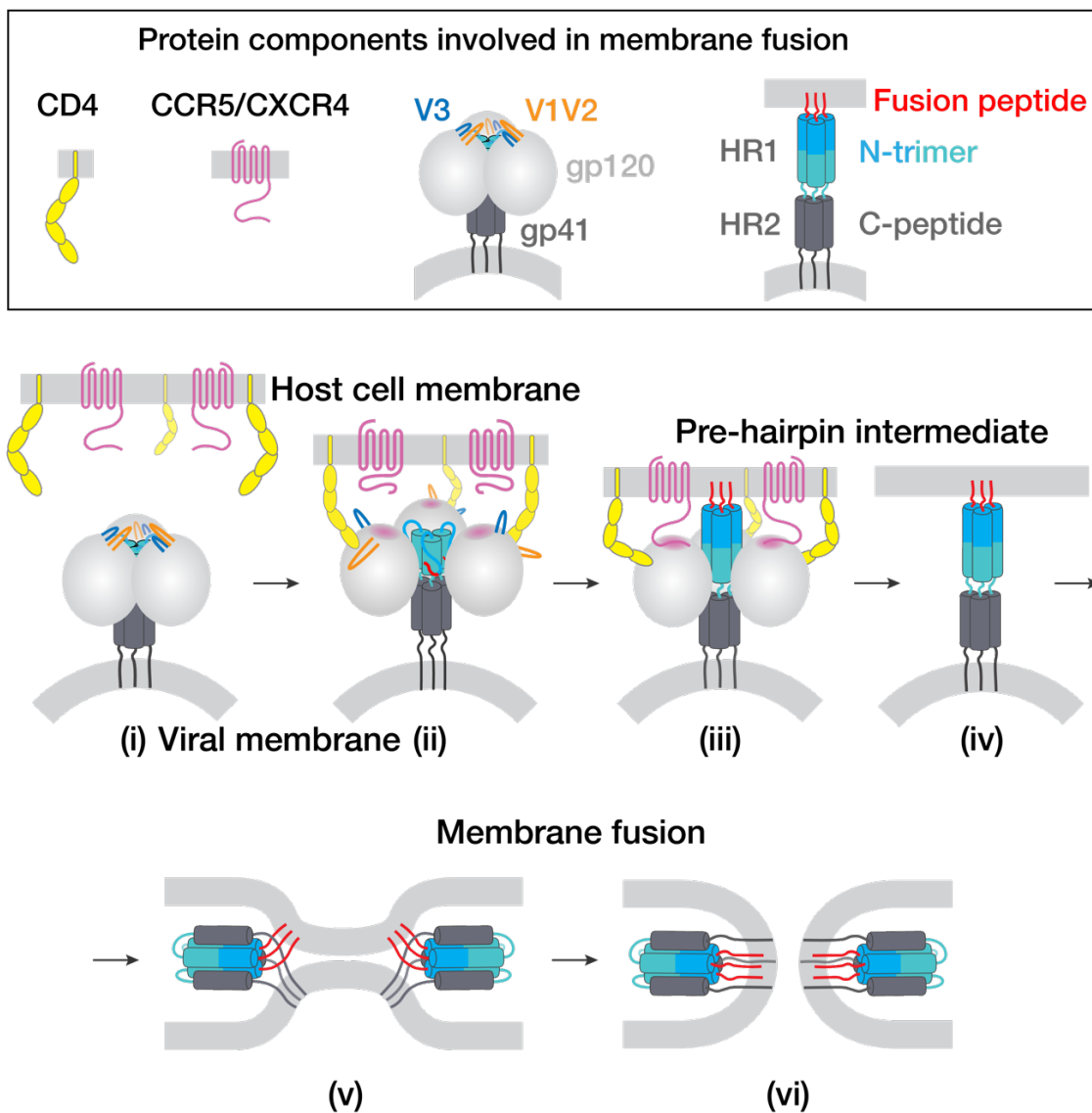


**Figure 2. A schematic view of the HIV-1 Env-mediated membrane fusion process.** Protein components involved in this process including CD4 and co-receptors CCR5/CXCR4, as well as a detailed representation of HIV-1 Env and the hypothetical model of Env gp41 post-fusion structures are shown in the box. (Adapted from Ladinsky et al., 2020).

As part of an effort to develop a soluble and native-like Env trimer, a strain of Env, BG505, was used and modified. Briefly, the C-terminal end of residue 664 was truncated to generate the soluble ecto-domain of Env. In addition, a disulfide bond was introduced to improve the stable association between gp120 and gp41 subunits (SOS mutation), a proline residue was introduced to replace residue I559, which further improved the stability by destabilizing the formation of “pre-hairpin” structure (IP mutation)<sup>7</sup>. This modified BG505 SOSIP.664 Env trimer has been widely used in both structural studies and vaccine development<sup>8</sup>. Soluble trimers of other strains can also be created by making similar mutations.

In this work, BG505 SOSIP, a soluble Env trimer derived from a clade A virus, and B41 SOSIP, one that was derived from a clade B virus<sup>9</sup>, together with the Env receptor CD4 as well as various types of antibodies, were used to investigate the biochemical and structural properties of HIV-1 Env trimer and to characterize the interactions between Env and various antibodies. In Chapters 2 and 3, we characterized multiple conformational states of HIV-1 Env that reflect its intrinsic conformational plasticity; these states provided evidence on the initial steps of Env conformational changes that would ultimately lead to membrane fusion.

## **Broadly neutralizing antibodies against HIV-1**

Distinct from most other viruses, the HIV-1 Env is usually heavily glycosylated with its protein epitopes camouflaged under the “glycan shields”, making it easier to escape immune surveillance<sup>10</sup>. Due to the unusually high mutation rates, numerous mutations can be introduced into the Env, making it challenging for the humoral immune system to keep up with the changes and develop efficient immune responses by generating effective antibodies against a broad range of mutated strains<sup>11</sup>. The competition between the “two titans of evolution” is exemplary of the prolonged battles between a fast-mutating virus and the human immune system attempting to come up with complicated solutions<sup>12</sup>. However, a small group of HIV infected individuals successfully developed antibodies that showed good potency and breadth against a wide range of HIV-1 viral strains<sup>13</sup>. These “broadly neutralizing antibodies”, or “bNAbs” usually took as long as several years to develop. bNAbs with high potency and wide coverage breadth have been pursued for prophylactic or therapeutic applications<sup>14</sup>. The neutralization activities of bNAbs are usually tested against a panel of viruses including viruses that are usually easy to neutralize, being categorized into the “tier 1” strains, as well as the “tier 2” strains, which are more representative of circulating viral strains and are harder to neutralize<sup>15</sup>. It is thus of great interest to develop vaccines that can elicit antibodies against a broad range of tier 2 viruses, including the strains that were not exposed to the immunizations (“heterologous” neutralization).

Structural studies of bNAbs have provided immense information for a better understanding of the recognition mechanisms of the antibodies. Using X-ray crystallography or cryo-electron microscopy (cryo-EM), the structural characterizations of bNAb-gp120 and bNAb-Env trimer complexes indicate that the epitopes are generally located on certain conserved regions of the Env<sup>8,12</sup>. Such regions include (1) the CD4 binding site (CD4bs), (2) the V2 apex, (3) the V3 region, (4) the gp120/gp41 interface region including the fusion peptide (FP), and (5) the MPER, or the membrane-proximal external region (Fig. 3)<sup>8,12</sup>.

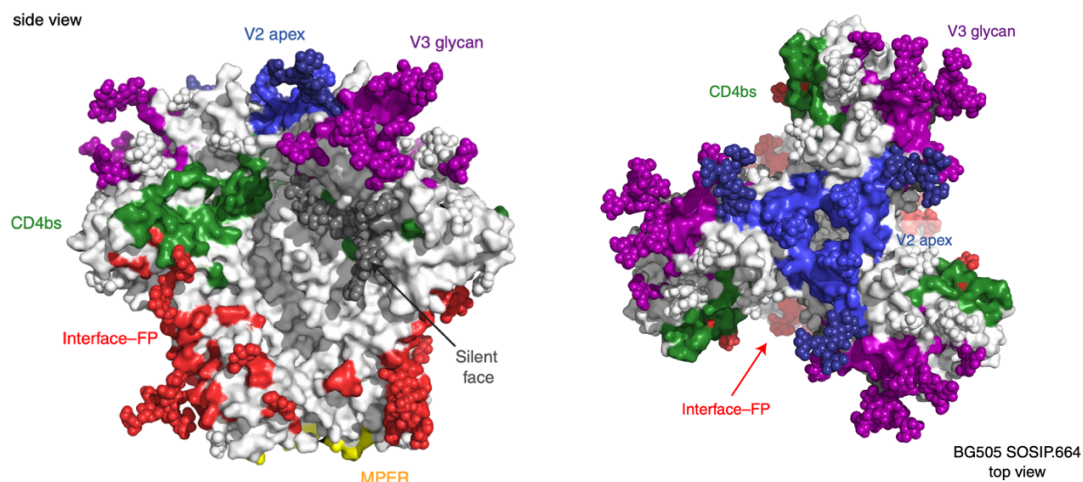


**Figure 3. Common epitopes on the HIV Env as recognized by bNAbs.** Side view (left) and top view (right) of an HIV strain BG505 Env. The bNAb epitopes are highlighted in colors: CD4bs in green, V2 apex is in blue, V3 region in purple, gp120/gp41 interface (including FP) in red, and MPER in yellow. (Adapted from Sok and Burton, 2018).

As the name suggests, the anti-CD4bs bNAbs target the region in the vicinity to the binding site of receptor CD4. Antibodies of this class include the VRC01-class bNAbs<sup>16</sup>, 3BNC117<sup>17</sup>, N6<sup>18</sup>, and IOMA<sup>19</sup>, etc. Because the CD4bs is involved in engaging receptor CD4, this epitope is one of the most conserved regions of Env. The CD4bs bNAbs generally showed best combinations of both potency and breadth<sup>20,12</sup>.

The V2 apex epitope is located around the apex region of Env trimer (Fig. 2). bNAbs targeting this region include PGT145, which contains a prolonged complementarity determining region heavy chain loop 3 (CDRH3) inserting into the threefold axis of the trimer<sup>21</sup>, PG9 and PG16<sup>22</sup>, CAP256-VRC26 lineage<sup>23</sup>, and N90-VRC38<sup>24</sup> etc. These antibodies' interaction with Env usually involves V2 region glycans such as N130, N156, N160, and N173.

The bNAbs targeting V3 region often engage in interactions with the Env V3 glycans. Some Abs of this class penetrate the glycan shield and interact with the conserved V3 GIDR motif.

bNAbs of this class include BG18<sup>25</sup>, PGT121<sup>26</sup>, and 10-1074<sup>27</sup>, etc., among which BG18 showed the best overall potency and breadth of this class.

The gp120/gp41 interface region is also a target for many bNAbs including 8ANC195<sup>17</sup>, PGT151<sup>28</sup>, VRC34<sup>29</sup>, and 35O22<sup>30</sup>, etc. Antibody 8ANC195 has been shown to bind to Env trimer in both ligand-free and CD4-bound state<sup>31</sup>, while most other Abs targeting the interface region interact with the fusion peptide (FP) located near the joining point between gp120 and gp41 before furin cleavage<sup>8</sup>. Although the hydrophobic FP is partly buried in some structures<sup>32</sup>, it is exposed in the Fab-Env complex structures where the interface-targeting antibodies made interactions with the FP<sup>28-30</sup>.

The MPER bNAbs, such as 10E8<sup>33</sup> or DH511<sup>34</sup>, recognize the Env region closer to the viral membrane. Compared to other bNAb classes, this class of bNAbs generally showed good breadth but less potency<sup>12</sup>.

Despite the isolations and well characterizations of bNAbs, to elicit protective bNAbs in humans through immunizations remains a challenge<sup>35</sup>. Some of the difficulties in vaccine design include the low immunogenicity of native Envs, the production of non-conserved, immunodominant off-target antibodies, and the production of strain-specific antibodies which lack the broad coverage against a wide range of viral strains, etc<sup>12,35</sup>. Comprehensive studies of bNAbs have allowed researchers to engineer immunogens through structure-based rational design<sup>36-38</sup>. In these efforts, to recapitulate the co-evolution between the virus and the human immune system, sequential immunizations were used to guide affinity maturation towards generating antibodies against the targeted, conserved regions of the Env<sup>37,38</sup>. In addition, in recent studies, immunogens were multimerized onto the surface of a particle to improve its immunogenicity and to elevate the immune response<sup>38</sup>.

### CD4-induced antibodies

The CD4-induced (CD4i) antibodies recognize the conserved regions of gp120 that are usually buried in ligand-free, closed Env trimer but are fully accessible when CD4 is bound. These regions are located at or near the co-receptor binding site<sup>39</sup>. In some cases, their binding involves direct interactions with CD4<sup>40</sup>. Although recognition of the conserved regions on gp120 gives these antibodies broad cross-reactivity, compared to the bNAbs, they showed weak neutralization potency<sup>41-43</sup>, perhaps due to the requirement of fully exposure of their epitopes or related to limited steric availability when such exposure takes place during the event of Env-mediated viral entry<sup>44</sup>. The CD4i antibodies were first structurally investigated when bound to monomeric gp120, in which the gp120 monomer adopts a conformation analogous to the Env's CD4-induced, fully-open conformation<sup>31,32,45,46</sup>.

Examples of CD4i antibodies include E51<sup>47</sup>, 17b<sup>48</sup>, 412d<sup>49</sup>, 21c<sup>43</sup>, etc. It has been suggested that engineered reagents that connect CD4i antibodies or CD4i antibody CDRs with CD4 can overcome the problem of steric inaccessibility of the antibody by exposing its gp120 binding site, these reagents were shown to potently neutralize multiple HIV-1 strains, indicating that they have promising therapeutic values through passive immunization and they were shown to protect animals from viral challenges through consistent *in vivo* expression<sup>50,51</sup>.

In Chapter II, we present structures of soluble Env trimer, BG505 SOSIP.664, in complex with sCD4 and a co-receptor mimicking, CD4i antibody, E51, whose CDRH3 region contains multiple potential sites of *O*-sulfated tyrosine (Tys), a signature residue that can also be found at the N-terminus of the co-receptor CCR5 and are considered to be essential for CCR5-Env interaction<sup>3,49,52</sup>.

## References

1. Harrison, S. C. Viral membrane fusion. *Virology* **479–480**, 498–507 (2015).
2. Barré-Sinoussi, F., Ross, A. L. & Delfraissy, J.-F. Past, Present and Future: 30 Years of HIV Research. *Nat. Rev. Microbiol.* **11**, 877–883 (2013).
3. Choe, H. *et al.* The Chemokine Receptors CCR3 and CCR5 Facilitate Infection by Primary HIV-1 Isolates. *Cell* **85**, 1135–1148 (1996).
4. Feng, Y., Broder, C. C., Kennedy, P. E. & Berger, E. A. HIV-1 Entry Cofactor: Functional cDNA Cloning of a Seven-Transmembrane, G Protein-Coupled Receptor. *Science* **272**, 872–877 (1996).
5. Chan, D. C. & Kim, P. S. HIV Entry and Its Inhibition. *Cell* **93**, 681–684 (1998).
6. Chan, D. C., Fass, D., Berger, J. M. & Kim, P. S. Core Structure of gp41 from the HIV Envelope Glycoprotein. *Cell* **89**, 263–273 (1997).
7. Sanders, R. W. *et al.* A Next-Generation Cleaved, Soluble HIV-1 Env Trimer, BG505 SOSIP.664 gp140, Expresses Multiple Epitopes for Broadly Neutralizing but Not Non-Neutralizing Antibodies. *PLoS Pathog.* **9**, e1003618 (2013).
8. Ward, A. B. & Wilson, I. A. The HIV-1 Envelope Glycoprotein Structure: Nailing Down a Moving Target. *Immunol. Rev.* **275**, 21–32 (2017).
9. Pugach, P. *et al.* A Native-Like SOSIP.664 Trimer Based on an HIV-1 Subtype B *env* Gene. *J. Virol.* **89**, 3380–3395 (2015).
10. Scanlan, C. N., Offer, J., Zitzmann, N. & Dwek, R. A. Exploiting the Defensive Sugars of HIV-1 for Drug and Vaccine Design. *Nature* **446**, 1038–1045 (2007).
11. Smyth, R. P., Davenport, M. P. & Mak, J. The Origin of Genetic Diversity in HIV-1. *Virus Res.* **169**, 415–429 (2012).
12. Sok, D. & Burton, D. R. Recent Progress in Broadly Neutralizing Antibodies to HIV. *Nat. Immunol.* **19**, 1179–1188 (2018).
13. Simek, M. D. *et al.* Human Immunodeficiency Virus Type 1 Elite Neutralizers: Individuals with Broad and Potent Neutralizing Activity Identified by Using a High-Throughput Neutralization Assay together with an Analytical Selection Algorithm. *J. Virol.* **83**, 7337–7348 (2009).

14. Hsu, D. C., Mellors, J. W. & Vasan, S. Can Broadly Neutralizing HIV-1 Antibodies Help Achieve an ART-Free Remission? *Front. Immunol.* **12**, 710044 (2021).
15. Montefiori, D. C., Roederer, M., Morris, L. & Seaman, M. S. Neutralization Tiers of HIV-1. *Curr. Opin. HIV AIDS* **13**, 128–136 (2018).
16. Wu, X. *et al.* Rational Design of Envelope Identifies Broadly Neutralizing Human Monoclonal Antibodies to HIV-1. *Science* **329**, 856–861 (2010).
17. Scheid, J. F. *et al.* Sequence and Structural Convergence of Broad and Potent HIV Antibodies That Mimic CD4 Binding. *Science* **333**, 1633–1637 (2011).
18. Huang, J. *et al.* Identification of a CD4-Binding-Site Antibody to HIV that Evolved Near-Pan Neutralization Breadth. *Immunity* **45**, 1108–1121 (2016).
19. Gristick, H. B. *et al.* Natively Glycosylated HIV-1 Env Structure Reveals New Mode for Antibody Recognition of the CD4-binding site. *Nat. Struct. Mol. Biol.* **23**, 906–915 (2016).
20. Zhou, T. *et al.* Structural Repertoire of HIV-1-Neutralizing Antibodies Targeting the CD4 Supersite in 14 Donors. *Cell* **161**, 1280–1292 (2015).
21. Lee, J. H. *et al.* A Broadly Neutralizing Antibody Targets the Dynamic HIV Envelope Trimer Apex via a Long, Rigidified, and Anionic  $\beta$ -Hairpin Structure. *Immunity* **46**, 690–702 (2017).
22. Wang, H. *et al.* Asymmetric recognition of HIV-1 Envelope trimer by V1V2 loop-targeting antibodies. *eLife* **6**, e27389 (2017).
23. Andrabi, R. *et al.* Glycans Function as Anchors for Antibodies and Help Drive HIV Broadly Neutralizing Antibody Development. *Immunity* **47**, 524–537.e3 (2017).
24. Cale, E. M. *et al.* Virus-like Particles Identify an HIV V1V2 Apex-Binding Neutralizing Antibody that Lacks a Protruding Loop. *Immunity* **46**, 777–791.e10 (2017).
25. Freund, N. T. *et al.* Coexistence of Potent HIV-1 Broadly Neutralizing Antibodies and Antibody-sensitive Viruses in a Viremic Controller. *Sci. Transl. Med.* **9**, eaal2144 (2017).
26. Walker, L. M. *et al.* Broad Neutralization Coverage of HIV by Multiple Highly Potent Antibodies. *Nature* **477**, 466–470 (2011).
27. Mouquet, H. *et al.* Complex-type N-glycan Recognition by Potent Broadly Neutralizing HIV Antibodies. *Proc. Natl. Acad. Sci.* **109**, E3268–E3277 (2012).

28. Falkowska, E. *et al.* Broadly Neutralizing HIV Antibodies Define a Glycan-Dependent Epitope on the Prefusion Conformation of gp41 on Cleaved Envelope Trimers. *Immunity* **40**, 657–668 (2014).
29. Kong, R. *et al.* Fusion Peptide of HIV-1 as a Site of Vulnerability to Neutralizing Antibody. *Science* **352**, 828–833 (2016).
30. Huang, J. *et al.* Broad and Potent HIV-1 Neutralization by a Human Antibody that Binds the gp41–gp120 Interface. *Nature* **515**, 138–142 (2014).
31. Wang, H., Barnes, C. O., Yang, Z., Nussenzweig, M. C. & Bjorkman, P. J. Partially Open HIV-1 Envelope Structures Exhibit Conformational Changes Relevant for Coreceptor Binding and Fusion. *Cell Host Microbe* **24**, 579–592.e4 (2018).
32. Yang, Z., Wang, H., Liu, A. Z., Gristick, H. B. & Bjorkman, P. J. Asymmetric Opening of HIV-1 Env Bound to CD4 and a Coreceptor-mimicking Antibody. *Nat. Struct. Mol. Biol.* **26**, 1167–1175 (2019).
33. Huang, J. *et al.* Broad and Potent Neutralization of HIV-1 by a gp41-specific Human Antibody. *Nature* **491**, 406–412 (2012).
34. Williams, L. D. *et al.* Potent and Broad HIV-neutralizing Antibodies in Memory B Cells and Plasma. *Sci. Immunol.* **2**, eaal2200 (2017).
35. Burton, D. R. *et al.* A Blueprint for HIV Vaccine Discovery. *Cell Host Microbe* **12**, 396–407 (2012).
36. Jardine, J. *et al.* Rational HIV Immunogen Design to Target Specific Germline B Cell Receptors. *Science* **340**, 711–716 (2013).
37. Escolano, A. *et al.* Immunization Expands B Cells Specific to HIV-1 V3 Glycan in Mice and Macaques. *Nature* **570**, 468–473 (2019).
38. Escolano, A. *et al.* Sequential Immunization of Macaques Elicits Heterologous Neutralizing Antibodies Targeting the V3-glycan Patch of HIV-1 Env. *Sci. Transl. Med.* **13**, eabk1533 (2021).
39. DeVico, A. CD4-Induced Epitopes in the HIV Envelope Glycoprotein, Gp120. *Curr. HIV Res.* **5**, 561–571 (2007).
40. Diskin, R., Marcovecchio, P. M. & Bjorkman, P. J. Structure of a Clade C HIV-1 gp120 Bound to CD4 and CD4-induced Antibody Reveals anti-CD4 Polyreactivity. *Nat. Struct. Mol. Biol.* **17**, 608–613 (2010).

41. Burton, D. R. *et al.* HIV Vaccine Design and the Neutralizing Antibody Problem. *Nat. Immunol.* **5**, 233–236 (2004).
42. Thali, M. *et al.* Characterization of Conserved Human Immunodeficiency Virus Type 1 gp120 Neutralization Epitopes Exposed Upon gp120-CD4 Binding. *J. Virol.* **67**, 3978–3988 (1993).
43. Xiang, S.-H., Doka, N., Choudhary, R. K., Sodroski, J. & Robinson, J. E. Characterization of CD4-Induced Epitopes on the HIV Type 1 gp120 Envelope Glycoprotein Recognized by Neutralizing Human Monoclonal Antibodies. *AIDS Res. Hum. Retroviruses* **18**, 1207–1217 (2002).
44. Labrijn, A. F. *et al.* Access of Antibody Molecules to the Conserved Coreceptor Binding Site on Glycoprotein gp120 Is Sterically Restricted on Primary Human Immunodeficiency Virus Type 1. *J. Virol.* **77**, 10557–10565 (2003).
45. Kwong, P. D. *et al.* Structure of an HIV gp120 Envelope Glycoprotein in Complex with the CD4 Receptor and a Neutralizing Human Antibody. *Nature* **393**, 648–659 (1998).
46. Ozorowski, G. *et al.* Open and Closed Structures Reveal Allostery and Pliability in the HIV-1 Envelope Spike. *Nature* **547**, 360–363 (2017).
47. Xiang, S.-H. *et al.* Epitope Mapping and Characterization of a Novel CD4-induced Human Monoclonal Antibody Capable of Neutralizing Primary HIV-1 Strains. *Virology* **315**, 124–134 (2003).
48. Sullivan, N. *et al.* CD4-Induced Conformational Changes in the Human Immunodeficiency Virus Type 1 gp120 Glycoprotein: Consequences for Virus Entry and Neutralization. *J. Virol.* **72**, 4694–4703 (1998).
49. Choe, H. *et al.* Tyrosine Sulfation of Human Antibodies Contributes to Recognition of the CCR5 Binding Region of HIV-1 gp120. *Cell* **114**, 161–170 (2003).
50. West, A. P. *et al.* Evaluation of CD4-CD4i Antibody Architectures Yields Potent, Broadly Cross-Reactive Anti-Human Immunodeficiency Virus Reagents. *J. Virol.* **84**, 261–269 (2010).
51. Dey, B., Del Castillo, C. S. & Berger, E. A. Neutralization of Human Immunodeficiency Virus Type 1 by sCD4-17b, a Single-Chain Chimeric Protein, Based on Sequential Interaction of gp120 with CD4 and Coreceptor. *J. Virol.* **77**, 2859–2865 (2003).

52. Farzan, M. *et al.* Tyrosine Sulfation of the Amino Terminus of CCR5 Facilitates HIV-1 Entry. *Cell* **96**, 667–676 (1999).

*Chapter 2***Asymmetric opening of HIV-1 Env bound to CD4 and a coreceptor-mimicking antibody****Abstract**

The HIV-1 envelope (Env) glycoprotein, a (gp120-gp41)<sub>3</sub> trimer, mediates fusion of viral and host cell membranes after gp120 binding to host receptor CD4. Receptor binding triggers conformational changes allowing coreceptor (CCR5) recognition through CCR5's tyrosine-sulfated N-terminus, release of the gp41 fusion peptide, and fusion. We present 3.3Å and 3.5Å cryo-EM structures of E51, a tyrosine-sulfated coreceptor-mimicking antibody, complexed with a CD4-bound open HIV-1 native-like Env trimer. Two classes of asymmetric Env interact with E51, revealing tyrosine-sulfated interactions with gp120 mimicking CCR5 interactions, and two conformations of gp120-gp41 protomers (A and B protomers in AAB and ABB trimers) that differ in their degree of CD4-induced trimer opening and induction of changes to the fusion peptide. By integrating the new structural information with previous closed and open envelope trimer structures, we modeled the order of conformational changes on the path to coreceptor binding site exposure and subsequent viral–host cell membrane fusion.

## Introduction

The HIV-1 envelope glycoprotein (Env), a homotrimer of gp120-gp41 heterodimers, mediates fusion of the host and viral membrane bilayers to allow entry of the HIV-1 capsid containing viral RNA into the host cell cytoplasm<sup>1</sup>. The fusion process is initiated by interactions between the Env gp120 subunit and the host receptor CD4, resulting in conformational changes that reveal the binding site for a host coreceptor, the CCR5 or CXCR4 chemokine receptor<sup>2,3</sup>. Coreceptor binding facilitates further changes leading to insertion of the gp41 fusion peptide into the host cell membrane and subsequent fusion<sup>1</sup>. Conformational changes induced by CD4 binding to trimeric HIV-1 Env have been characterized by cryo-electron tomography of virion-bound Envs<sup>4</sup> and higher resolution single-particle cryo-EM structures of soluble, native-like Env trimers lacking membrane and cytoplasmic domains and including stabilizing mutations (SOSIP Envs)<sup>5-7</sup>. Mutations introduced into soluble SOSIP Env trimers ('SOS' mutations A501C<sub>gp120</sub>, T605C<sub>gp41</sub> and the 'IP' mutation I559P<sub>gp41</sub>)<sup>8</sup> prevent HIV-1 infection when introduced into virion-bound Envs<sup>9</sup>, as expected since the substitutions were designed to stabilize the prefusion Env conformation<sup>8</sup>. However, SOSIP Env structures can undergo conformational changes upon binding to CD4; thus SOSIP structures have defined a closed, pre-fusion Env state in which the gp120 V1V2 loops shield the coreceptor binding site on V3 and an open CD4-bound trimeric state with outwardly rotated gp120 subunits and V1V2 loops displaced by ~40Å to expose the V3 loops and coreceptor binding site<sup>5-7,10</sup> (Supplementary Video). Both the closed and open CD4-bound states are consistent with the structures of native virion-bound Envs derived by cryo-electron tomography and sub-tomogram averaging<sup>4</sup>.

As the only viral protein on the surface of HIV-1 virions, HIV-1 Env is the target of host antibodies whose epitopes have been mapped onto structures of Env glycoprotein trimers<sup>11</sup>. One class of antibodies, the CD4-induced (CD4i) antibodies, recognizes conserved regions of gp120 at or near the coreceptor binding site that are exposed by conformational changes caused by CD4 binding<sup>12</sup>. These antibodies are often cross-reactive but not very potent<sup>13-16</sup>, perhaps related to limited steric accessibility when Env on the viral membrane is complexed with CD4 on the target cell<sup>17</sup>. CD4i antibodies were initially characterized structurally as complexes with monomeric gp120 cores (gp120

constructs with truncations in the N- and C-termini, V1V2, and V3), as exemplified by the first gp120 crystal structure in which CD4i antibody 17b and soluble CD4 (sCD4) were complexed with a gp120 core<sup>18</sup>. The CD4i epitope on monomeric gp120 cores comprises the base of the V3 loop and the bridging sheet (a four-stranded anti-parallel  $\beta$ -sheet involving the gp120  $\beta$ 20 and  $\beta$ 21 strands preceding the V5 loop and the  $\beta$ 2 and  $\beta$ 3 strands at the base of V1V2). Confirming that the coreceptor binding site on gp120 also involves the bridging sheet and V3, a cryo-EM structure of a sCD4-bound full-length monomeric gp120 complexed with CCR5 showed interactions of the CCR5 N-terminal residues with the four-stranded bridging sheet and insertion of gp120 V3 loop into the chemokine binding pocket formed by the CCR5 transmembrane helices<sup>19</sup>. The structure also revealed contacts of N-terminal *O*-sulfated tyrosines on CCR5 that enhance viral entry (Tys10<sub>CCR5</sub> and Tys14<sub>CCR5</sub>)<sup>20</sup> with residues at the base of gp120 V3<sup>19</sup>.

CD4i antibodies mimic host coreceptors by requiring conformational changes within Env trimers for binding. In addition, some CD4i antibodies; e.g., the E51 and 412d antibodies that were isolated from the same HIV-1-infected donor<sup>21,22</sup>, mimic N-terminal residues of CCR5 by including sulfotyrosines in their heavy chain complementarity determining region 3 (CDRH3) regions<sup>20,23</sup>. Current structures of CD4i antibodies bound to sCD4-bound Env trimers are limited to complexes with 17b and 21c<sup>5,7</sup>, antibodies that do not include tyrosine-sulfated CDRH3 regions. Here we present 3.3 Å and 3.5 Å resolution cryo-EM structures of E51, the more potent of the pair of tyrosine-sulfated CD4i antibodies<sup>21-23</sup>, bound to open sCD4-SOSIP Env trimer complexes, allowing comparisons of sulfated tyrosine recognition by a CD4i antibody and by CCR5. Both E51-sCD4-Env structures exhibit deviations from 3-fold Env symmetry in the degree to which the three gp120-gp41 protomers open in response to sCD4 binding and in the extent of sCD4- and Fab-induced structural changes relayed to gp41 and the fusion peptide. Together with comparisons with previous structures, including complexes of CCR5-sCD4-monomeric gp120<sup>19</sup>, CD4i-sCD4-Env trimers<sup>5,7</sup>, and CD4i-sCD4-monomeric gp120<sup>24,25</sup>, the new structures define structural effects of CDRH3 tyrosine sulfation, illustrate the potential for Env trimer asymmetry, and facilitate understanding of conformational changes leading to Env-mediated fusion of viral and host cell membranes.

## Results

### **Cryo-EM Structures of Env trimer in complex with sCD4 and E51 Fab**

We previously described structures of clade A BG505 and clade B B41 native-like soluble Env trimers (SOSIP.664 trimers<sup>8</sup>) complexed with sCD4, the CD4i antibodies 17b or 21c, and the gp120-gp41 interface antibody 8ANC195<sup>6,7</sup>. We observed conformational changes, including rotation and displacement of gp120 subunits, displacement of the gp120 V1V2 region from the apex to the sides of the trimer, exposure of V3, and a more compact conformation of the gp41 HR1<sub>c</sub> helices. As defined by measurements between 3-fold symmetry-related residues in gp120 that were outwardly displaced in response to sCD4 binding<sup>7</sup>, we described the trimers in the 17b-sCD4-Env-8ANC195 and 21c-sCD4-Env-8ANC195 complexes as partially open, as compared with the fully-open Env conformation in a 17b-sCD4-B41 complex<sup>5</sup>, concluding that 8ANC195 binding induced partial closure of open sCD4-bound Env trimers<sup>7,26</sup>.

In this study, we prepared fully-open sCD4-bound BG505 SOSIP.664 Env trimer and used cryo-EM to investigate the structural details of sulfotyrosine interactions with the exposed coreceptor binding site in an E51-sCD4-BG505 complex. E51 Fab, BG505 SOSIP, and sCD4 domains 1 and 2 were expressed and purified as described<sup>7</sup> with modifications for E51 including co-expression with tyrosylprotein sulfotransferase II (TPST II)<sup>27</sup> and isolation of tyrosine-sulfated Fab (Extended Data 1a). Mass spectrometric analyses revealed up to two sulfated tyrosines within the E51 Fab (Extended Data 1b). Single-particle cryo-EM structures were solved using complexes containing E51 Fab with two sulfotyrosines to resolutions of 3.3 Å and 3.5 Å for two conformational classes of the E51-sCD4-BG505 complex (denoted here as class I and class II) (Table 1, Extended Data 2,3). Both structures involved an asymmetric Env trimer complexed with three sCD4s and three E51 Fabs (Fig. 1a,b). Each of the three gp120-gp41 protomers exhibited outwardly rotated gp120 subunits compared to closed Env trimers, a largely disordered and exposed V3 loop, a displaced V1V2 region, and a four-stranded gp120 bridging sheet (Fig. 1b; Supplementary Video). The E51 Fab epitope on gp120 overlaps with the epitopes for the CD4i antibodies 17b and 21c (Fig. 1c). Consistent with mass spectrometric identification of sulfated tyrosines in E51 Fab (Extended Data 1b), we found density for two sulfated tyrosines within the E51 CDRH3

(Extended Data 4). While Tys100I<sub>E51 HC</sub> showed clear density for both the aromatic ring and sulfate group, the density for Tys100F<sub>E51 HC</sub> was weaker (Extended Data 4a).

### **Sulfotyrosines on E51 recognize conserved positive patches on gp120**

In common with the epitopes of CCR5 and the CD4i antibodies such as 17b and 21c, the E51 epitope on gp120 involves the base of V3 and residues within the four-stranded  $\beta$ 20- $\beta$ 21- $\beta$ 2- $\beta$ 3 bridging sheet (Fig. 2), and like 17b and 21c, E51 also contacts the CD4-binding site loop (Supplementary Note 1). E51 Fab contacts gp120 with all three CDRs of its heavy chain, but its light chain does not participate in gp120 recognition (Fig. 2a,b). Contacts between the E51 heavy chain and gp120 could be divided into two categories: (i) CDRH1 and CDRH2 contacts with gp120 bridging sheet residues and CDRH3 stacking on top of the bridging sheet (Fig. 2a,b), and (ii) interactions between CDRH3 sulfotyrosines and positively-charged gp120 residues (Fig. 2c).

The E51 CDRH3 sulfotyrosines, Tys100I<sub>E51 HC</sub> and Tys100F<sub>E51 HC</sub>, play prominent roles in E51's interface with gp120 (Fig. 2a). The aromatic ring of E51 Tys100I<sub>E51 HC</sub> is stacked above the guanidinium group of Arg327<sub>gp120</sub> (base of the V3 loop) through a cation- $\pi$  interaction, while the sulfate group interacts electrostatically with Lys421<sub>gp120</sub>, which is N-terminal to the  $\beta$ 20 strand of the bridging sheet (Fig. 2a). Tys100F<sub>E51 HC</sub> interacts electrostatically with Arg419<sub>gp120</sub> and is in the vicinity of Lys421<sub>gp120</sub>, with which it could interact with a cation- $\pi$  interaction. The E51 sulfotyrosine interactions can be compared with interactions of monomeric gp120 with sulfated tyrosines within the N-terminal loop of CCR5 and in the CD4i antibody 412d, as visualized in structures of CCR5-sCD4-gp120<sub>monomer</sub><sup>19</sup> and 412d-sCD4-gp120<sub>monomer</sub><sup>25</sup> complexes. Superimposition of the gp120 portions of the E51-sCD4-BG505, CCR5-sCD4-gp120, and 412d-sCD4-gp120 complexes showed that a CCR5 sulfated tyrosine that is required for binding to gp120-sCD4 complexes and for inhibition of viral entry into host cells<sup>28</sup> (Tys10<sub>CCR5</sub>) was oriented similarly with respect to gp120 as Tys100I<sub>E51 HC</sub> and made analogous interactions. These interactions were also shared with the orientation and interactions of Tys100<sub>412d</sub>, a sulfated tyrosine in the 412d Fab<sup>25</sup> (Fig. 2a). The 412d antibody included another sulfated tyrosine, Tys100C<sub>412d</sub>, which mimicked the interactions of another required CCR5 sulfated tyrosine, Tys14<sub>CCR5</sub> (Fig. 2a).

To further characterize E51 recognition of sCD4-bound Env, we compared the structures of the variable domains of free E51 (PDB 1RZF)<sup>22</sup> and E51 complexed with Env trimer (this study). The E51 V<sub>L</sub> domain showed no major structural changes between bound and free forms (root mean square deviation, r.m.s.d., for superimposition of 112 V<sub>L</sub> Ca atoms = 0.4 Å) (Fig. 2d,e), consistent with no V<sub>L</sub> contacts in E51 with gp120. By contrast, the E51 V<sub>H</sub> domain buried 723 Å<sup>2</sup> at the interface with gp120. Major changes between the free and bound E51 V<sub>H</sub> domains involved the CDRH3 loop, which was largely disordered in free E51 Fab (12 disordered residues spanning Gly99<sub>E51 HC</sub>–Asp100<sub>E51 HC</sub>, which included two sulfated tyrosines<sup>22</sup>), but adopted an ordered conformation stabilized by contacts with gp120 in bound E51 (Fig. 2d,e) (r.m.s.d. = 1.0 Å calculated for 121 ordered Ca residues in bound versus free E51 V<sub>H</sub>). The ordered CDRH3 conformation in bound E51 Fab included 1.5 turns of α-helix (residues Ala98<sub>E51 HC</sub>–Ala100<sub>E51 HC</sub>) followed by the two sulfated tyrosines (Tys100<sub>F<sub>E51 HC</sub></sub> and Tys100<sub>I<sub>E51 HC</sub></sub>) (Fig. 2d).

### **BG505 Env trimer adopts two distinct sCD4-bound open states when complexed with E51**

Whereas other structures of CD4i-sCD4-Env complexes (open and partially-open CD4i-sCD4-Env structures) are three-fold symmetric<sup>5,7</sup>, the E51-sCD4-BG505 complexes are asymmetric, exhibiting two distinct conformations referred to here as class I and class II (Fig. 3a). The class I and class II Env trimers are distinguished by containing different proportions of two distinct gp120-gp41 protomer conformations, defined by differences in the gp120 core (gp120 residues excluding V1V2 and V3) and in gp41 (Fig. 3a; Supplementary Video). The class I Env trimer contained two protomers in conformation A and one protomer in conformation B (AAB trimer), whereas the class II Env trimer contained one protomer in conformation A and two protomers in conformation B (ABB trimer) (Fig. 3a). When compared with gp120s from partially-open Env protomers in a 17b-sCD4-BG505-8ANC195 complex<sup>7</sup> and a 17b-sCD4-B41 complex with a fully-open symmetric Env trimer<sup>5</sup>, the protomer A conformation was intermediate between the conformations of the protomers in the partially-open and fully-open Env trimers, whereas the protomer B conformation corresponded to the protomer conformation in the fully-open Env trimer (Fig.

3b; Table S1). We found no classes containing symmetric Env trimers with all three protomers adopting the same conformation.

To compare and quantify the A and B gp120-gp41 protomer conformations, we started by aligning on an unaltered region at the gp120 base that is in common amongst the six Env protomers within the class I and class II Env structures. This region is formed by a three-stranded  $\beta$ -sheet (N- and C-terminal gp120 strands ( $\beta_4$  and  $\beta_{26}$ ) and the N-terminal gp41  $\beta$ -strand), about which the gp41 heptad repeat 2 (HR2) helices are wrapped (Fig. 4a; Supplementary Video). Upon sCD4 binding, the core of gp120 in the closed Env trimer conformation is displaced relative to this region, pivoting around a hinge surrounding residues Gly41<sub>gp120</sub> and Pro493<sub>gp120</sub> (Fig. 4a). The A and B protomer conformations can be distinguished after superimposing the hinge region  $\beta$ -strands (gp120  $\beta_4$  and  $\beta_{26}$ ) from the six protomers in the class I and class II trimers as follows: (i) gp120-gp41 protomer conformation A: a conformation in which the gp120 core is located closer to the central axis of the trimer than in fully-open sCD4-bound trimers<sup>5</sup>, but further from the central axis than in partially-open sCD4-bound trimers<sup>7</sup>, and (ii) gp120-gp41 protomer conformation B: a conformation corresponding to fully-open sCD4-bound trimers<sup>5</sup> in which gp120 is further from the central axis (Fig. 3a,b). The centers of mass (c.o.m.) of the gp120 cores in conformations A and B differed by 7.3 Å (calculated for 345 Ca atoms), and lines joining the centers of mass to the hinge residue Pro493<sub>gp120</sub> differed an angle of 11.4° (Fig. 4b).

### **Transition between open gp120-gp41 protomer conformations demonstrate plasticity of gp41 HR1<sub>C</sub>**

Conformational differences in gp41 between protomer conformations A and B include changes in the gp41 HR1<sub>C</sub> helix. In closed and sCD4-bound partially-open Env trimer structures, three gp41 HR1<sub>C</sub> segments form a three-helix bundle around a three-fold symmetric Env trimer axis<sup>7</sup>, whereas the gp41 HR1<sub>C</sub> helices deviated from three-fold symmetry in the E51-sCD4-bound-class I and class II Env trimers. After superimposition of the protomer A and B gp120  $\beta_4$  and  $\beta_{26}$  strands, the C-terminal portion of the HR1<sub>C</sub> helix (Arg588<sub>gp41</sub>-Trp596<sub>gp41</sub>) was similar between the protomer A and protomer B conformations (angle between the two helical axes = 2.5°), whereas the N-terminal portion

(Leu565<sub>gp41</sub>–Glu584<sub>gp41</sub>) showed deviations up to 11.3 Å at the N-termini of the helices and a helical axis angle difference of 22.5°, resulting in a bent protomer A HR1<sub>C</sub> helix and a straight protomer B HR1<sub>C</sub> helix (Fig. 4c). The straight conformation of the protomer B HR1<sub>C</sub> helix allowed insertion of the Trp571<sub>gp41</sub> sidechain into a pocket located below the loop connecting gp120 α<sub>0</sub> helix and β<sub>0</sub> strand, where it is sandwiched by hydrophobic residues Phe53<sub>gp120</sub> and Val75<sub>gp120</sub>, whereas the Trp571<sub>gp41</sub> sidechain in the bent protomer A HR1<sub>C</sub> helix is above the loop, preventing the α<sub>0</sub> helix and β<sub>0</sub> strand from adopting the B conformation (Fig. 4d).

The short gp120 α<sub>0</sub> helix conformation frees up space that allowed straightening of the gp41 HR1<sub>C</sub> helix; in addition, the gp120 α<sub>0</sub> helix is adjacent to the N-terminus of the HR1<sub>C</sub> from a neighboring protomer in conformation B, but not to the HR1<sub>C</sub> from a neighboring protomer in conformation A (Fig. 4e). As a result, a conserved histidine residue (His72<sub>gp120</sub>) of the conformation B gp120 α<sub>0</sub> is brought in proximity to residue Pro559<sub>gp41</sub> of the neighboring gp41 HR1<sub>C</sub>, enabling extension of ordered density for the N-terminus of the gp41 HR1<sub>C</sub> helix by four residues (His560<sub>gp41</sub>–Glu564<sub>gp41</sub>), as compared to the counterpart region of gp41 adjacent to a conformation A gp120 α<sub>0</sub> helix, in which ordered density does not extend beyond Pro559<sub>gp41</sub> (Fig. 4e).

### **The fusion peptide conformation is coupled to Env protomer conformational states**

While the conformation of the fusion peptide in closed Env structures is either disordered (e.g., PDB codes 4NCO and 3J5M) or in a loop conformation (e.g., PDBs 5CEZ, 5CJX, 4ZMJ) (with the exception of closed Envs in which the fusion peptide is directly stabilized by antibodies such as PGT151<sup>29</sup> and VRC34<sup>30</sup>), the fusion peptide formed a partial helix in a partially-open Env trimer complexed with 17b, sCD4 and 8ANC195<sup>7</sup> (Extended Data 5). In our E51-sCD4-BG505 complex structures, a full-length ordered α-helix was found for the fusion peptide in protomer A, which resides in a hydrophobic environment that includes gp120 β-strands and the fusion peptide proximal region (FPPR; residues 530<sub>gp41</sub>–545<sub>gp41</sub>, as defined in ref.<sup>31</sup>). In contrast, for gp120-gp41 protomer conformation B in which gp120 is further displaced from the Env trimer axis, the outermost gp120 β-strand (β<sub>0</sub>) is elevated with respect to the Env trimer base, whereas the FPPR is lower. The straight protomer B

HR1<sub>C</sub> helix, but not the bent protomer A HR1<sub>C</sub> helix (Fig. 4c), results in displacement of the protomer B fusion peptide from the hydrophobic environment it occupies in the protomer A conformation. The result of these conformational changes is exposure of the fusion peptide residues to solvent, where it adopts a less-ordered loop structure in protomer B than the helical conformation in protomer A (Fig. 5; Supplementary Video). The conformational differences in the protomer A and B fusion peptide conformations are anchored at the sidechain of Phe522<sub>gp41</sub>, which has been described as a pivot point for the flexible fusion peptide<sup>32</sup>, and whose orientation differs between the A and B protomer conformations (Fig. 5). Phe522<sub>gp41</sub> also serves as an anchor point for fusion peptide conformational changes in closed Env trimer structures bound to PGT151<sup>29</sup> or VRC34<sup>10</sup>. In our structures, the transition from conformation A to B was accompanied by the release of hydrophobic residues Phe522<sub>gp41</sub> and Leu523<sub>gp41</sub>, resulting in reorientation of their side chains (Fig. 5; Supplementary Video).

## Discussion

The HIV-1 Env trimer functions in the first step of viral infection: fusion of the viral and host lipid bilayers to allow entry of the HIV-1 capsid and its RNA into the host cell cytoplasm<sup>1</sup>. Membrane fusion requires major conformational changes in Env, including CD4-induced and(or) stabilized opening of the closed prefusion Env resulting in an open trimer that exposes the coreceptor binding site, rearrangement to allow insertion of the gp41 fusion peptide into the host cell membrane upon coreceptor binding, membrane fusion, and culmination a post-fusion gp41 helical bundle structure<sup>1</sup>. Structural information for a subset of these conformational states exists: (i) closed, prefusion HIV-1 Env structures have been characterized by crystallographic and cryo-EM structures of Env trimers<sup>10</sup>, (ii) sCD4-bound open Env trimer structures<sup>5-7</sup>, including those reported here, defining structural rearrangements resulting from receptor binding, and (iii) the post-fusion six-helical bundle structures of gp41<sup>33,34</sup>.

We know less about the conformational changes that occur after CD4 binding and before six-helical gp41 bundle formation because there is currently no structural information for sCD4 plus coreceptor-bound Env trimers. However, a sCD4- and CCR5-bound cryo-EM structure of a gp120 monomer revealed the CCR5 footprint on gp120, including interactions of the tyrosine-sulfated N-terminus of CCR5<sup>19</sup>. The CCR5 binding site on gp120 overlaps with the binding sites of CD4i antibodies, which mimic host coreceptors by requiring CD4-induced conformational changes within Env for binding, and CD4i antibodies sometimes further resemble CCR5 by including tyrosines modified by sulfation<sup>20,23,35</sup>. Structures of CD4i-sCD4-Env trimers can therefore be used to infer Env trimer rearrangements required for coreceptor binding, and if including a tyrosine-sulfated CD4i antibody, to gain understanding of the role of tyrosine sulfation in recognition of HIV-1 Env. Here we report cryo-EM structures of E51, a tyrosine-sulfated CD4i antibody, complexed with an open sCD4-bound BG505 Env trimer. The structures define interactions of two E51 sulfated tyrosines with gp120 and reveal unexpected asymmetry in sCD4-bound Env trimers.

**Env interactions of E51 sulfated tyrosines.**

The E51-sCD4-BG505 structures revealed V1V2 displacement from the trimer apex to its sides, which exposes the gp120 V3 region to allow interactions with the E51 CDRH3 (Supplementary Video). As in other CD4-CD4-Env trimer structures<sup>5-7</sup>, the E51 interaction with V3 involved the base of the loop (Fig. 1b). By contrast, CCR5 interacts extensively with the exposed V3 loop<sup>19</sup> that is disordered in CD4i-sCD4-Env trimer structures<sup>5-7</sup>. In the E51-sCD4-BG505 structures, EM density for the two sulfated tyrosines (Tys100F<sub>E51 HC</sub> and Tys100I<sub>E51 HC</sub>) in E51 Fab (Extended Data 1) allowed a detailed description of electrostatic and cation- $\pi$  interactions between the Tys residues and gp120 (Fig. 2a). One of the E51 residues (Tys100I<sub>E51 HC</sub>) made analogous interactions with gp120 as a CCR5 sulfated tyrosine and a sulfated tyrosine within the 412d CD4i antibody<sup>25</sup> (Fig. 2a). Structural comparisons of the E51, 412d, and CCR5 complexes with trimeric (for E51) or monomeric (for 412d and CCR5) Envs showed that each of the tyrosine-sulfated CD4i Fabs included one sulfated tyrosine (Tys100I<sub>E51 HC</sub> and Tys100<sub>412d</sub>) that directly mimicked a CCR5 sulfated tyrosine and an additional sulfated tyrosine (Tys100F<sub>E51 HC</sub> and Tys100C<sub>412d</sub>) that made distinct interactions with gp120 (Fig. 2a).

Comparisons of the interactions of CD4-bound gp120 with E51's CDRH3 and with CCR5<sup>19</sup> suggest a possible scenario for the high potency of eCD4-Ig, a reagent in which a sulfopeptide corresponding to the E51 CDRH3 was fused to the C-terminus of CD4-Fc<sup>27,36</sup>. Namely, the effects of electrostatic interactions of E51 sulfotyrosines with positively-charged residues on gp120 in combination with interactions of the short helix in the CDRH3 of bound E51 (Fig. 2d) (if the helix forms in the context of the CDRH3 sulfopeptide) with the four-stranded gp120 bridging sheet (Fig. 2a) could contribute to specific binding of eCD4-Ig to the sCD4-induced Env conformation in which these regions are accessible. By contrast, these regions are buried in the closed Env conformation in which the bridging sheet has only three strands that differ in topology from the four-stranded bridging sheet in open sCD4-bound Env conformations (Fig. 6a-d; Supplementary Video).

**A model of Env fusion activation.** Although previous sCD4-bound Env structures were three-fold symmetric<sup>5-7</sup>, the E51-sCD4-BG505 complex structures displayed Env trimer

asymmetry, including differences in the degree of gp120 rearrangement and distinct conformations for specific structural elements within gp120-gp41 protomers. Given the relatively small number of available sCD4-bound open Env structures, it is unclear why the Env trimers in the E51-sCD4-Env structures were asymmetric. However, these new open Env conformations can be used to deduce likely states of structural changes in HIV-1 Env upon CD4 binding. Comparison of the class I and class II E51-sCD4-Env structures with previous closed and partially-open Env structures suggest a model for the initial sCD4-induced conformational changes that lead to coreceptor binding and fusion (Fig. 6a-d). As previously described, sCD4 binding to gp120 subunits within Env trimer leads gp120 rotation and outward displacement<sup>4</sup> and to repositioning of the V1V2 domain from the trimer apex in closed Env to the sides of trimer in sCD4-bound Env<sup>6</sup> (Supplementary Video), resulting in formation of the four-stranded gp120 bridging sheet and exposure of the coreceptor binding site on V3<sup>7</sup>. The rotation and displacement of gp120 subunits in sCD4-bound Env trimer structures results in loss of intra-protomer gp120 contacts, a conformation that is either captured by sCD4 during Env “breathing” and (or) is driven by CD4 binding that induces the straightening of the gp41 HR1C helix observed in the protomer B conformation (Fig. 4c). Apparently synchronized conformational changes that differentiate the less-open protomer A conformation (Fig. 6c) and the fully-open protomer B conformation (Fig. 6d) include: (i) gp120 outward displacement that opens space for extension of the HR1C<sub>gp41</sub> N-terminus, (ii) displacement of the gp120  $\alpha_0$  helix closer to HR1C<sub>gp41</sub> N-terminus of the neighboring protomer to facilitate a loop-to-helix transition at the HR1C<sub>gp41</sub> N-terminus, and (iii) elevation of the gp120  $\beta_0$  strand and lowering of the portion of the gp41 helix C-terminal to the fusion peptide, presumably releasing the fusion peptide from the hydrophobic environment observed in the closed<sup>10</sup>, partially-open sCD4-bound Env structures<sup>7</sup>, and protomer A conformations.

We now have structural information relevant to sCD4-induced (or captured) conformational changes in four distinct Env trimer conformations: closed<sup>10</sup> (Fig. 6a), partially-open sCD4-bound<sup>7</sup> (Fig. 6b), the sCD4-bound protomer A in the E51-sCD4-BG505 structures (Fig. 6c), and the fully-open conformation of the sCD4-bound protomer B in the E51-sCD4-BG505 structures (this study) (Fig. 6d) and in the 17b-sCD4-B41 Env structure<sup>5</sup>. These

conformations may represent snapshots of transitions from closed Env trimer (Fig. 6a) to various forms of partially-open trimers (Fig. 6b,c), prior to adopting the fully-open sCD4-bound Env conformation (Fig. 6d) that can interact with coreceptor to undergo further changes resulting in full release of the gp41 fusion peptide. Thus the ability of single-particle cryo-EM to reveal multiple conformations of a protein-protein complex facilitates understanding of conformational changes required during the function of a complicated process such as HIV-1 Env-mediated membrane fusion.

### **Acknowledgements**

We thank M. Farzan, A.P. West, and C.O. Barnes for helpful discussions. Structural studies were performed in the Biological and Cryogenic Transmission Electron Microscopy Center at Caltech with assistance from directors A. Malyutin and S. Chen. We thank the Gordon and Betty Moore and Beckman Foundations for gifts to Caltech to support electron microscopy, Z. Yu (Janeila Farm) for advice on cryo-EM, J. Vielmetter and the Caltech Protein Expression Center for protein production, and M. Shahgholi and the Caltech Protein Exploration Laboratory for mass spectrometry analyses. This work was supported by the National Institute of Allergy and Infectious Diseases of the National Institutes of Health Grant HIVRAD P01 P01AI10014 (P.J.B.) and the National Institutes of Health Grant P50 8 P50 AI150464-13 (P.J.B.).

## Methods

### Protein expression and purification

A native-like, soluble HIV Env gp140 trimer BG505 SOSIP.664 construct including 'SOS' mutations (A501C<sub>gp120</sub>, T605C<sub>gp41</sub>), the 'IP' mutation (I559P<sub>gp41</sub>), introduction of an *N*-linked glycosylation site mutation (T332N<sub>gp120</sub>) and improved furin protease cleavage site (REKR to RRRRRR), and truncation after the C-terminus of gp41 residue 664<sup>8</sup> subcloned into the pTT5 expression vector (National Research Council of Canada) and expressed by transient expression in HEK293-6E cells. BG505 Env trimer was purified from HEK 6E cell supernatants by 2G12 immunoaffinity and size-exclusion chromatography (SEC) using a Superdex 200 Increase 10/300 GL (GE Life Sciences) as described<sup>26</sup>.

The heavy and light chains of 6x-His tagged E51 Fab were co-expressed with tyrosylprotein sulfotransferase II (TPST II)<sup>27</sup> in HEK293-6E cells and purified from transiently-transfected cell supernatants by Ni-NTA chromatography followed by SEC. To separate differentially tyrosine-sulfated species, purified E51 Fab in Tris-Cl pH 9.0 was applied to a Mono Q 5/50 GL anion exchange column (GE Life Sciences) and eluted using a linear salt gradient from 0 mM to 1 M NaCl. Fractions corresponding to three Fab species (Extended Data 1a) were buffer exchanged during SEC into TBS (20 mM Tris-HCl, pH 8.0, 150 mM NaCl, 0.02% NaN<sub>3</sub>).

C-terminally 6x-His tagged sCD4 (D1D2 domain residues 1-186) was expressed in HEK293-6E cells and purified from transiently-transfected cell supernatants by Ni-NTA chromatography followed by SEC as described<sup>7</sup>.

### Mass spectrometric characterization of E51 Fab

E51 Fab samples were analyzed by LC-MS in the positive ion mode using an LCT Premier XE Time-of-Flight mass spectrometer (Waters Corporation). The sample was introduced by a 2.1x50 mm, 450Å, 2.7µm particle BioResolv mAb PolyPhenyl column (Waters Corporation) using a 7-minute gradient of water and acetonitrile with 0.1% formic acid. Raw spectra were averaged and deconvoluted with the MassLynx software (Waters Corporation).

### **Cryo-EM sample preparation**

E51-sCD4-BG505 complexes were generated by incubating purified BG505 SOSIP.664 trimer with E51 and sCD4 at a molar ratio of 4:4:1 (E51:sCD4:Env trimer) at room temperature for 2 hours, transferred to 4°C overnight, and then concentrated to 1.2 mg/mL. Cryo-EM grids were prepared using a Mark IV Vitrobot (ThermoFisher) operated at 10°C and 100% humidity. 3.2  $\mu\text{L}$  of concentrated sample was applied to 300 mesh Quantifoil R2/2 grids, blotted for 4 s, and then plunge-frozen in liquid ethane that is surrounded by liquid nitrogen.

### **Cryo-EM data collection and processing**

Cryo-grids were loaded onto a 300kV Titan Krios electron microscope (ThermoFisher) equipped with a GIF Quantum energy filter (slit width 20 eV) operating at a nominal 130,000x magnification. Images were recorded on a K2 Summit direct electron detector (Gatan) operating in counting mode with a pixel size of  $1.057 \text{ \AA} \cdot \text{pixel}^{-1}$ . The defocus range was set to 1-2.8  $\mu\text{m}$ . Each image was exposed for 8 s and dose-fractionated into 40 subframes with a total dose of  $64 \text{ e}^- \cdot \text{pixel}^{-1}$ , generating a dose rate of  $1.6 \text{ e}^- \cdot \text{pixel}^{-1} \cdot \text{subframe}^{-1}$ . A total of 3128 images were motion-corrected using MotionCor2<sup>37</sup> without binning. Micrographs CTF were estimated using Gctf 1.06<sup>38</sup>. Initially, ~1000 particles were manually picked and reference-free 2D classes were generated using RELION<sup>39,40</sup>. Particles from good 2D classes were used as references for particle picking using RELION AutoPicking<sup>39,40</sup>. A total of 941,841 particles used for three rounds of reference-free 2D classification in RELION<sup>39,40</sup>. After removing ice contaminants, damaged particles and aggregates, 687,259 particles from good classes were combined and used for 3D classification (Extended Data 2a). Low-pass (80  $\text{\AA}$ ) filtered coordinates from a partially-open sCD4-bound BG505 SOSIP Env trimer (PDB 6CM3) were used as a reference for initial 3D classifications. Two major classes (class I and class II) were generated from the first round of 3D classification. Particles from good classes were combined for a second round of 3D classification using the class I map low-pass filtered to 80  $\text{\AA}$ . Both 3D classification steps were performed assuming C1 symmetry. Class I contained 320,895 particles and class II contained 182,970 particles (Extended Data 2b). 3D auto-refinement for both classes were performed assuming C1 symmetry with the E51 Fab C<sub>H</sub>C<sub>L</sub> domains and the sCD4 D2

domain masked out, generating 3.8 Å and 3.9 Å resolution maps for class I and class II, respectively, whereas 3D auto-refinements performed using C3 symmetry produced maps with overall resolutions worse than 7 Å for both classes (data not shown). Particle CTF refinement, particle polishing, and post processing were performed in RELION<sup>39,40</sup> for the two classes of asymmetric maps, which produced two 3D reconstructions with overall resolutions of 3.3 Å for class I and 3.5 Å for class II, calculated using the gold-standard FSC 0.143 criterion<sup>41</sup> (Extended Data 3).

### **Model building**

Coordinates for gp120, gp41, E51 Fab, and sCD4 D1 were fitted into the corresponding regions of the density maps. The following coordinate files were used for initial fitting: BG505 gp120 monomer, gp41 monomer, and sCD4 D1 from the partially-open complex (PDB 6CM3), and E51 Fab from its crystal structure (PDB 1RZF). Coordinates for the two classes of complex structures as well as the *N*-linked glycans were manually refined and built in Coot<sup>42</sup>. Multiple rounds of whole-complex refinement using *phenix.real\_space\_refine*<sup>43,44</sup> and manual refinement were performed to correct for interatomic bonds and angles, clashes, residue side chain rotamers, and residue Ramachandran outliers.

### **Structural analyses**

Buried surface areas were calculated using PDBePISA<sup>45</sup> and a 1.4 Å probe. Potential hydrogen bonds were assigned using the geometry criteria with separation distance of <3.5 Å and A-D-H angle of >90°. The maximum distance allowed for a potential van der Waals interaction was 4.0 Å. Protein surface electrostatic potentials were calculated in PyMol (Schrödinger LLC). Briefly, hydrogens were added to proteins using PDB2PQR<sup>46</sup>, and an electrostatic potential map was calculated using APBS<sup>47</sup>.

### **Data availability**

The structural coordinates were deposited into the Worldwide Protein Data Bank (wwPDB) with accession code 6U0L (class I E51-BG505 SOSIP.664-sCD4 complex) and 6U0N (class II E51-BG505 SOSIP.664-sCD4 complex). EM density maps were deposited into EMDb

with accession numbers EMD-20605 (class I) and EMD-20608 (class II). Other data are available upon reasonable request.

## Figures and Tables

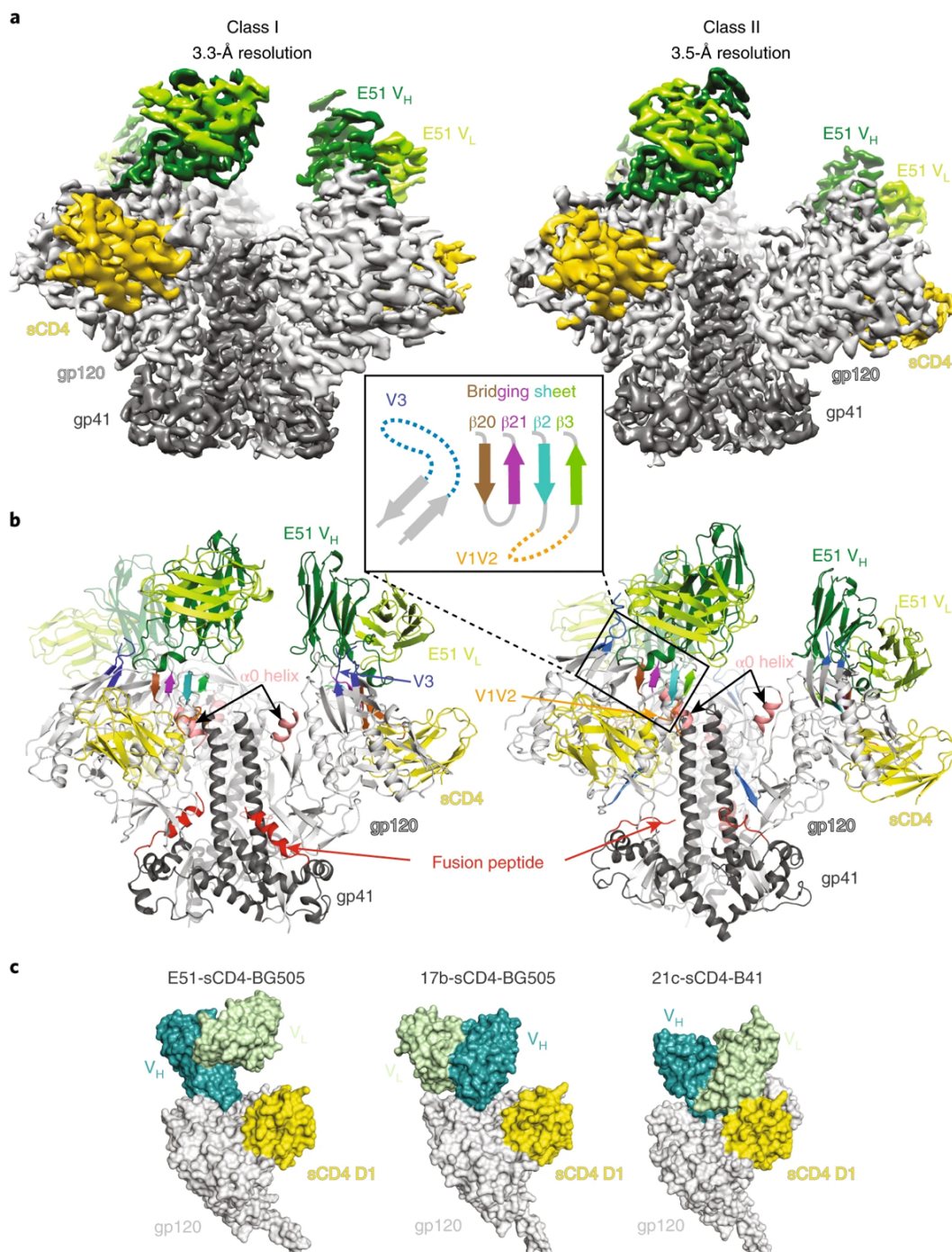


**Figure 1. The Env protomers in E51-sCD4-BG505 complexes adopt two distinct conformations. a, Cryo-EM density maps of class I and class II E51-sCD4-BG505**

structures. **b**, Cartoon representations of Envs from the two structural classes. Inset shows a topology diagram for the four-stranded bridging sheet and the exposed V3 loop (mostly disordered) that comprise part of the E51 epitope on gp120. **c**, Surface representations comparing CD4i Fabs (E51, 17b, and 21c) bound to the gp120-sCD4 portions of CD4i-sCD4-Env trimer complex structures (PDBs 6CM3 and 6EDU for the 17b and 21c complex structures, respectively).

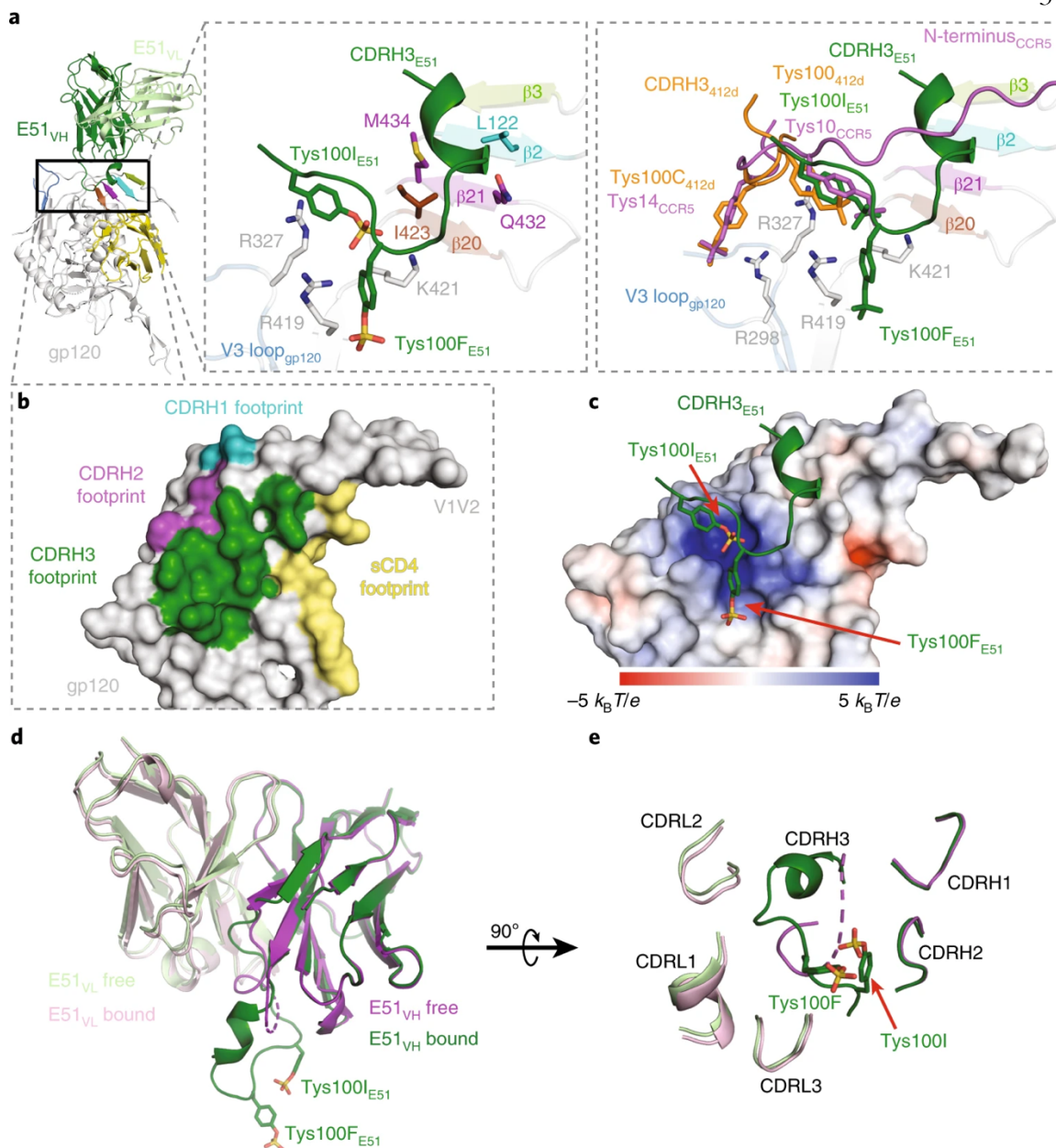


**Figure 2. E51 Fab interacts extensively with gp120.** **a**, Cartoon representation of E51-gp120 portion of E51-sCD4-BG505 structure (left). Middle inset shows a close-up with the four-stranded bridging sheet (colors as shown in Fig. 1b) and interface residues shown as sticks. Right inset shows a superimposition of regions containing sulfated tyrosines in structures of E51-sCD4-BG505, CCR5-sCD4-gp120 (PDB 6MEO), and 412d-sCD4-gp120 (PDB 2QAD) complexes. **b**, Surface representation of gp120 with contacts by E51 CDRs and sCD4 highlighted. **c**, Electrostatic surface of gp120 overlaid with CDRH3 of bound

E51. Sulfated tyrosines highlighted as sticks. **d**, Superimposition of  $V_H$ - $V_L$  domains of bound and free E51 (PDB 1RZF)<sup>22</sup>. Ordered sulfated tyrosines are highlighted as sticks on the CDRH3 of the bound E51 Fab structure. A dashed line for the CDRH3 in the free structure indicates a disordered region. **e**, E51 combining site (90° rotation from orientation in panel d) with ordered sulfated tyrosines highlighted as sticks.

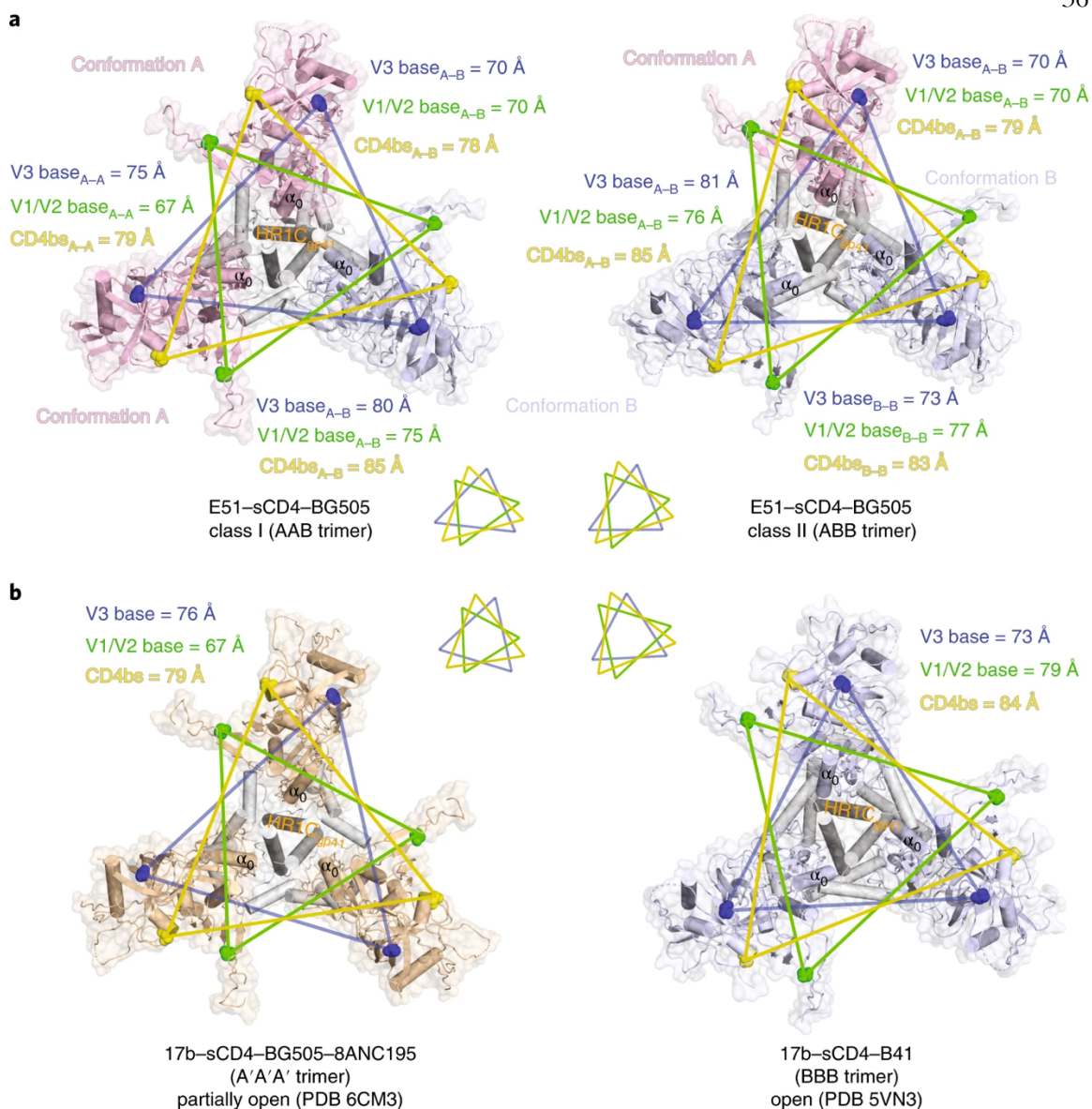


**Figure 3. BG505 Env trimers are asymmetric in the class I and class II E51-sCD4-BG505 structures.** **a**, Top-down views of BG505 trimers in class I (left) and class II (right) conformations with the protomer conformation A in light pink and the protomer conformation B in light blue. Inter-protomer distances between three residues (V3 base residue His330<sub>gp120</sub>, V1/V2 base residue Pro124<sub>gp120</sub>, and CD4 binding site (CD4bs) residue Asp368<sub>gp120</sub>) are indicated in colored lines on the structures and shown schematically as triangles below the structures. **b**, Top-down views of Env trimers in symmetric CD4i-sCD4-Env complex structures. Inter-protomer distances between the three residues used for analysis in panel **a** are indicated in colored lines on the structures and shown schematically

as triangles above the structures. A' denotes the conformation of protomers in a partially-open sCD4-bound structure (PDB 6CM3)<sup>7</sup>.

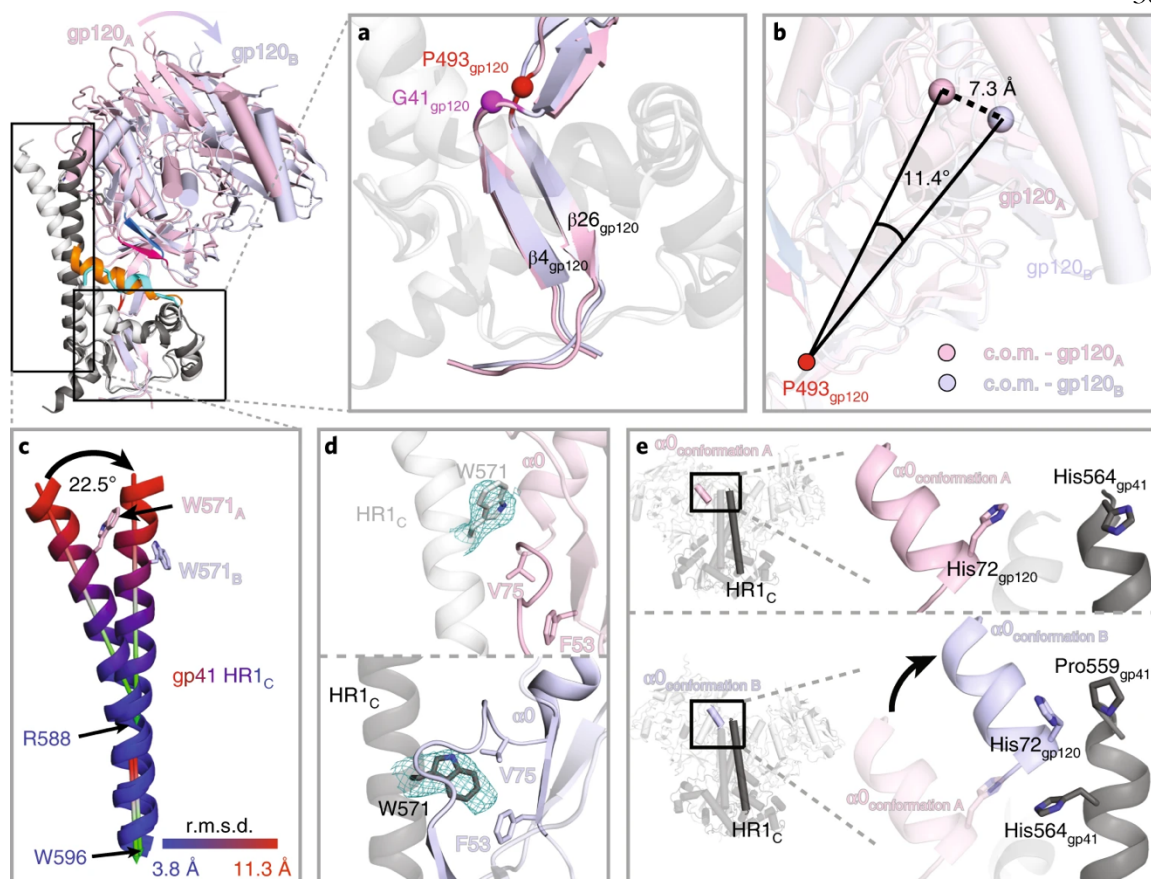


**Figure 4. Protomers A and B exhibit different structural features (see also Supplementary Video).** Top left, overlay of cartoon representations of gp120 conformations A (pink) and B (light blue) and gp41 conformations A (light grey) and B (dark grey). Insets show close-up views of features discussed in the text. **a**, Superimposition of gp120  $\beta 4$  and  $\beta 26$  strands in protomers A and B. **b**, Definition of lines joining the hinge residue Pro493<sub>gp120</sub> to the center of mass (c.o.m.) of the gp120s in conformations A and B. The lines differed by an angle of 11.4° and a displacement of 7.3 Å. **c**, Differences in the protomer A and B HR1C helices. After superimposition of gp120  $\beta 4$  and  $\beta 26$  strands in protomers A and B (panel a), the C-terminal portion of the HR1<sub>C</sub> helix (Arg588<sub>gp41</sub>–Trp596<sub>gp41</sub>) was similar between the two conformations (angle between the two helical axes of 2.5°), whereas the N-terminal portion (Leu565<sub>gp41</sub>–Glu584<sub>gp41</sub>) showed deviations up to 11.3 Å at the helix N-termini and a helical axis angle difference of 22.5°. **d**, Comparison of the location and conformation of gp41 HR1C residue Trp571<sub>gp41</sub> in protomer conformations

A (top) and B (bottom). **e**, The gp120  $\alpha 0$  helix in conformation B, but not conformation A, facilitates an extension of the gp41 HR1C N-terminus of a neighboring protomer.

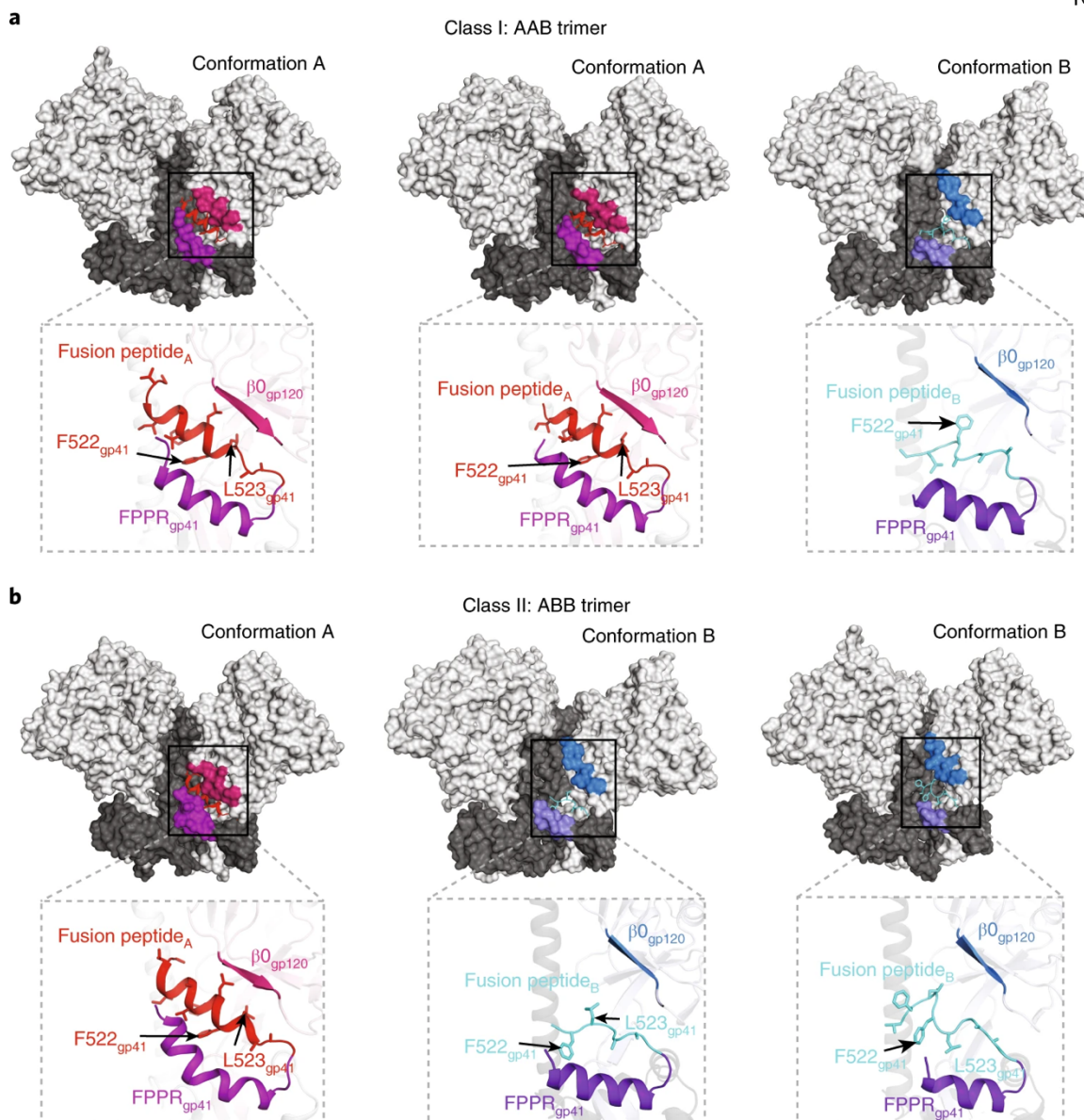


**Figure 5. gp41 exhibits different conformations in protomers A and B (see also Supplementary Video).** **a**, Class I Env trimer. The gp41 fusion peptide is  $\alpha$ -helical in two conformation A protomers in the class I structure (AAB trimer), and adopts a partially-ordered loop structure in the conformation B protomer. **b**, Class II Env trimer. The fusion peptide is  $\alpha$ -helical in one conformation A protomer and in two conformation B protomers in the class II structure (ABB trimer).

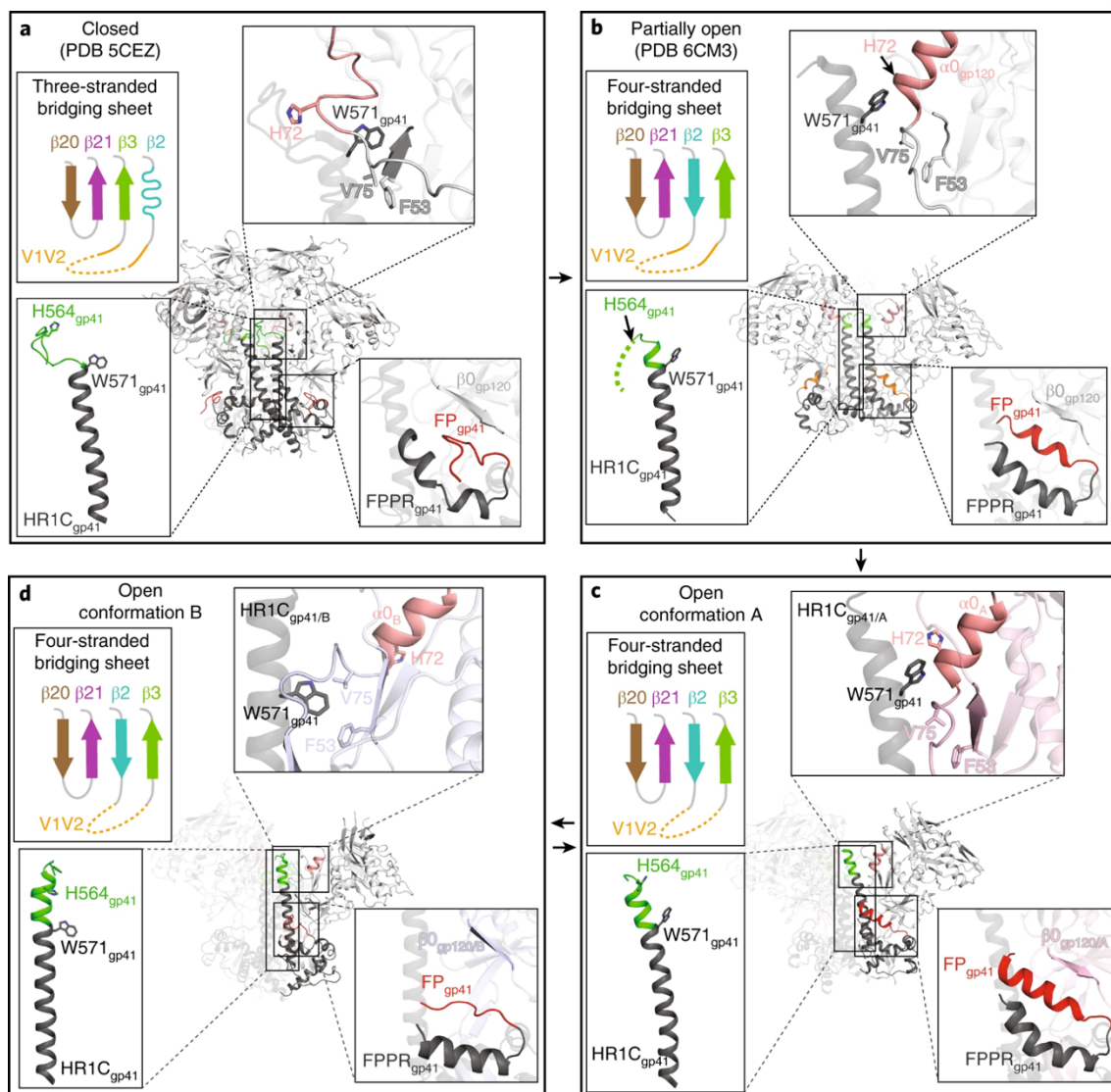
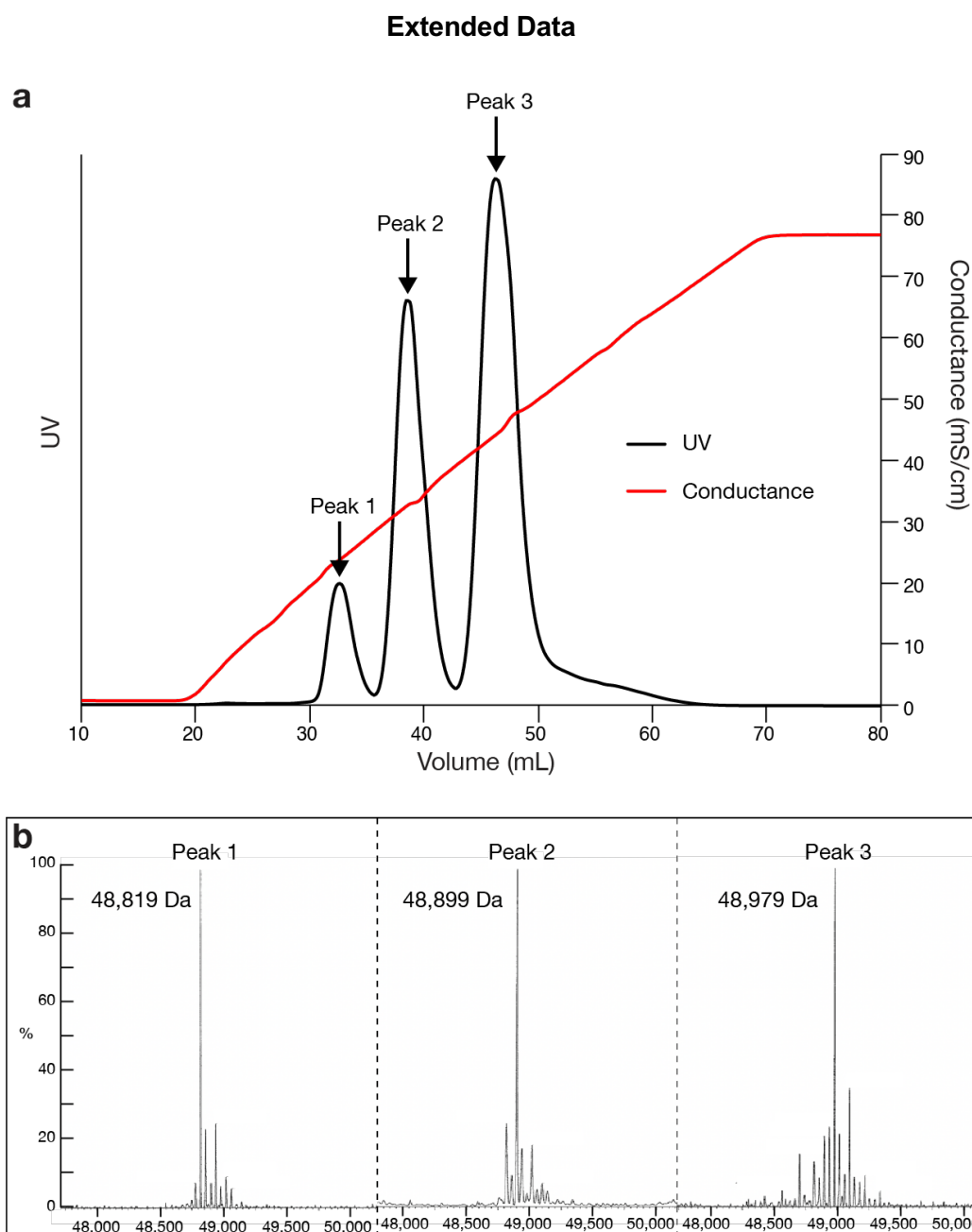


**Figure 6. Summary of conformational changes described in text between closed and various open Env conformations (see also Supplementary Video).** Env conformations are indicated, along with the complex from which the Env structure was derived. **a**, Closed Env trimer conformation (PDB 5CEZ). **b**, Partially-open sCD4-bound Env conformation (PDB 6CM3). **c**, Open conformation A (intermediate between partially-open and fully-open sCD4-bound Env conformations). **d**, Fully-open sCD4-bound Env conformation B.

**Table 1. Cryo-EM data collection, refinement, and validation statistics**

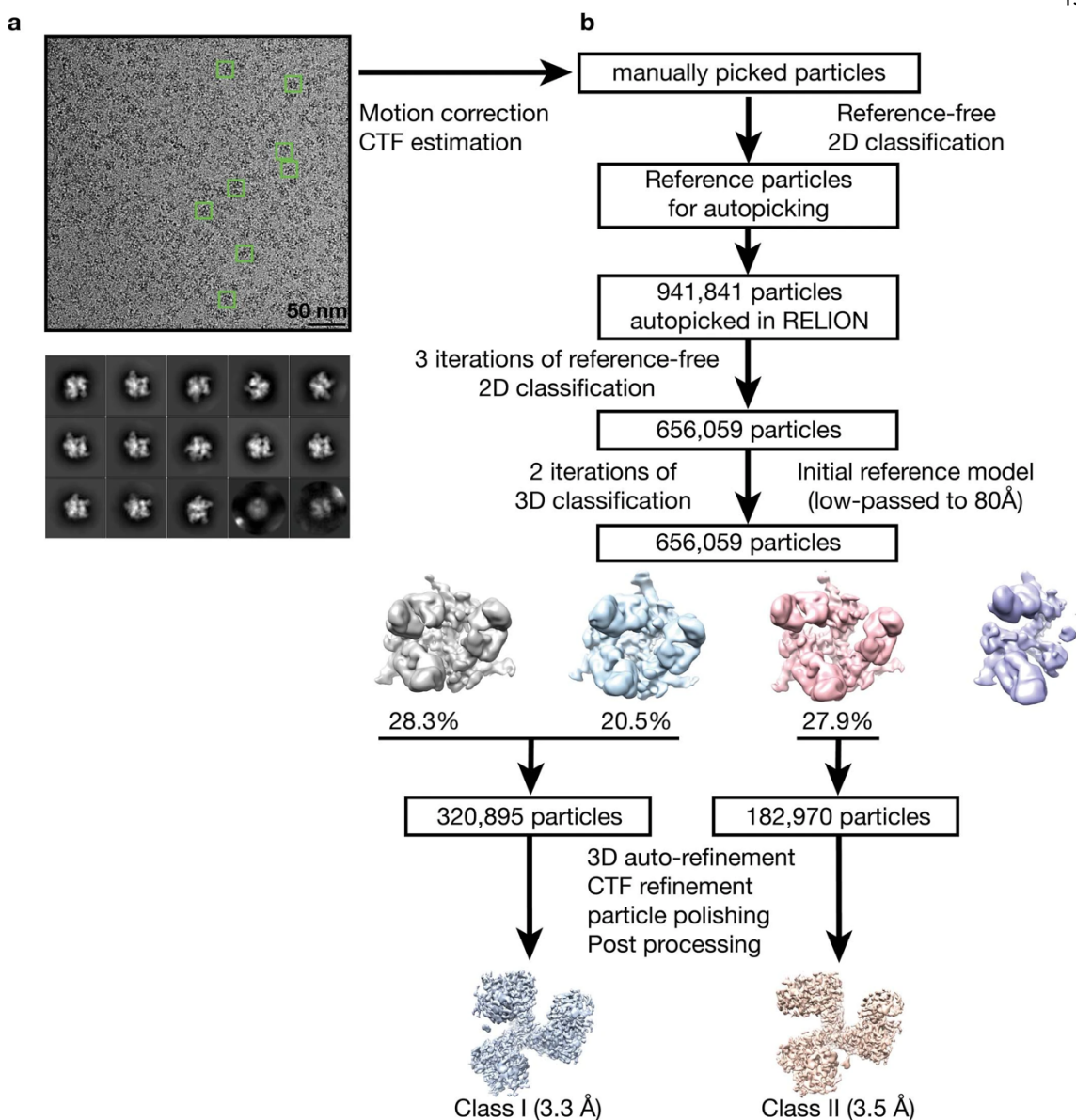
	BG505 SOSIP-sCD4-E51 Class I (EMDB-20605; PDB 6U0L)	BG505 SOSIP-sCD4-E51 Class II (EMDB-20608; PDB 6U0N)
<b>Data collection and processing</b>		
Magnification (nominal)	130,000x	130,000x
Voltage (kV)	300	300
Electron exposure (e <sup>-</sup> /Å <sup>2</sup> )	64	64
Defocus range (μm)	1 - 2.8	1 - 2.8
Pixel size (Å)	1.057	1.057
Symmetry imposed	C1	C1
Initial particle images (no.)	941,841	941,841
Final particle images (no.)	320,895	182,970
Map resolution (Å)	3.31	3.49
FSC threshold	0.143	0.143
Map resolution range (Å)	3.3 - 5.2	3.5 - 5.2
<b>Refinement</b>		
Initial model used (PDB code)	6CM3 (partial*)	6CM3 (partial*)
Model resolution (Å)		
FSC threshold - 0.143	3.2	3.3
Model resolution range (Å)	3.2 - 5.2	3.3 - 5.2
Map sharpening <i>B</i> factor (Å <sup>2</sup> )	-90	-80
Model composition		
Non-hydrogen atoms	19,624	19,322
Protein residues	2502	2489
Ligands	NAG: 35 BMA: 3 MAN: 8	NAG: 34 BMA: 3 MAN: 6
<i>B</i> factors (Å <sup>2</sup> )		
Protein	68	84
Ligand	69	87
R.m.s. deviations		
Bond lengths (Å)	0.009	0.006
Bond angles (°)	1.025	0.914
Validation		
MolProbity score	2.17	1.84
Clashscore	6.01	5.68
Poor rotamers (%)	1.0	0.35
Ramachandran plot		
Favored (%)	90.6	90.5
Allowed (%)	9.4	9.5
Disallowed (%)	0	0

\* Used coordinates of trimeric gp120-gp41 as the reference model



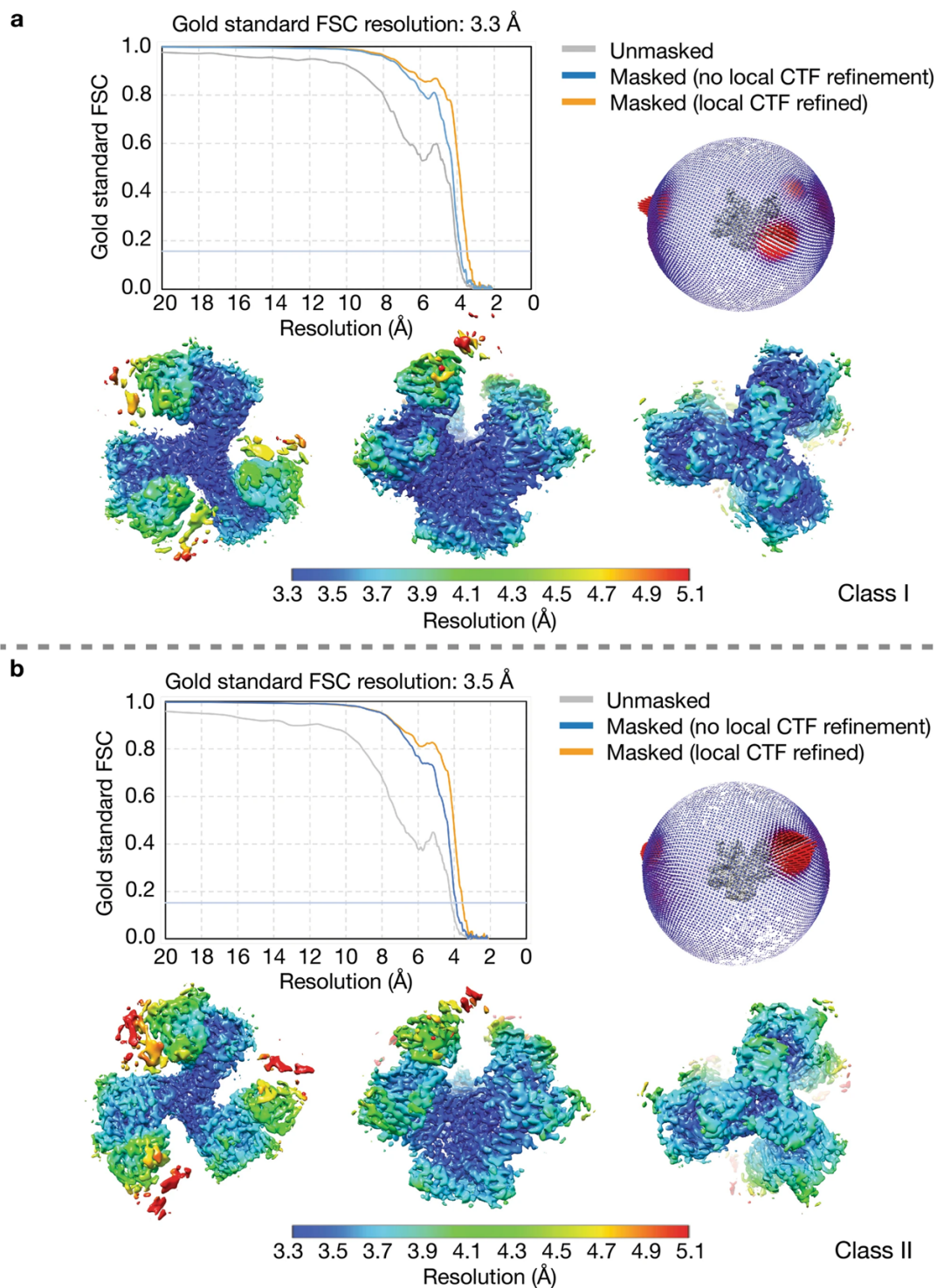
**Extended Data Figure 1. Mass spectrometry characterization of E51 Fab. a,** Peak fractions from anion exchange chromatography of E51 Fab. **b,** Mass spectra of the three E51 peaks from panel a. The molecular mass for Peak 1 corresponded within 27 Da to the predicted mass for unmodified E51 Fab (48,791 Da), suggesting this E51 Fab fraction contained no sulfated tyrosines. The molecular masses for Peaks 2 and 3 were each increased by 80 Da from the preceding peak, corresponding to the molecular weight of a

SO<sup>3-</sup> group (80 Da). These results are consistent with the identification of Peaks 2 and 3 as E51 Fab with one and two sulfated tyrosines, respectively. Peak 3 was used for preparing complexes for cryo-EM.



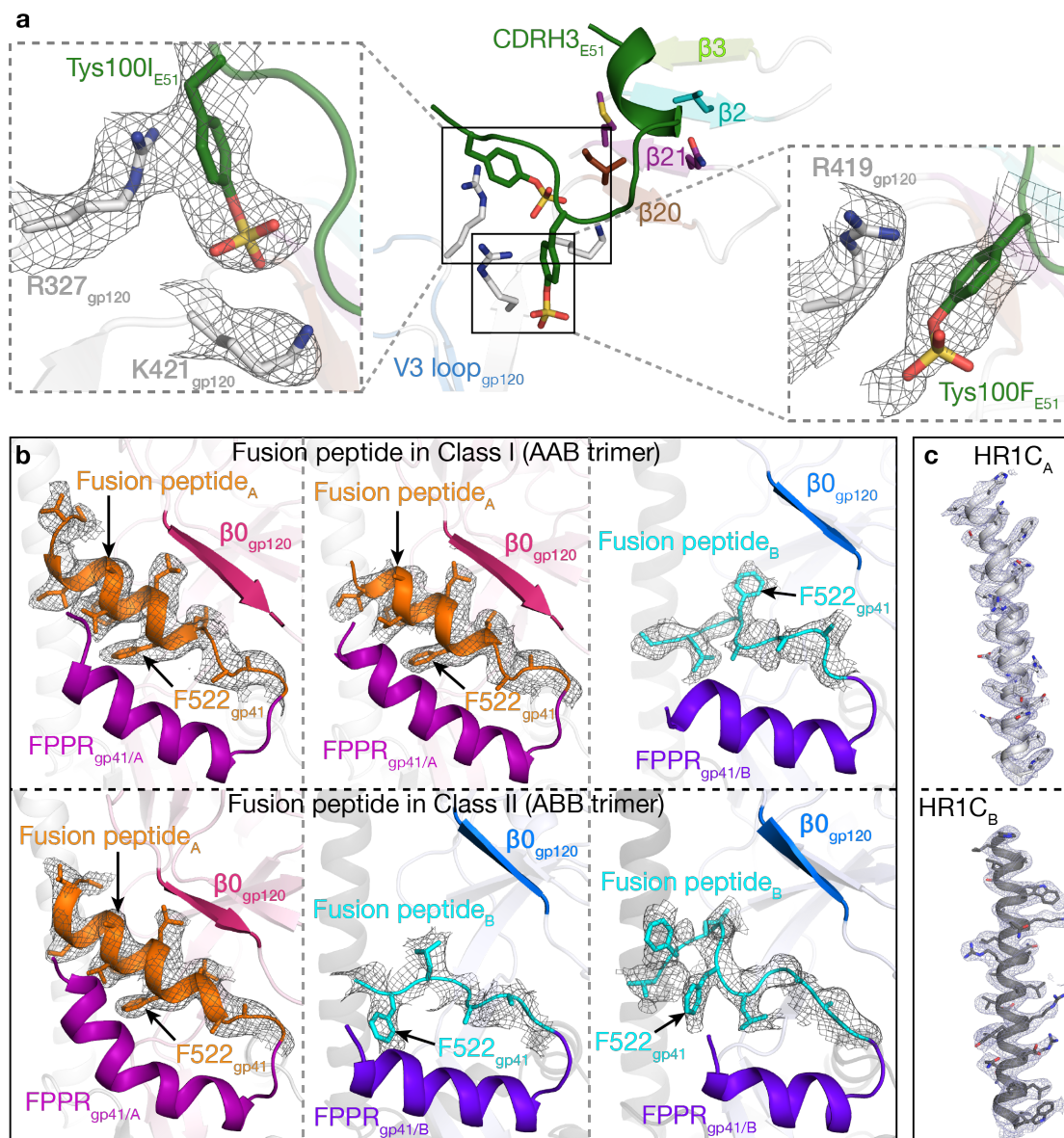
**Extended Data Figure 2. Data processing for BG505 SOSIP-sCD4-E51 complex structures.** **a**, Example of a motion-corrected and dose-weighted micrograph of E51-sCD4-BG505 complexes (representative individual particles in boxes). Scale bar = 50 nm. Defocus was  $\sim 2.6$   $\mu\text{m}$  underfocus. **b**, Data processing scheme. Collected micrographs were motion-corrected using MotionCor2 (ref.<sup>1</sup>) without binning. Contrast transfer functions (CTFs) were estimated using Gctf 1.06 (ref.<sup>2</sup>).  $\sim 1,000$  particles were manually picked and subjected to 2D classification in RELION<sup>3,4</sup>. Particles from good classes were used as references for automatic particle picking using RELION AutoPicking. 941,841 autopicked

particles were subjected to three rounds of reference-free 2D classification. In each round, particles from good 2D classes were selected, which gave 656,059 particles. Subsequently, using the Env trimer portion of an 80 Å low-pass filtered partially-open trimeric BG505 SOSIP structure (PDB 6CM3) as the reference model, first round of 3D classification was performed assuming C1 symmetry. Particles from good classes were combined and used for a second round of 3D classification with C1 symmetry. The resulting maps could be grouped into two classes: class I (320,895 particles) and class II (182,970 particles). Maps from the two classes were refined separately assuming C1 symmetry with the sCD4 D2 domain and E51 Fab C<sub>H</sub>C<sub>L</sub> domains masked out. After CTF refinement, movie refinement, and particle polishing, the class I and class II post-processed maps were refined to 3.3 Å and 3.5 Å resolution (FSC 0.143), respectively (Fig. S3).

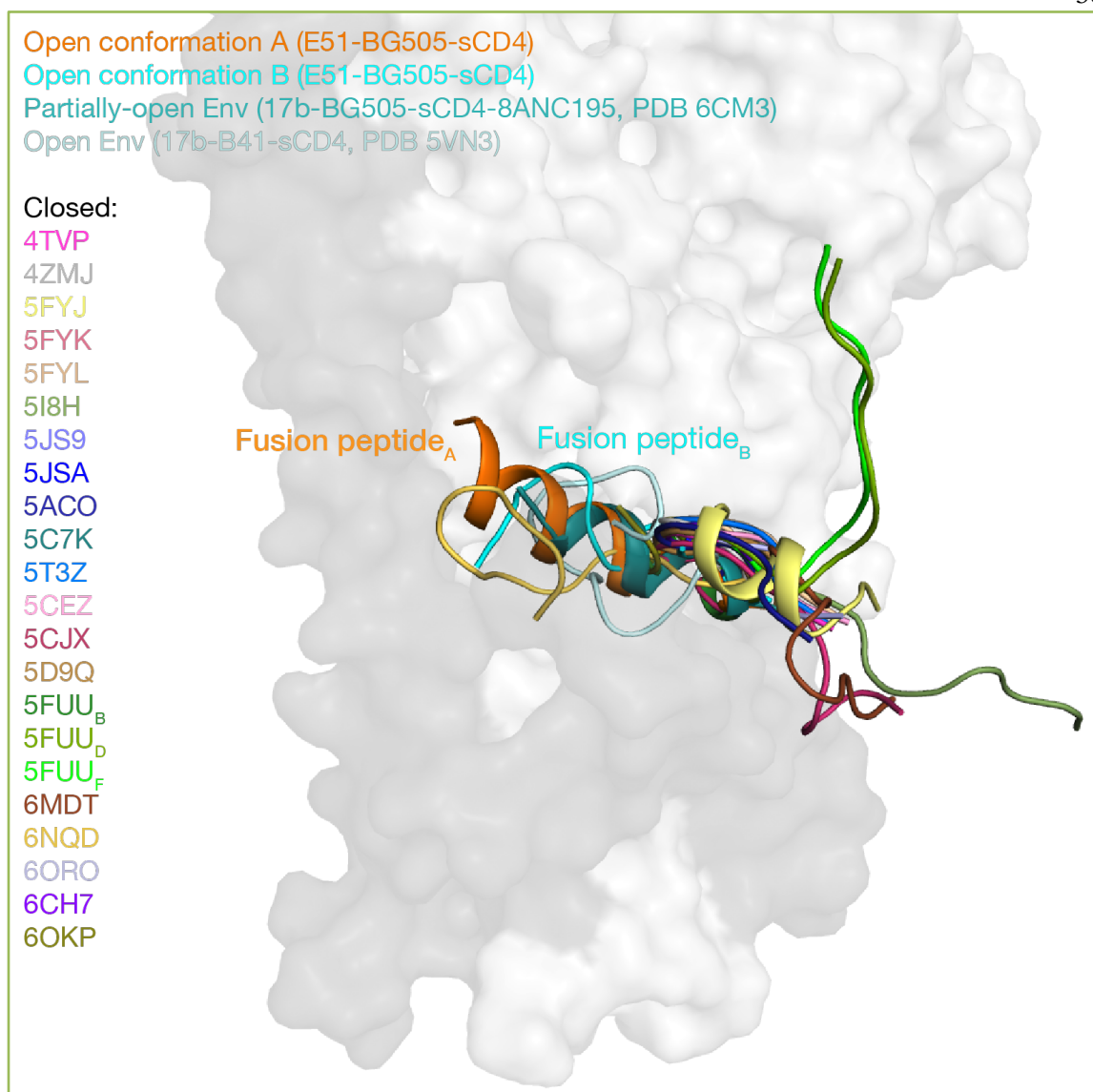


**Extended Data Figure 3. Validation of the BG505 SOSIP-sCD4-E51 complex structures.** Class I (panel a) and class II (panel b) E51-sCD4-BG505 complex structures. Top left in both panels: Gold-standard Fourier Shell Correlations (FSCs) of two classes of

maps. Top right: Orientation distributions for class I and class II structures. Bottom: Local resolution estimations for class I and class II density maps (calculated using the local resolution program in RELION<sup>3,4</sup>).



**Extended Data Figure 4.** Representative densities for class I and class II E51-sCD4-BG505 complex structures. **a**, Densities for residues involved in E51 CDRH3 sulfotyrosine interactions. **b**, Densities for fusion peptides in protomers A (top) and B (bottom). **c**, Densities for HR1<sub>C</sub> helices in protomers A (top) and B (bottom).



**Extended Data Figure 5. Comparison of fusion peptide conformations in Env structures.** The fusion peptide is orange in the conformation A protomer, cyan in the conformation B protomer (from the E51-sCD4-BG505 complex structures reported here), teal in a partially-open 17b-sCD4-BG505-8ANC195 complex (PDB 6CM3), and pale cyan in a fully-open 17b-sCD4-B41 complex (PDB 5VN3). Fusion peptides from Env trimers in a closed, prefusion conformation are color coded as shown for their PDB IDs. References for structures are listed below.

## Supplementary Information

E51-sCD4-BG505	ENLWVTVVYGVFVWKDAETTLFCASDAKAYETEKHNWVWATHACVPTDPNPFQEIHLNVTE	<u>α0</u>	<u>β0</u>	
CCR5-sCD4-gp120	DNLWVTVVYGVFVWKDAETTLFCASDAKAYETEKHNWVWATHACVPTDPNPFQEIHLNVTE			
17b-sCD4-8ANC195-BG505	ENLWVTVVYGVFVWKDAETTLFCASDAKAYETEKHNWVWATHACVPTDPNPFQEIHLNVTE			
21c-sCD4-8ANC195-B41	AKKVVTVVYGVFVWKDAETTLFCASDAKAYETEKHNWVWATHACVPTDPNPFQEIHLNVTE			
	40	72		
E51-sCD4-BG505	EFNMWKNMVEQMHTDIIISLWDQSLKPCVKLTPLCVTLQCTNVTTNIT-----	<u>α1</u>	<u>β2</u>	<u>V1V2</u>
CCR5-sCD4-gp120	NFNMWKNMVEQMHTDIIISLWDQSLKPCVKLTPLCVTLQCTNVTTNIT-----			
17b-sCD4-8ANC195-BG505	EFNMWKNMVEQMHTDIIISLWDQSLKPCVKLTPLCVTLQCTNVTTNIT-----			
21c-sCD4-8ANC195-B41	NFNMWKNMVEQMHTDIIISLWDQSLKPCVKLTPLCVTLQCTNVTTNIT-----			
	100	122		
E51-sCD4-BG505	DDMRGELKNCSEFNMTTELDRKKQKVYSLFYRLDQVQINENQGNRSNNSNKEYRLINCNST	<u>V1V2</u>		
CCR5-sCD4-gp120	GIDKGEIKNCSEFNMTTELDRKKQKVYSLFYRLDQVQINENQGNRSNNSNKEYRLINCNST			
17b-sCD4-8ANC195-BG505	DDMRGELKNCSEFNMTTELDRKKQKVYSLFYRLDQVQINENQGNRSNNSNKEYRLINCNST			
21c-sCD4-8ANC195-B41	KMETGEMKNCSEFNMTTELDRKKQKVYSLFYRLDQVQINENQGNRSNNSNKEYRLINCNST			
	164			
E51-sCD4-BG505	AITQACPKVSFEPIPIHYCAPAGFAILKCKDKKFNFTGPCPSVSTVQCTHGIRPVVSTQL	<u>β3</u>		
CCR5-sCD4-gp120	VITQACPKVTFEPIPIHYCTFAGYAILKCNKGFNGTGPCNVSSTVQCTHGIRPVVSTQL			
17b-sCD4-8ANC195-BG505	AITQACPKVSFEPIPIHYCAPAGFAILKCKDKKFNFTGPCPSVSTVQCTHGIRPVVSTQL			
21c-sCD4-8ANC195-B41	VITQACPKVSFEPIPIHYCAPAGFAILKCNKGFNGTGPCNVSSTVQCTHGIRPVVSTQL			
	202			
E51-sCD4-BG505	LLNGSLAEEVMIRESNITNNAKNIIVQFNTPVQINCTRPNNTRKSIIRIGPGQAFYATG	<u>V3</u>		
CCR5-sCD4-gp120	LLNGSLAEEVMIRESNITNNAKNIIVQFNTPVQINCTRPNNTRKSIIRIGPGQAFYATG			
17b-sCD4-8ANC195-BG505	LLNGSLAEEVMIRESNITNNAKNIIVQFNTPVQINCTRPNNTRKSIIRIGPGQAFYATG			
21c-sCD4-8ANC195-B41	LLNGSLAEEVMIRESNITNNAKNIIVQFNTPVQINCTRPNNTRKSIIRIGPGQAFYATG			
	261	300		
E51-sCD4-BG505	DIIGDIHQAHCVNSKATWNETLQVVKQLRKHFGNNTIIRFANSSGGDLEVTTHSFNCGG	<u>V3</u>	<u>CD4bs loop</u>	
CCR5-sCD4-gp120	DIIIGDIHQAHCVNSKATWNETLQVVKQLRKHFGNNTIIRFANSSGGDLEVTTHSFNCGG			
17b-sCD4-8ANC195-BG505	DIIGDIHQAHCVNSKATWNETLQVVKQLRKHFGNNTIIRFANSSGGDLEVTTHSFNCGG			
21c-sCD4-8ANC195-B41	DIIIGDIHQAHCVNSKATWNETLQVVKQLRKHFGNNTIIRFANSSGGDLEVTTHSFNCGG			
	327	369		
E51-sCD4-BG505	EFFYCNSTGLFNSTWISNTSVQGSNSTGSNDSITLPCRIKQIINMWQRIGQAMYAPPIQG	<u>V4</u>	<u>β20</u>	<u>β21</u>
CCR5-sCD4-gp120	EFFYCNSTGLFNSTWISNTSVQGSNSTGSNDSITLPCRIKQIINMWQRIGQAMYAPPIQG			
17b-sCD4-8ANC195-BG505	EFFYCNSTGLFNSTWISNTSVQGSNSTGSNDSITLPCRIKQIINMWQRIGQAMYAPPIQG			
21c-sCD4-8ANC195-B41	EFFYCNSTGLFNSTWISNTSVQGSNSTGSNDSITLPCRIKQIINMWQRIGQAMYAPPIQG			
	381	421	432	
E51-sCD4-BG505	VIRCVSNITGLILTRDGGSTN-STTETFRPGGDMRDNRSELYKYKVVVIEPLGVAPTR	<u>V5</u>	<u>β26</u>	
CCR5-sCD4-gp120	KIKCSSNITGLILTRDGGSTN-STTETFRPGGDMRDNRSELYKYKVVVIEPLGVAPTR			
17b-sCD4-8ANC195-BG505	VIRCVSNITGLILTRDGGSTN-STTETFRPGGDMRDNRSELYKYKVVVIEPLGVAPTR			
21c-sCD4-8ANC195-B41	QIRCSSNITGLILTRDGGSTN-STTETFRPGGDMRDNRSELYKYKVVVIEPLGVAPTR			
	442	493		
E51-sCD4-BG505	CKRRVVG	X = residues contacted by Fabs or CCR5		
CCR5-sCD4-gp120	-----	□ = residues contacted by sulfated tyrosines		
17b-sCD4-8ANC195-BG505	CKRRVVG	■ = disordered regions		
21c-sCD4-8ANC195-B41	CKRRV--			

Supplementary Note 1. Sequence alignment of gp120s from structures of the indicated complexes demonstrates similarities and differences in interactions.

Trimer state	Trimer type	Ligand(s)	Method	PDB	Resolution (Å)	Distance(s) between V3 (His330) (Å)	Distance(s) between V1/V2 (Pro124) (Å)	Distance(s) between CD4bs (Asp368) (Å)
Closed	BG505 SOSIP.664	8ANC195	X-ray	5CJX	3.6	68	14	54
Closed	BG505 SOSIP.664	PGT122, 35O22	X-ray	4TVP	3.5	69	15	55
Closed	BG505 SOSIP.664	PGT122	X-ray	4NCO	4.7	70	14	56
Closed	BG505 SOSIP.664	3H+109L 35O22	X-ray	5CEZ	3	69	14	56
Closed	BG505 SOSIP.664	IOMA, 35O22	X-ray	5T3Z	3.5	69	14	54
Closed	JR-FL EnvΔCT	PGT151	cryo-EM	5FUU	4.2	69	16	56
Partially open	BG505 SOSIP.664	sCD4, 17b 8ANC195	cryo-EM	6CM3	3.5	76	67	79
Partially open	B41 SOSIP.664	sCD4, 21c 8ANC195	cryo-EM	6EDU	4.1	73	69	79
Open	B41 SOSIP.664	sCD4, 17b	cryo-EM	5VN8	3.6	73	79	84
Open (Class I)	BG505 SOSIP.664	sCD4, E51	cryo-EM	6u0L	3.3	75, 80, 70	67, 75, 70	79, 85, 78
Open (Class II)	BG505 SOSIP.664	sCD4, E51	cryo-EM	6u0N	3.5	81, 73, 70	76, 77, 70	85, 83, 79

**Supplementary Table 1. Distance comparisons in Env trimer structures.** Structures are grouped into four conformational states: closed (unliganded and bound to Fabs), partially open (bound to 8ANC195, sCD4, and either 17b or 21c), and open (bound to sCD4 and 17b), and the open class I and class II E51-sCD4-BG505 complexes (this study). The PDB identifier is given for each structure. PDB coordinates for gp120 subunits within a trimer were used to measure distances on adjacent protomers between V3 base residue His330<sub>gp120</sub>, V1V2 base residue Pro124<sub>gp120</sub>, and the CD4 binding site residue Asp368<sub>gp120</sub>.

PDB	Supplementary PDB References for Extended Data Figure 5
6CM3	Wang, H., Barnes, C.O., Yang, Z., Nussenzweig, M.C. & Bjorkman, P.J. Partially Open HIV-1 Envelope Structures Exhibit Conformational Changes Relevant for Coreceptor Binding and Fusion. <i>Cell Host Microbe</i> <b>24</b> , 579-592 e4 (2018)
5VN3	Ozorowski, G. et al. Open and closed structures reveal allostery and pliability in the HIV-1 envelope spike. <i>Nature</i> <b>547</b> , 360-363 (2017)
4TVP	Pancera, M. et al. Structure and immune recognition of trimeric pre-fusion HIV-1 Env. <i>Nature</i> <b>514</b> , 455-61 (2014)
4ZMJ	Kwon, Y.D. et al. Crystal structure, conformational fixation and entry-related interactions of mature ligand-free HIV-1 Env. <i>Nat Struct Mol Biol</i> <b>22</b> , 522-31 (2015)
5FYJ	Stewart-Jones, G.B.E. et al. Trimeric HIV-1-Env Structures Define Glycan Shields from Clades A, B, and G. <i>Cell</i> <b>165</b> , 813-26 (2016)
5FYK	Stewart-Jones, G.B.E. et al. Trimeric HIV-1-Env Structures Define Glycan Shields from Clades A, B, and G. <i>Cell</i> <b>165</b> , 813-26 (2016)
5FYL	Stewart-Jones, G.B.E. et al. Trimeric HIV-1-Env Structures Define Glycan Shields from Clades A, B, and G. <i>Cell</i> <b>165</b> , 813-26 (2016)
5I8H	Kong, R. et al. Fusion peptide of HIV-1 as a site of vulnerability to neutralizing antibody. <i>Science</i> <b>352</b> , 828-33 (2016)
5JS9	Kong, L. et al. Uncleaved prefusion-optimized gp140 trimers derived from analysis of HIV-1 envelope metastability. <i>Nat Commun</i> <b>7</b> , 12040 (2016)
5JSA	Kong, L. et al. Uncleaved prefusion-optimized gp140 trimers derived from analysis of HIV-1 envelope metastability. <i>Nat Commun</i> <b>7</b> , 12040 (2016)
5ACO	Lee, J.H., de Val, N., Lyumkis, D. & Ward, A.B. Model Building and Refinement of a Natively Glycosylated HIV-1 Env Protein by High-Resolution Cryoelectron Microscopy. <i>Structure</i> <b>23</b> , 1943-51 (2015)
5C7K	Kong, L. et al. Complete epitopes for vaccine design derived from a crystal structure of the broadly neutralizing antibodies PGT128 and 8ANC195 in complex with an HIV-1 Env trimer. <i>Acta Crystallogr D Biol Crystallogr</i> <b>71</b> , 2099-108 (2015)
5T3Z	Gristick, H.B. et al. Natively glycosylated HIV-1 Env structure reveals new mode for antibody recognition of the CD4-binding site. <i>Nat Struct Mol Biol</i> <b>23</b> , 906-915 (2016)
5CEZ	Garces, F. et al. Affinity Maturation of a Potent Family of HIV Antibodies Is Primarily Focused on Accommodating or Avoiding Glycans. <i>Immunity</i> <b>43</b> , 1053-63 (2015)

5CJX	Scharf, L. et al. Broadly Neutralizing Antibody 8ANC195 Recognizes Closed and Open States of HIV-1 Env. <i>Cell</i> <b>162</b> , 1379-90 (2015)
5D9Q	Jardine, J.G. et al. Minimally Mutated HIV-1 Broadly Neutralizing Antibodies to Guide Reductionist Vaccine Design. <i>PLoS Pathog</i> <b>12</b> , e1005815 (2016)
5FUU	Lee, J.H., Ozorowski, G. & Ward, A.B. Cryo-EM structure of a native, fully glycosylated, cleaved HIV-1 envelope trimer. <i>Science</i> <b>351</b> , 1043-8 (2016)
6MDT	Kumar, S. et al. Capturing the inherent structural dynamics of the HIV-1 envelope glycoprotein fusion peptide. <i>Nat Commun</i> <b>10</b> , 763 (2019).
6NQD	Ananthaswamy, N. et al. A sequestered fusion peptide in the structure of an HIV-1 transmitted founder envelope trimer. <i>Nat Commun</i> <b>10</b> , 873 (2019)
6OKP	Schoofs, T. et al. Broad and Potent Neutralizing Antibodies Recognize the Silent Face of the HIV Envelope. <i>Immunity</i> <b>50</b> , 1513-1529 e9 (2019)
6ORO	Barnes, C.O. et al. Structural characterization of a highly-potent V3-glycan broadly neutralizing antibody bound to natively-glycosylated HIV-1 envelope. <i>Nat Commun</i> <b>9</b> , 1251 (2018)
6CH7	Escolano, A. et al. Immunization expands B cells specific to HIV-1 V3 glycan in mice and macaques. <i>Nature</i> (2019)

**Supplementary Table 2. PDB entries for structures presented in Extended Data Figure 5 and their corresponding references.**

## References

1. Harrison, S.C. Viral Membrane Fusion. *Virology* **479-480**, 498-507 (2015).
2. Choe, H. et al. The Beta-chemokine Receptors CCR3 and CCR5 Facilitate Infection by Primary HIV-1 Isolates. *Cell* **85**, 1135-48 (1996).
3. Feng, Y., Broder, C.C., Kennedy, P.E. & Berger, E.A. HIV-1 Entry Cofactor: Functional cDNA Cloning of a Seven-transmembrane, G protein-coupled Receptor. *Science* **272**, 872-7 (1996).
4. Liu, J., Bartesaghi, A., Borgnia, M.J., Sapiro, G. & Subramaniam, S. Molecular Architecture of Native HIV-1 gp120 Trimers. *Nature* **455**, 109-13 (2008).
5. Ozorowski, G. et al. Open and Closed Structures Reveal Allostery and Pliability in the HIV-1 Envelope Spike. *Nature* **547**, 360-363 (2017).
6. Wang, H. et al. Cryo-EM Structure of a CD4-bound Open HIV-1 Envelope Trimer Reveals Structural Rearrangements of the gp120 V1V2 Loop. *Proc. Natl. Acad. Sci.* **113**, E7151-E7158 (2016).
7. Wang, H., Barnes, C.O., Yang, Z., Nussenzweig, M.C. & Bjorkman, P.J. Partially Open HIV-1 Envelope Structures Exhibit Conformational Changes Relevant for Coreceptor Binding and Fusion. *Cell Host & Microbe* **24**, 579-592 e4 (2018).
8. Sanders, R.W. et al. A Next-generation Cleaved, Soluble HIV-1 Env Trimer, BG505 SOSIP.664 gp140, Expresses Multiple Epitopes for Broadly Neutralizing but not Non-neutralizing Antibodies. *PLoS Pathog.* **9**, e1003618 (2013).
9. Alshafiq, N., Debbeche, O., Sodroski, J. & Finzi, A. Effects of the I559P gp41 Change on the Conformation and Function of the Human Immunodeficiency Virus (HIV-1) Membrane Envelope Glycoprotein Trimer. *PLoS One* **10**, e0122111 (2015).
10. Ward, A.B. & Wilson, I.A. The HIV-1 Envelope Glycoprotein Structure: Nailing Down a Moving Target. *Immunol. Rev.* **275**, 21-32 (2017).
11. Burton, D.R. & Hangartner, L. Broadly Neutralizing Antibodies to HIV and Their Role in Vaccine Design. *Annu. Rev. Immunol.* **34**, 635-59 (2016).
12. DeVico, A.L. CD4-induced Epitopes in the HIV Envelope Glycoprotein, gp120. *Curr. HIV Res.* **5**, 561-71 (2007).
13. Burton, D.R. et al. HIV Vaccine Design and the Neutralizing Antibody Problem. *Nat. Immunol.* **5**, 233-6 (2004).

14. Thali, M. et al. Characterization of Conserved Human Immunodeficiency Virus Type 1 gp120 Neutralization Epitopes Exposed Upon gp120-CD4 Binding. *J. Virol* **67**, 3978-88 (1993).
15. Xiang, S.H., Doka, N., Choudhary, R.K., Sodroski, J. & Robinson, J.E. Characterization of CD4-induced Epitopes on the HIV Type 1 gp120 Envelope Glycoprotein Recognized by Neutralizing Human Monoclonal Antibodies. *AIDS Res. Hum. Retroviruses* **18**, 1207-17 (2002).
16. Decker, J.M. et al. Antigenic Conservation and Immunogenicity of the HIV Coreceptor Binding Site. *J. Exp. Med.* **201**, 1407-19 (2005).
17. Labrijn, A.F. et al. Access of Antibody Molecules to the Conserved Coreceptor Binding Site on Glycoprotein gp120 is Sterically Restricted on Primary Human Immunodeficiency Virus Type 1. *J. Virol.* **77**, 10557-65 (2003).
18. Kwong, P.D. et al. Structure of an HIV gp120 Envelope Glycoprotein in Complex with the CD4 Receptor and a Neutralizing Human Antibody. *Nature* **393**, 648-59 (1998).
19. Shaik, M.M. et al. Structural Basis of Coreceptor Recognition by HIV-1 Envelope Spike. *Nature* **565**, 318-323 (2019).
20. Farzan, M. et al. Tyrosine Sulfation of the Amino Terminus of CCR5 Facilitates HIV-1 Entry. *Cell* **96**, 667-76 (1999).
21. Xiang, S.H. et al. Epitope Mapping and Characterization of a Novel CD4-induced Human Monoclonal Antibody Capable of Neutralizing Primary HIV-1 Strains. *Virology* **315**, 124-134 (2003).
22. Huang, C.C. et al. Structural Basis of Tyrosine Sulfation and VH-gene Usage in Antibodies that Recognize the HIV Type 1 Coreceptor-binding Site on gp120. *Proc. Natl. Acad. Sci. U S A* **101**, 2706-11 (2004).
23. Choe, H. et al. Tyrosine Sulfation of Human Antibodies Contributes to Recognition of the CCR5 Binding Region of HIV-1 gp120. *Cell* **114**, 161-70 (2003).
24. Diskin, R., Marcovecchio, P.M. & Bjorkman, P.J. Structure of a Clade C HIV-1 gp120 Bound to CD4 and CD4-induced Antibody Reveals Anti-CD4 Polyreactivity. *Nat. Struct. Mol. Biol.* **17**, 608-13 (2010).

25. Huang, C.C. et al. Structures of the CCR5 N-Terminus and of a Tyrosine-sulfated Antibody with HIV-1 gp120 and CD4. *Science* **317**, 1930-4 (2007).
26. Scharf, L. et al. Broadly Neutralizing Antibody 8ANC195 Recognizes Closed and Open States of HIV-1 Env. *Cell* **162**, 1379-90 (2015).
27. Gardner, M.R. et al. AAV-expressed eCD4-Ig Provides Durable Protection from Multiple SHIV Challenges. *Nature* **519**, 87-91 (2015).
28. Cormier, E.G. et al. Specific Interaction of CCR5 Amino-terminal Domain Peptides Containing Sulfotyrosines with HIV-1 Envelope Glycoprotein gp120. *Proc. Natl. Acad. Sci. U S A* **97**, 5762-7 (2000).
29. Lee, J.H., Ozorowski, G. & Ward, A.B. Cryo-EM Structure of a Native, Fully Glycosylated, Cleaved HIV-1 Envelope Trimer. *Science* **351**, 1043-8 (2016).
30. Kong, R. et al. Fusion Peptide of HIV-1 as a Site of Vulnerability to Neutralizing Antibody. *Science* **352**, 828-33 (2016).
31. Kumar, S. et al. Capturing the Inherent Structural Dynamics of the HIV-1 Envelope Glycoprotein Fusion Peptide. *Nat. Commun.* **10**, 763 (2019).
32. Dingens, A.S. et al. Complete Functional Mapping of Infection- and Vaccine-elicited Antibodies Against the Fusion Peptide of HIV. *PLoS Pathog.* **14**, e1007159 (2018).
33. Chan, D.C., Fass, D., Berger, J.M. & Kim, P.S. Core Structure of gp41 from The HIV Envelope Glycoprotein. *Cell* **89**, 263-73 (1997).
34. Weissenhorn, W., Dessen, A., Harrison, S.C., Skehel, J.J. & Wiley, D.C. Atomic Structure of the Ectodomain from HIV-1 gp41. *Nature* **387**, 426-30 (1997).
35. Dorfman, T., Moore, M.J., Guth, A.C., Choe, H. & Farzan, M. A Tyrosine-sulfated Peptide Derived from the Heavy-chain CDR3 Region of an HIV-1-neutralizing Antibody Binds gp120 and Inhibits HIV-1 Infection. *J. Biol. Chem.* **281**, 28529-35 (2006).
36. Fellingner, C.H. et al. eCD4-Ig Limits HIV-1 Escape More Effectively than CD4-Ig or a Broadly Neutralizing Antibody. *J. Virol.* (2019).
37. Zheng, S.Q. et al. MotionCor2: Anisotropic Correction of Beam-induced Motion for Improved Cryo-electron Microscopy. *Nat. Methods* **14**, 331-332 (2017).

38. Zhang, K. Gctf: Real-time CTF Determination and Correction. *J. Struct. Biol.* **193**, 1-12 (2016).
39. Zivanov, J. et al. New Tools for Automated High-resolution Cryo-EM Structure Determination in RELION-3. *Elife* **7**(2018).
40. Scheres, S.H. RELION: implementation of a Bayesian approach to cryo-EM structure determination. *J. Struct. Biol.* **180**, 519-30 (2012).
41. Scheres, S.H. & Chen, S. Prevention of Overfitting in Cryo-EM Structure Determination. *Nat. Methods* **9**, 853-4 (2012).
42. Emsley, P., Lohkamp, B., Scott, W.G. & Cowtan, K. Features and Development of Coot. *Acta. Crystallogr. D Biol. Crystallogr.* **66**, 486-501 (2010).
43. Adams, P.D. et al. PHENIX: A Comprehensive Python-based System for Macromolecular Structure Solution. *Acta. Crystallogr. D Biol. Crystallogr.* **66**, 213-21 (2010).
44. Afonine, P.V. et al. Real-space Refinement in PHENIX for Cryo-EM and Crystallography. *Acta. Crystallogr. D Struct. Biol.* **74**, 531-544 (2018).
45. Krissinel, E. & Henrick, K. Inference of Macromolecular Assemblies from Crystalline State. *J Mol Biol* **372**, 774-97 (2007).
46. Dolinsky, T.J. et al. PDB2PQR: Expanding and Upgrading Automated Preparation of Biomolecular Structures for Molecular Simulations. *Nucleic Acids Res.* **35**, W522-5 (2007).
47. Baker, N.A., Sept, D., Joseph, S., Holst, M.J. & McCammon, J.A. Electrostatics of Nanosystems: Application to Microtubules and the Ribosome. *Proc. Natl. Acad. Sci.* **98**, 10037-41 (2001).

*Chapter 3***Neutralizing antibodies induced in immunized macaques recognize the CD4-binding site on an occluded-open HIV-1 envelope trimer****Abstract**

Broadly-neutralizing antibodies (bNAbs) against HIV-1 Env can protect from infection. We characterize Ab1303 and Ab1573, heterologously-neutralizing CD4-binding site (CD4bs) antibodies, isolated from sequentially-immunized macaques. Ab1303/Ab1573 binding is observed only when Env trimers are not constrained in the closed, prefusion conformation. Fab-Env cryo-EM structures show that both antibodies recognize the CD4bs on Env trimer with an 'occluded-open' conformation between closed, as targeted by bNAbs, and fully-open, as recognized by CD4. The occluded-open Env trimer conformation includes outwardly-rotated gp120 subunits, but unlike CD4-bound Envs, does not exhibit V1V2 displacement, 4-stranded gp120 bridging sheet, or co-receptor binding site exposure. Inter-protomer distances within trimers measured by double electron-electron resonance spectroscopy suggest an equilibrium between occluded-open and closed Env conformations, consistent with Ab1303/Ab1573 binding stabilizing an existing conformation. Studies of Ab1303/Ab1573 demonstrate that CD4bs neutralizing antibodies that bind open Env trimers can be raised by immunization, thereby informing immunogen design and antibody therapeutic efforts.

## Introduction

Human immunodeficiency virus-1 (HIV-1) is the causative agent behind the ongoing AIDS pandemic affecting millions of people worldwide. Although HIV-1 infection induces neutralizing antibodies against the viral envelope glycoprotein trimer (Env), the large number of viral strains in a single infected person and across the infected population means that commonly-produced strain-specific antibodies do not clear the infection<sup>1</sup>. However, a fraction of infected patients produce broadly neutralizing antibodies (bNAbs) that could provide protection from HIV-1 infection if an efficient means of eliciting such antibodies is developed<sup>2,3</sup>. However, vaccines to elicit such bNAbs are challenging to develop because heavily somatically mutated bNAbs usually arise only after years of virus-antibody co-evolution in their hosts<sup>2,3</sup>.

Neutralizing antibodies against HIV-1 are exclusively directed against Env, the only viral protein on the surface of the virion<sup>4,5</sup>. HIV-1 Env is a homotrimer of gp120-gp41 heterodimers that mediates fusion of the host and viral membrane bilayers to allow entry of viral RNA into the host cell cytoplasm<sup>6</sup>. Fusion is initiated when the Env gp120 subunit contacts the host receptor CD4, resulting in conformational changes that reveal the binding site for a host coreceptor in the chemokine receptor family<sup>7,8</sup>. Coreceptor binding to gp120 results in further conformational changes including insertion of the gp41 fusion peptide into the host cell membrane<sup>6</sup>.

Conformations of trimeric HIV-1 Envs have been investigated using single-particle cryo-EM to derive structures of soluble, native-like Env trimers lacking membrane and cytoplasmic domains and including stabilizing mutations (SOSIP.664 Envs)<sup>9</sup>. Such structures defined a closed, pre-fusion Env state in which the coreceptor binding site on gp120 variable loop 3 (V3) is shielded by the gp120 V1V2 loops<sup>10</sup>, and open CD4-bound Env trimer states with outwardly rotated gp120 subunits and V1V2 loops displaced by ~40Å to expose the V3 loops and coreceptor binding site<sup>11-14</sup>.

Structurally-characterized anti-HIV-1 bNAbs recognize the closed, pre-fusion Env state<sup>10</sup> with the exception of one of the first HIV-1 bNAbs to be discovered: an antibody called b12

that was isolated from a phage display screen<sup>15</sup>. Like more recently identified bNAbs<sup>16,17</sup>, b12 binds to an epitope overlapping with the CD4-binding site (CD4bs) on gp120<sup>18</sup>. However, the Env trimer state recognized by b12 represents an ‘occluded-open’ conformation in which the gp120 subunits are rotated out from the central trimer axis, but V1V2 is not displaced to the sides of the Env trimer<sup>11,12,14</sup>.

As compared with a library screen that would not preserve correct heavy chain-light chain pairing, Ab1303 and Ab1573 were isolated by single cell cloning from SOSIP-binding B cells derived from sequentially-immunized non-human primates (NHPs)<sup>19</sup>. Both antibodies exhibited broad, but weak, heterologous neutralization and were mapped by competition ELISA as recognizing the CD4bs<sup>19</sup>. Here we show that, in common with b12 but not with other CD4bs bNAbs, neither antibody binds Env trimer when it is locked into the closed, prefusion state that is recognized by other CD4bs bNAbs. To elucidate the conformational state of Env recognized by these monoclonal antibodies (mAbs), we solved single-particle cryo-EM structures of a SOSIP Env trimer complexed with either Ab1303 or Ab1573 Fabs. The structures revealed that these mAbs recognized Env trimers with gp120 subunits that had rotated outwards to create an occluded-open trimer conformation that differed from the closed, prefusion Env conformation and from the open conformation of CD4-bound Env trimers<sup>11-14</sup>. To further investigate the occluded-open Env trimer conformation, we used double electron-electron resonance (DEER) spectroscopy to determine if this conformation was detectable in a solution of unliganded HIV-1 Env trimers. By measuring inter-protomer distances between V1V2 loops in the presence and absence of Ab1303 and Ab1573, we found evidence for the conformation recognized by these antibodies in unliganded trimers, suggesting that Ab1303 or Ab1573 binding stabilized a pre-existing Env conformation.

In this work, in contrast to previous structures of CD4bs bNAb-closed Env trimer complexes<sup>10</sup> and CD4-bound open Env conformation structures<sup>11-14</sup>, the Ab1303 and Ab1573 structures revealed a new mode of naturally-induced CD4bs antibody-Env interaction. Furthermore, when combined with DEER spectroscopy data, these structures define Env trimer conformational state intermediates between the closed and CD4-bound open conformations. Although Ab1303 and Ab 1573 are not as broad or potent as CD4bs

bNAbs isolated from infected human donors, discovery of the Env structure recognized by these mAbs reveals an unanticipated target that could be exploited for immunogen design.

## Results

### **Heterologously neutralizing mAbs Ab1303 and Ab1573 were elicited in NHPs after sequential immunization with designed immunogens**

The V3-glycan patch immunogen RC1 was modified from the V3 immunogen 11MUTB<sup>20</sup> by mutating a potential *N*-linked glycan site (PNGS) to remove the *N*-glycan attached to Asn156<sub>gp120</sub><sup>21</sup>. RC1 and 11MUTB were both derived from the clade A BG505 SOSIP.664 native-like Env trimer<sup>9</sup>. We constructed RC1-4fill and 11MUTB-4fill by modifying RC1 and 11MUTB, respectively, to insert PNGSs to add glycans to residues 230<sub>gp120</sub>, 241<sub>gp120</sub>, 289<sub>gp120</sub>, and 344<sub>gp120</sub> to reduce antibody responses to off-target epitopes<sup>22-24</sup>. Immunogens were multimerized on VLPs using the SpyTag-SpyCatcher system<sup>25,26</sup> to enhance avidity effects and limit antibody access to the Env trimer base. The mAbs described here were isolated from NHPs immunized sequentially as shown in Supplementary Fig.1a. As described elsewhere<sup>19</sup>, we obtained weak heterologously neutralizing antisera from the sequentially-immunized NHPs, and mAb sequences were generated by single cell cloning from B cells that were captured as described using BG505 and B41 SOSIP baits<sup>27</sup>. Here we investigated Ab1303 and Ab1573, which unexpectedly recognized the CD4bs rather than the V3-glycan patch that was targeted in the sequential immunization scheme.

Ab1303 sequences were derived from rhesus macaque germline V gene segments IGHV4-160\*01 and IGLV4-97\*01 gene segments for heavy and light chains, respectively, and exhibited 8.3% and 8% amino acid changes due to somatic hypermutations, respectively (Supplementary Fig.1b). Ab1573 sequences were derived from IGHV1-198\*02 and IGLV1-64\*01 gene segments and contained 7.3% and 10.5% somatic hypermutation changes, respectively (Supplementary Fig.1b). Neutralizing activities of the two antibodies were reported elsewhere<sup>19</sup>. The HIV-1 strains chosen for neutralization measurements were derived from the 12-strain global panel of HIV-1 reference strains<sup>28</sup> plus seven other HIV-1 strains including BG505, from which the RC1-4fill and 11MUT-4fill immunogens were derived. We found that Ab1303 neutralized 12 of the 19 cross-clade strain panel with IC<sub>50</sub> values <100 µg/mL, whereas Ab1573 neutralized five strains in the panel with IC<sub>50</sub> values <100 µg/mL<sup>19</sup>. Although the neutralization potencies were generally weak, both mAbs

exhibited heterologous neutralization, with Ab1303 neutralizing >60% of the viruses in the cross-clade panel when evaluated at high concentrations.

### **Ab1303/Ab1573 bound a non-closed Env trimer conformation with varying stoichiometries**

To verify that Ab1303 and Ab1573 recognized the CD4bs on Env trimer, we repeated competition ELISA experiments conducted with RC1 trimer<sup>19</sup>, this time using BG505 trimer (Fig. 1a). We first immobilized randomly-biotinylated BG505 Env trimers on streptavidin plates and then added antibody Fabs targeting either the CD4bs (3BNC117)<sup>16</sup>, the V3-glycan patch (10-1074)<sup>29</sup>, V1V2 (PG16)<sup>30</sup>, or the fusion peptide (VRC34)<sup>31</sup>. Subsequently, either Ab1303 or Ab1573 IgGs were added, the plates were washed, and the degree of binding was detected. The binding of Ab1303 IgG was essentially unaffected in the Env trimer samples that were complexed with 10-1074, PG16, or VRC34 compared to the control with no competitor (Ab1303 IgG alone), but its binding to BG505 Env was reduced in the presence of 3BNC117 Fab (Fig. 1a). Similar results were found for Ab1573, although the presence of PG16 and VRC34 Fabs also reduced the binding somewhat (Fig. 1a). From these results, we concluded that both antibodies recognized the CD4bs on BG505 SOSIP. CD4bs bNAbs such as VRC01, 3BNC117, and IOMA bind closed, prefusion state Env trimers<sup>32-34</sup>. An exception to this finding for CD4bs antibodies is b12, a more weakly neutralizing antibody selected from a phage display derived from antibody genes isolated from an HIV-positive individual bone marrow<sup>15</sup>. Unlike all other human CD4bs bNAbs characterized to date, b12 binds to an “occluded open” Env trimer conformation in which gp120 subunits are rotated outwards from the central trimer axis but the V1V2 loops are not displaced from their positions on top of the gp120 subunits<sup>11</sup>.

To determine if Ab1303 and Ab1573 recognize closed Env trimers, we assessed their ability to bind Env trimer captured with PGT145, a V1V2 bNAb that recognizes a quaternary epitope at the trimer apex<sup>33</sup>. Unlike other V1V2 bNAbs such as PG16 that can recognize both closed and open Env trimers<sup>35</sup>, PGT145 locks Envs into a closed, prefusion state<sup>33</sup>. In this experiment, we captured BG505 with PGT145 IgG on an ELISA plate and compared binding of Ab1303, Ab1573, a conventional CD4bs bNAb that recognizes closed Env trimer

(IOMA)<sup>32</sup>, and b12 Fab that binds to an “occluded open” trimer (Fig. 1b). IOMA showed binding to BG505 captured by PGT145, consistent with IOMA-BG505 complex structure with a closed conformation trimer<sup>32</sup> (Fig. 1b). By contrast, b12 did not bind to BG505 that was captured by PGT145, as the b12 epitope is occluded in the closed Env conformation<sup>11</sup> (Fig. 1b). Similar to the results for b12, Ab1303 and Ab1573 did not bind BG505 that was captured by PGT145, suggesting that the closed Env trimer occludes epitopes for Ab1303 and Ab1573 (Fig. 1b).

To further characterized the interactions of Ab1303 and Ab1573 with Env trimer, we performed size-exclusion chromatography coupled with multi-angle light scattering (SEC-MALS) to determine the absolute molecular masses of the complexes and therefore the number of Fabs bound per trimer. Complexes formed by incubating mAb Fabs with BG505 trimer at various temperatures were analyzed by SEC-MALS. Compared to BG505 trimer alone (~310 kDa apparent mass including glycans), incubation of Ab1303 Fab with trimer at 22°C for one hour resulted in a complex with an average molecular mass of 370 kDa, equivalent to ~1.1 Fabs per trimer, whereas incubation at 37°C for one hour produced complexes with an average molecular mass of 443 kDa, corresponding to ~3 Fabs per trimer (Fig. 1c). In the case of Ab1573 complexes, one-hour incubations at 22°C and 37°C produced up to ~1 and ~2.6 copies of Fabs per trimer on average (Fig. 1c). Notably, peaks corresponding to the Ab1303 Fab-BG505 complex from the 22°C incubation condition and the Ab1573 Fab-BG505 complexes from both temperature conditions were broad, consistent with a mixture of sub-stoichiometric populations being present under these conditions. These observations suggest that physiological temperature could result in the antibody binding sites on Env being more accessible, facilitating binding of Ab1303 and Ab1573 by more frequent Env transitions between different conformational states at higher temperature.

### **Ab1303 and Ab1573 occlude the CD4bs on gp120**

To further explore the interactions of Ab1303 and Ab1573 with Env trimer, we solved 1.51Å and 2.24Å crystal structures of unbound Ab1303 and Ab1573 Fabs (Supplementary Table 1; Supplementary Fig.1c) and single-particle cryo-EM structures of BG505 SOSIP.664

complexed with Ab1303 and Ab1573 to resolutions of 4.0Å and 4.1Å, respectively (Fig. 2a,b, Supplementary Fig.2, and Supplementary Table 2). Prior to cryo-EM data collection, the Fabs were incubated with BG505 at 37°C for two hours to achieve an approximate 3:1 Fab to BG505 trimer stoichiometry.

We first compared the structures of the unbound Fabs to their structures when bound to Env trimer. For both antibodies, there were no major structural changes between their free (solved by X-ray crystallography) and bound (solved by cryo-EM) forms: Root mean square deviations, rmsds, for superimposition of free and bound Ab1303 V<sub>H</sub> and V<sub>L</sub> (235 Ca atoms) were 0.72Å, and 0.89Å for superimposition of free and bound Ab1573 V<sub>H</sub> and V<sub>L</sub> (231 Ca atoms), with minimal differences in the complementarity determining region (CDR) loops (Supplementary Fig.1d). Thus, Ab1303 and Ab1573 bound their Env antigen targets using preformed antibody combining sites, rather than undergoing structural rearrangements to accommodate their targets.

The cryo-EM structures of both Fab complexes with Env trimer showed three bound Fabs that interacted with the CD4bs of each gp120 protomer (Fig. 2a,b; Fig. 3). The binding sites for Ab1303 and Ab1573 on gp120 were located in an area that is surrounded by three *N*-glycan patches: the Asn363<sub>gp120</sub>/Asn386<sub>gp120</sub> glycans located near the base of V3, the Asn197<sub>gp120</sub> glycan in the V1V2 region, and the Asn276<sub>gp120</sub> glycan near the bottom of gp120 (Fig. 2a,b). The epitope of Ab1303 comprised 1430Å<sup>2</sup> of buried surface area (BSA) on gp120, of which 879Å<sup>2</sup> were buried by the heavy chain and 551Å<sup>2</sup> were buried by the light chain (Fig. 3a,g). The heavy chain complementarity determining region 3 (CDRH3) of Ab1303 makes extensive contacts with gp120, including an antibody residue Arg100<sub>B<sub>HC</sub></sub> that is stabilized by neighboring Trp100<sub>A<sub>HC</sub></sub> through cation-π interaction, contributes a salt bridge with gp120 residue Asp457<sub>gp120</sub> and hydrogen bonds with the Arg456<sub>gp120</sub> carbonyl group and with the Ser365<sub>gp120</sub> sidechain, forming a stable interaction network (Fig. 3b). Residue Tyr100<sub>E<sub>HC</sub></sub> of CDRH3 hydrogen bonded with Gln428<sub>gp120</sub> and Asp474<sub>gp120</sub> (Fig. 3b). Residue D368<sub>gp120</sub> in the CD4 binding loop, which plays an important role in CD4 binding<sup>36</sup>, was positioned in proximity to the Ab1303 light chain and excluded from solvent by adjacent CDRL3 residues such as Trp91<sub>LC</sub>. In the case of Ab1573, 646Å<sup>2</sup> of surface area

was buried by  $V_H$  and  $762\text{\AA}^2$  buried by  $V_L$ , composing a total of  $1408\text{\AA}^2$  of BSA on gp120 (Fig. 3c,g). Two salt bridges were found at the Ab1573-gp120 interface: between CDRH3 residue Asp97<sub>HC</sub> and Arg476<sub>gp120</sub>, and between CDRH1 residue Arg31<sub>HC</sub> and Asp113<sub>gp120</sub> (Fig. 3d). Compared with the Ab1573 and Ab1573 footprints on gp120, contacts by b12 are dominated by its  $V_H$  domain (Fig. 3e), with no contacts by  $V_L$  except for a small region of BSA ( $340\text{\AA}^2$ ) on V1V2 (Fig. 3f,g). A large portion of CD4 binding loop including residue Asp368<sub>gp120</sub> was positioned between Ab1573 CDRH3 and CDRL3.

In addition to their protein epitopes, Ab1303 and Ab1573 also contacted *N*-linked glycans on gp120. The light chains of both Fabs were adjacent to the *N*-glycans attached to Asn197<sub>gp120</sub> and Asn276<sub>gp120</sub>. When compared to an Env structure that does not have an antibody bound in this vicinity (PDB 5FYL), the Asn197<sub>gp120</sub> side chain was rotated  $\sim 180^\circ$  in the Ab1303- and Ab1573-bound structures, and the Asn197<sub>gp120</sub> glycans underwent large displacements. In addition, the Asn276<sub>gp120</sub> glycan was shifted slightly to facilitate Fab binding (Supplementary Fig. 3).

To further characterize the antibody epitope, we compared our structures with those of other CD4bs-Env complexes. The  $V_H$  domains of Ab1303 and Ab1573 were positioned close to the gp120 inner domain, which is not fully exposed in the closed Env conformation, whereas the  $V_L$  domains were sandwiched between Asn363<sub>gp120</sub>/Asn386<sub>gp120</sub> and Asn276<sub>gp120</sub> glycans (Fig. 4). While the b12  $V_H$  is positioned similarly on gp120 as the  $V_H$  domains of Ab1303 and Ab1573 (Fig. 3a,c,e), the b12  $V_L$  is closer to the gp120 V1V2, which constitutes the only contacts made by the b12  $V_L$  with gp120 (Fig. 3e-g). By contrast, other CD4bs bNAbs  $V_HV_L$  domains share similar binding poses; they are located further from the gp120 inner domain and are lined up almost parallel to the trimer three-fold axis, with  $V_H$  near the Asn363<sub>gp120</sub>/Asn386<sub>gp120</sub> and Asn197<sub>gp120</sub> glycans and  $V_L$  adjacent to the Asn276<sub>gp120</sub> glycan (Fig. 4), and to accommodate such poses, Asn276 glycans need to be displaced further away by antibodies light chains.

**Ab1303 and Ab1503 bind an occluded-open state of Env trimer**

The trimers in the Ab1303-Env and Ab1573-Env complexes differed in conformation from the closed, prefusion Env conformation, each exhibiting a more open state that exposed portions of the gp120 that were otherwise buried (Fig. 5a,b). To characterize these differences, we mapped the trimer epitope regions from each antibody-bound open conformation onto a closed, prefusion trimer Env structure. For both complexes, a portion of the epitope was solvent inaccessible in the closed trimer state but was exposed in the antibody-bound open state (Fig. 5a,b; red highlighted regions). The Ab1303 contacts that are buried in a closed trimer were contacted exclusively on the occluded, open trimer by its  $V_H$  domain (Fig. 5a), which buried  $286\text{\AA}^2$  of gp120 surface area that would be inaccessible on a closed trimer. The contact residues buried in the closed Env state by Ab1573 also involved only its  $V_H$  domain (Fig. 5b), burying a discontinuous  $137\text{\AA}^2$  of gp120 surface area. In addition, docking of Ab1303 (Fig. 5c) or Ab1573 (Fig. 5d) onto a closed trimer structure results in steric clashes. These results are consistent with the ELISA demonstration that Ab1303 and Ab1573 did not bind the closed, prefusion Env trimers (Fig. 1b).

To compare and quantify outward displacements of gp120 protomers in different Env states, we measured inter-protomer distances of selected residues located in the CD4bs, V1V2 base, and V3 base of a closed BG505 Env trimer with analogous residues in BG505 trimers bound to Ab1303 or Ab1573 (Fig. 5e). Inter-protomer distances were increased in the Ab1303- and Ab1573-bound trimers compared with the closed trimer, providing a quantitative measurement of openness. In addition, differences in the three inter-protomer distances for each measurement within the Ab1303- and Ab1573-bound Envs demonstrated trimer asymmetry compared with the symmetric closed trimer conformation. Comparisons with a structure of B41 SOSIP bound to b12 Fab<sup>11</sup> showed that the Ab1303- and Ab1573-bound trimers resembled the b12-bound Env state more than the closed state, although the b12-bound trimer structure was three-fold symmetric (Fig. 5e). Finally, measurements for all four of these trimers differed from the CD4-bound open state exemplified by the structure of a CD4-bound asymmetrically open BG505 trimer<sup>14</sup> and a CD4-bound symmetrically open B41 trimer<sup>11</sup> (Fig. 5e).

Despite Env trimer opening, the gp120 V1V2 and V3 regions in the Ab1303-BG505 and Ab1573-BG505 structures exhibited only minor local structural rearrangements in which the gp120s were displaced as nearly rigid bodies from their central positions in the closed trimer structure (Fig. 6a; Movie S1). Thus, most of each gp120 subunit, including the V1V2 and V3 regions, remained unchanged between the closed Env conformation and the open Ab1303- and Ab1573-bound Env trimers (Fig. 6a, left and middle); the rmsd for superimposition of 347 gp120 Ca atoms (Gly41<sub>gp120</sub> to Pro493<sub>gp120</sub> excluding disordered residues) was  $\sim 1.3\text{\AA}$ . By contrast, when bound to CD4, Env trimer opening did not result from rigid body rotations of gp120; instead the V1V2 loops were displaced from apex of each gp120 apex to the sides of the Env trimer to expose the coreceptor-binding site on V3, and portions of V1V2 and V3 were disordered<sup>11,12,14</sup> (Fig. 6a, right). In addition, the gp120  $\beta 2$  and  $\beta 3$  strands at the beginning and end of the V1V2 loop switched positions with respect to their locations in closed, prefusion Env trimers to form a four-stranded anti-parallel  $\beta$ -sheet (4-stranded bridging sheet) (Fig. 6b, right) instead of the 3-stranded sheet in closed Env structures (Fig. 6b; left) (Movie S1). Notably, the ‘occluded open’ Env trimer conformations observed upon binding of Ab1303, Ab1573, or b12 included the 3-stranded sheet found in the closed, prefusion Env trimer rather than the 4-stranded bridging sheet in open, CD4-bound Env trimers (Fig. 6b; middle; Movie S1).

Local structural rearrangements in Asp57<sub>gp120</sub> - Ala73<sub>gp120</sub>, residues that are immediately N-terminal to the gp120  $\alpha_0$  region (residues Lys65<sub>gp120</sub> - Ala73<sub>gp120</sub>), provided further evidence that the Ab1303- and Ab1573-bound trimers adopted a state distinct from the closed state recognized by CD4bs bNAbs: in the closed state, residues Asp57<sub>gp120</sub> - Glu62<sub>gp120</sub> formed a  $\beta$ -strand and a short loop (Fig. 6c, left), whereas they formed a two-turn  $\alpha$ -helix and the  $\alpha_0$  residues remained as a loop in Ab1303/Ab1573-bound open conformation (Fig. 6c, middle). By contrast, in the CD4-bound fully-open state, the Asp57<sub>gp120</sub> - Glu62<sub>gp120</sub> segment formed a  $\beta$ -strand and short loop; whereas the  $\alpha_0$  segment (residues Lys65<sub>gp120</sub> - Ala73<sub>gp120</sub>), which was a loop in both the closed and the Ab1303/Ab1573-bound open states, was an  $\alpha$ -helix in the CD4-bound fully-open state (Fig. 6c, right). The structural rearrangement of  $\alpha_0$  was accompanied by protein sidechain repositioning: in the closed and Ab1303/1573-

bound open states, the Trp69<sub>gp120</sub> sidechain was sandwiched between the  $\alpha_1$  helix and  $\beta_4$  strand and His66<sub>gp120</sub> was solvent exposed, whereas in the CD4-bound open state, the Trp69<sub>gp120</sub> sidechain was rearranged such that the His66<sub>gp120</sub> sidechain occupied a nearly analogous position (Fig. 6c).

The conformation of the C-terminal portion of gp41 heptad repeat segment 1 (HR1<sub>c</sub>) also exhibited changes between the closed, Ab1303- and Ab1573-bound open, and CD4-bound open Env trimer states. In closed prefusion Env trimers, residues N-terminal to Thr569<sub>gp41</sub> adopted a loop structure (Fig. 6c, left). Outward rotations of the gp120 subunits in the Ab1303-/Ab1573-bound open Env created space for the gp41 HR1<sub>c</sub> to extend its three-helix coiled-coil structure, lengthening the  $\alpha$ -helices by 1.5 turns (Fig. 6c, middle). Additional outward gp120 rotations combined with V1V2 and V3 displacements created more space for the central  $\alpha$ -helices in the CD4-bound fully-open state; thus gp41 residues that were disordered in the closed and occluded open trimer states extended the HR1<sub>c</sub> N-terminal helical structure by another helical turn, with ordered residues terminating at around residue Pro559<sub>gp41</sub><sup>11-14</sup>, the site of the Ile-to-Pro stabilizing mutation in SOSIPs<sup>9</sup> (Fig. 6c, right). Thus, the Ab1303- and Ab1573-bound Env structures revealed an occluded-open trimer state distinct from both the closed, prefusion and the CD4-bound fully-open trimer conformations.

### **DEER suggests that the unliganded Env trimers contain both occluded-open and other Env conformations**

To evaluate the conformational flexibility of ligand-free and antibody-bound trimer in solution, we used double electron-electron resonance (DEER) spectroscopy to probe interprotomer distances between V1V2 regions in different Env trimer states. DEER can be used to derive distances between electron spin pairs ranging from 17-80Å by detecting their respective dipolar interactions<sup>37</sup>. By recording a snapshot of the equilibrium distance distributions of flash-frozen samples, DEER data report molecular motions in solution to provide insight into conformational heterogeneity. We previously used DEER to evaluate spin-labeled BG505 and B41 SOSIPs in the presence and absence of antibodies, CD4, and a small molecule ligand, finding a relatively homogeneous trimer apex, more

conformational heterogeneity at the trimer base, and inter-protomer distances between spin labels that were consistent with bNAb-bound closed Env structures and CD4-bound open Env structures<sup>38</sup>.

In the present studies, we introduced a free cysteine into a gp120-gp41 protomer of the BG505 SOSIP in order to use site-directed spin labeling<sup>39</sup> to covalently attach a nitroxide spin label with a V1 side chain<sup>40</sup>. This approach results in three spin labels on each Env, which form a triangle of spin labels, either equilateral, isosceles, or scalene depending on whether the labeled Env adopts a three-fold symmetric or asymmetric conformation. Thus, DEER measurements in a conformationally-rigid Env trimer would report one distance in a symmetric Env and two or more distances in asymmetric Envs. The most probable distance in a DEER distribution is defined by the largest peak area and represents the dominant structural state in a population of states. The presence of multiple peaks in a DEER distribution indicates conformational heterogeneity, with individual peak widths related to the flexibility of that conformation and of the attached spin label<sup>39,41</sup>. In general, peaks representing 17–65Å distances can be assigned with confidence, whereas distances > 65Å are detected with less accuracy<sup>37</sup>.

To choose a site for spin labeling, we used the Ab1303- and Ab1573-Env structures to identify solvent-exposed residues, which when spin-labeled, would result in distinguishable inter-protomer distances in different Env conformations. We also restricted candidate sites to residues located in a  $\beta$ -sheet to minimize potential flexibility of the attached spin label and excluded residues that were involved in interactions with other residues to avoid disrupting protein folding. The optimal candidate residue, V1V2 residue Ser174<sub>gp120</sub>, fulfilled these criteria, with inter-protomer C $\alpha$ -C $\alpha$  distances measured as 38Å in a closed Env structure, ranging from 40Å–60Å in the asymmetric Ab1303- and Ab1573-bound Env structures, 67Å in a b12-bound Env, and ~157Å (far out of DEER range) in a CD4-bound open Env (Fig. 7a). Although the V1 spin label is small (about the size of an amino acid) and contributes limited width to DEER distance distributions<sup>42</sup>, distances between spin label side chains measured by DEER only rarely equal the C $\alpha$ -C $\alpha$  inter-protomer distance since the radical center is found on the nitroxide ring, not the peptide linkage. As such, DEER results can be complicated by conformational heterogeneity and

flexibility intrinsic to the protein studied. In addition, previous work to model V1 nitroxide side chain rotamers on BG505 Env DEER target sites suggested that differences in V1 rotamers can contribute to measured DEER distances<sup>38</sup>.

The S174C mutant version of BG505 SOSIP was expressed, purified, and labeled with the V1 side chain. Ab1303 and Ab1573 Fabs were added at a 3-molar excess to V1-labeled BG505, and liganded and unliganded samples were incubated at 37°C for three hours before being flash-frozen in liquid nitrogen for resonance measurements. The DEER spectrum of unliganded BG505 (black trace in Fig. 7b,c) showed a complicated collection of peaks, indicating conformational heterogeneity of the V1V2 region in the vicinity of gp120 residue 174. These results differ from previous DEER experiments from which we derived BG505 V1V2 distances from spectra recorded after incubation at 4°C, which showed a more homogeneous distance distribution with a dominant peak observed at the expected inter-protomer distance<sup>38</sup>. In the present experiments, one of the major peaks, centered at ~38Å, corresponds to the residue 174 inter-protomer distance in a closed BG505 Env structure (Fig. 7b,c; red vertical line). The other major peaks for the unliganded BG505 sample, including major peaks at distances between ~20Å and ~35Å, were not readily interpretable based on closed SOSIP Env structures. However, the presence of the inter-protomer distances other than 38Å suggests that the unliganded BG505 SOSIP trimer can adopt conformational states in addition to the known closed, prefusion conformation. The broad heterogeneity of conformational states seen here may have been induced by incubation at 37°C.

We also collected DEER data for BG505 complexes with Ab1303 and Ab1573 (green and cyan traces in Figures 7B and C, respectively). Some of the short distance peaks, most notably a single major peak at ~24Å, were observed for both antibody-bound Envs (Fig. 7B,C). In addition to this structurally uninterpretable peak, also present in both spectra were peaks at ~43Å and ~55Å, likely corresponding to the structurally-measured inter-protomer distance of 40Å/46Å (measured distance 1 for Ab1303-Env and Ab1573 Env complexes) and a combination of the 53Å/58Å (Ab1303) and 53Å/60Å (Ab1573) distances (measured distances 2 and 3; green vertical lines in Fig. 7b; cyan vertical lines in Fig. 7c). Peaks at or

close to these distances were found in the unliganded BG505 DEER spectrum, suggesting that the conformational states observed for Ab1303/Ab1573-binding Env also exist at a lower population in unliganded BG505. Interestingly, peaks near 67Å – the measured inter-protomer distance for residue 174 in a b12-bound Env trimer – are observed in both the Ab1303-bound and Ab1573-bound Envs (major peak in Ab1303-bound Env spectrum; a minor peak in the Ab1573-bound spectrum), suggesting that binding of these antibodies induced a sub-population of Envs with a b12-bound conformation that was not captured in the cryo-EM structures.

## Discussion

Many HIV-1 vaccine efforts focus on using soluble Env trimers as immunogens to raise bNAbs<sup>43</sup>. Here we characterize Ab1303 and Ab1573, two CD4bs bNAbs raised by sequential immunization in NHPs of SOSIP trimer immunogens attached to VLPs<sup>19</sup>. Unexpectedly, both antibodies bind the CD4bs of an open form of HIV-1 Env trimer rather than the closed, prefusion state typically targeted by bNAbs raised in humans by natural infection<sup>10</sup>. In common with CD4-bound Envs, the trimer conformation recognized by Ab1303 and Ab1573 includes outward rotations of gp120, but the gp120 V1V2 loops are not rearranged to expose the coreceptor binding site on V3; thus, the Env trimer is open but the co-receptor binding site is occluded. The Ab1303/Ab1573-bound occluded-open Env trimer conformation shares structural features with the conformation recognized by b12<sup>11</sup>, an early CD4bs bNAb isolated from a phage display library<sup>15</sup>. Of relevance to immunogen design efforts is whether the occluded-open Env conformation exposes new epitopes that might elicit off-target non-neutralizing antibodies against trimer surfaces that would be buried in closed, prefusion Env trimers. Comparisons of BSAs between closed and occluded-open Env structures show that regions of V1V2 that are inaccessible in closed trimers (purple in Supplementary Fig. 4) might be accessible for antibody binding in the occluded-open Env conformation.

The question of which features of an Env-binding ligand induce an open coreceptor-binding HIV-1 Env conformation is prompted by the existence of two distinct open trimer conformations (Fig. 6a): (i) the CD4-bound open trimer, a coreceptor-binding conformation in which V1V2 relocates to the sides of the Env trimer to expose V3 and form a 4-stranded gp120 bridging  $\beta$ -sheet<sup>11-14</sup>, versus (ii) the occluded-open trimer in which the gp120s rotate outwards, but V1V2 remains “on top” of gp120 to shield the coreceptor binding site. Structures of the b12-Env<sup>11</sup> and the Ab1303/Ab1573-Env complexes reported here demonstrate that Env opening through gp120 rotation is not sufficient to induce the further structural rearrangements associated with CD4 binding (Fig. 6b.c). One difference that distinguishes CD4 from b12, Ab1303, Ab1573 and most other CD4bs bNAbs is that the antibodies lack a counterpart of CD4 residue Phe43, which inserts into the “Phe43” pocket on gp120<sup>44</sup>. We showed that small molecule CD4 mimetic entry inhibitors that insert into

the gp120 Phe43 pocket recognize the CD4-bound open trimer conformation<sup>35</sup>, whereas CD4 mimetics drugs that bind orthogonally to the Phe43 pocket bind closed, prefusion Envs<sup>45</sup>. Interaction with the gp120 Phe43 pocket may be necessary for recognition of the CD4-bound open trimer conformation, but is unlikely to be sufficient since CD4bs bNAb such as N6<sup>46</sup> contain a CD4 Phe43 counterpart within their CDRH2 region, yet bind closed, prefusion Env trimers<sup>47</sup>.

Our findings suggest that portions of the Ab1303 and Ab1573 epitopes on gp120 are buried on a closed, prefusion Env trimer (Fig. 5a) and that there are potential steric clashes between the Fabs and Env when they are docked onto their respective binding sites of closed Env (Fig. 5c,d). This implies that the Env trimer conformation that triggers development of this type of CD4bs bNAb is similar or equivalent to the occluded-open Env conformation described here. Indeed, DEER spectroscopy experiments suggested that a population of unliganded BG505 SOSIP Envs that had been incubated at 37°C adopted a conformation consistent with the occluded-open conformation recognized by Ab1303 and Ab1573 (Fig. 7), therefore this conformation may have been present on at least a subset of the SOSIP-based immunogens used in the sequentially-immunized NHPs from which these antibodies were derived<sup>19</sup>. In addition, the Env trimers of HIV-1 strains that are neutralized by Ab1303 and Ab1573<sup>19</sup> may more readily adopt the occluded-open conformation than Envs in neutralization-resistant strains.

The DEER results, together with the demonstration of temperature-dependent changes in Ab1303 and Ab1573 binding stoichiometry, suggest that physiological temperature facilitates conformational changes in soluble Env trimers that result in the occluded-open state. Our previous DEER studies to probe conformations of Env SOSIPs conducted with 4°C incubations concluded that unliganded SOSIPs showed conformations that were consistent with the closed pre-fusion trimer conformation, with no evidence for the CD4- or b12-bound open states<sup>38</sup>. For example, DEER spectra of the unliganded BG505 SOSIP labeled in V1V2 (residue 173) prepared at 4°C showed a dominant inter-protomer distance signal between 30-40Å, consistent with distances measured for the closed Env conformation<sup>38</sup>. In this study, the comparable unliganded BG505 SOSIP sample labeled in

V1V2 (residue 174) prepared at 37°C reported interspin distances consistent with the Ab1303/Ab1573-bound occluded-open trimer conformation. This suggests that at 37°C, the temperature at which antibodies are generated *in vivo*, Env trimers attached to VLPs can adopt different conformational states between defined closed and open conformations. Whether the occluded-open conformation is present on membrane-bound viral Env trimers remains unknown, but the isolation of the b12 bNAb from a phage display library constructed using bone marrow from an HIV-1–infected individual is consistent with the idea that viruses include Envs with this or a similar conformation. The discovery that the b12-bound conformation of HIV-1 Env trimer is recognized by vaccination-induced neutralizing antibodies suggests the occluded-open conformation of HIV-1 as a potential target for immunogen design.

## Acknowledgements

We thank Anthony P. West (Caltech) for help with analysis of antibody sequences. Cryo-EM was performed in the Beckman Institute Resource Center for Transmission Electron Microscopy at Caltech with assistance from directors A. Malyutin and S. Chen. We thank the Gordon and Betty Moore and Beckman Foundations for gifts to Caltech to support the Molecular Observatory (Dr. Jens Kaiser, director) and the beamline staff at SSRL for data collection assistance. Use of the Stanford Synchrotron Radiation Lightsource, SLAC National Accelerator Laboratory, is supported by the U.S. Department of Energy, Office of Science, Office of Basic Energy Sciences under Contract No. DE-AC02-c76SF00515. The SSRL Structural Molecular Biology Program is supported by the DOE Office of Biological and Environmental Research, and by the National Institutes of Health, National Institute of General Medical Sciences (P41GM103393). The contents of this publication are solely the responsibility of the authors and do not necessarily represent the official views of NIGMS or NIH. We thank Jost Vielmetter and Pauline Hoffman at the Beckman Institute Protein Expression Center at Caltech for protein production, John Moore (Weill Cornell Medical College) for the BG505 stable cell line, Kristie M. Gordon (The Rockefeller University) for assistance with flow cytometry, and Rogier W. Sanders and Marit J. van Gils (Academisch Medisch Centrum Universiteit van Amsterdam) for providing AviTagged and biotinylated BG505 and B41 SOSIP trimers for sorting. This work was supported by the National Institute of Allergy and Infectious Diseases (NIAID) HIVRAD P01 AI100148 (to P.J.B. and M.C.N.), Gates CAVD grant INV-002143 (to P.J.B., M.A.M., and M.C.N.), NIH P50 AI150464 (P.J.B.). M.C.N. is an HHMI Investigator.

## Methods

### Protein expression and purification

The native-like, soluble HIV Env gp140 trimer BG505 SOSIP.664 construct with 'SOS' mutations (A501C<sub>gp120</sub>, T605C<sub>gp41</sub>), the 'IP' mutation (I559P<sub>gp41</sub>), *N*-linked glycosylation site mutation (T332N<sub>gp120</sub>), an enhanced furin protease cleavage site (REKR to RRRRRR), and truncation after the C-terminus of gp41 residue 664<sup>9</sup> was cloned into pTT5 vector (National Research Council of Canada) and expressed in transiently-transfected Expi293F cells. For DEER experiments involving nitroxide spin labeling, BG505 SOSIP.664 was modified to include a free cysteine at residue Ser174<sub>gp120</sub> (S174C) by site-directed mutagenesis as described<sup>38</sup>. BG505 and BG505 S174C mutant Env trimers were purified from transfected cell supernatants as described<sup>48</sup> by 2G12 immunoaffinity and size-exclusion chromatography (SEC) with a HiLoad 16/600 Superdex 200 pg column followed by Superose 6 Increase 10/300 GL column (Cytiva).

The heavy and light chains of 6x-His tagged Ab1303 and Ab1573 Fabs were expressed in transiently-transfected Expi293F cells and purified by Ni-NTA chromatography followed by SEC as described<sup>19</sup>. IgG proteins were expressed in transiently-transfected Expi293F cells and purified by protein A affinity chromatography (Cytiva) followed by SEC as described<sup>21,48</sup>.

### Competition ELISA

BG505 SOSIP trimers were randomly biotinylated using the EZ-Link NHS-PEG4-Biotin kit (Thermo Fisher Scientific) according to the manufacturer's guidelines. Based on the Pierce Biotin Quantitation kit (Thermo Fisher Scientific), the number of biotin molecules per protomer was estimated to be 1.5. Biotinylated BG505 SOSIP trimers were immobilized on Streptavidin-coated 96-well plates (Thermo Fisher Scientific) at a concentration of 5 µg/mL in blocking buffer (1% BSA +1% goat serum in TBS-T) for 1 hour at room temperature (RT). After washing plates once in TBS-T, plates were incubated with a Fab derived from a bNAb that targets the V3 loop (10-1074), the fusion peptide (VRC34), the V1V2 loop (PG16), or the CD4bs (3BNC117), at a concentration of 100 µg/mL in blocking buffer for 1 hour at RT. After washing plates twice in TBS-T, a concentration series of Ab1303 or Ab1573 IgG was

added to the Fab-BG505 complexes with a top concentration of 100 µg/mL in blocking buffer and 4-fold dilutions for 1 hour at 37°C. After washing plates three times in TBS-T, bound IgG was detected using an HRP-conjugated goat anti-human Fc antibody (Southern Biotech) at a dilution of 1:10,000 in blocking buffer for 1 hour at RT. After washing plates three times with TBS-T, 1-Step Ultra TMB substrate (Thermo Fisher Scientific) was added for 5 min and plates were analyzed using a plate reader (BioTek).

### **PGT145 capture ELISA**

This capture ELISA was performed as described previously with minor modifications<sup>9</sup>. Briefly, Corning Costar 96-Well Assay high binding plates (07-200-39) were coated and incubated overnight at 4°C with PGT145 IgG at 5 µg/ml in 0.1 M NaHCO<sub>3</sub> (pH 9.6). Unbound PGT145 IgG was removed, and wells were blocked with 3% BSA in TBS-T (20mM Tris, 150 mM NaCl, 0.1% Tween20) for 1 hour at room temperature. BG505 SOSIP.664 was added at 10 µg/ml and incubated for 1 hour at room temperature, then removed. Serially diluted Fabs in 3% bovine serum albumin in TBS-T were added, incubated at room temperature for 2 hours, then washed three times with TBS-T. Horseradish peroxidase labeled mouse anti-His tag antibody (GenScript: A00186) was added for 30 minutes at 1:1000 dilution, followed by 3 washes with TBS-T. 1-Step™ Ultra TMB-ELISA Substrate Solution (ThermoFisher Scientific: 34029) was added for colorimetric detection. Color development was quenched with 1.0 N HCl, and absorption was measure at 450 nm. Two independent, biological replicates were performed.

### **Multiangle light scattering coupled with size-exclusion chromatography**

Protein mixtures were characterized by size-exclusion chromatography/multiangle light scattering (SEC-MALS) on a Superose 6 10/300 GL column. The column was connected in-line with a light scattering detector (DAWN HELEOS II; Wyatt Technology), a dynamic light-scattering detector (DynaPro Nanostar; Wyatt Technology), and a refractive index detector (Optilab t-rEX; Wyatt Technology). Data were collected at room temperature with a flow rate of 0.5 mL/min. Data were analyzed and molecular mass estimations were generated using ASTRA 6 software (Wyatt Technology).

### **X-ray crystallography**

Crystallization screens for Ab1303 Fab and Ab1573 Fab were performed using the sitting drop vapor diffusion method at room temperature by mixing concentrated Fabs with an equal amount of reservoir solution (Hampton Research) using a TTP Labtech Mosquito automatic microliter pipetting robot. Ab1303 Fab crystals were obtained in 10% (v/v) PEG 200, 0.1M Bis-Tris propane (pH 9.0), and 18% w/v PEG 8,000. Ab1573 Fab crystals were obtained in 0.1M Tris (pH 8.2), 26% (w/v) PEG 4000. Ab1303 Fab crystals were directly looped and cryopreserved in liquid nitrogen, whereas Ab1573 Fab was briefly mixed with 15% glycerol cryoprotectant solution before cryopreservation in liquid nitrogen.

X-ray diffraction data were collected at Stanford Synchrotron Radiation Lightsource (SSRL) beamline 12-1 equipped with an Eiger X 16M pixel detector (Dectris) at a wavelength of 0.97946Å. Recorded data were indexed, integrated, scaled in XDS<sup>49,50</sup> and merged with AIMLESS v0.7.4<sup>51</sup>. The structure of Ab1303 Fab was determined by molecular replacement using PHASER v2.8.2<sup>52</sup> and a search model comprising separate V<sub>H</sub>-V<sub>L</sub> and C<sub>H1</sub>-C<sub>L</sub> domains of a human antibody (PDB 4YK4) with the CDR loops removed. The structure of Ab1573 Fab was determined similarly, except using the Ab1303 Fab as the search model. Coordinates of both Fabs were refined using Phenix v1.19.2<sup>53,54</sup> and iterations of manual building in Coot v0.9<sup>55</sup> (Supplementary Table 2).

### **Cryo-EM sample preparation**

Ab1303-BG505 and Ab1573-BG505 complexes were prepared by incubating purified and concentrated Ab1303 and Ab1573 Fabs with BG505 SOSIP.664 trimer at a molar ratio of (3.6:1 Fab:Env) at 37°C for 2 hours. A final concentration of 0.05% (w/v) fluorinated octylmaltoside (Anatrace) was added to both samples immediately before cryo-freezing. Cryo-EM grids were prepared using a Mark IV Vitrobot (ThermoFisher) operated at 12°C and 95% humidity. 2.6 µL of concentrated sample was applied to 300 mesh Quantifoil R1.2/1.3 grids, blotted for 4 seconds, and grids were then vitrified in liquid ethane. The 12°C temperature of the Vitrobot reduced ice on the grids and prevented fog building up in the chamber. For sample freezing, multiple pairs of tweezers preheated to 37°C before picking up a new grid. The time between loading a sample drop onto a grid and plunge

freezing was only a few seconds. Thus, the 37°C temperature of the Fab:Env incubation was likely to have been maintained during the few seconds in the 12°C Vitrobot.

### **Cryo-EM data collection and processing**

Cryo-grids were loaded onto a 200kV Talos Arctica electron microscope (ThermoFisher) (Ab1303-BG505 complex) or a 300kV Titan Krios electron microscope (ThermoFisher) equipped with a GIF Quantum energy filter (slit width 20 eV) operating at a nominal 105,000x magnification (Ab1573-BG505). For data collection on the Krios, defocus ranges for both Ab1303-BG505 and Ab1573-BG505 datasets were set to 1.4-3.0  $\mu\text{m}$ . Movies were recorded using a 6k x 4k Gatan K3 direct electron detector operating in super-resolution mode with a pixel size of 0.869  $\text{\AA}\cdot\text{pixel}^{-1}$  (Arctica) or 0.855  $\text{\AA}\cdot\text{pixel}^{-1}$  (Krios) and collected using SerialEM v3.7 software. The recorded movies were sectioned into 40 subframes with a total dose of 60  $\text{e}^{-}\cdot\text{\AA}^{-2}$ , generating a dose rate of 1.5  $\text{e}^{-}/\text{\AA}^2\cdot\text{subframe}$ . A total of 8,036 (Ab1303-BG505) and 8,478 (Ab1573-BG505) movies were motion-corrected using MotionCor2<sup>56</sup> with 2x binning. The CTFs of motion-corrected micrographs were estimated using CTFFIND v4.1.14<sup>57</sup>. For both datasets, a set of ~1000 particles were manually picked and reference-free 2D classes were selected for automatic particle picking using RELION AutoPicking<sup>58,59</sup>. Automatically picked particles were subjected to iterations of reference-free 2D class averaging. A closed-conformation trimer (PDB 5CEZ) map that was low-pass filtered to 80 $\text{\AA}$  was used as reference for 3D classifications and high-resolution 3D refinement in RELION v3.1<sup>58,59</sup>. CTF refinements were performed on particles used previously in 3D refinement, and the CTF-refined particles were subsequently polished and subjected to a last iteration of 3D refinement and map sharpening. 3D FSCs of maps were calculated using the Remote 3DFSC Processing Server as described<sup>60</sup>. Local resolutions of the refined maps were calculated using RELION v3.1<sup>58,59</sup>.

### **Model building**

Coordinates for gp120, gp41, Ab1303 Fab, and Ab1573 Fab were fitted into the corresponding regions of the density maps. The following coordinate files were used for initial fitting: BG505 gp120 monomer (PDB 5T3Z), gp41 monomer (PDB 5T3Z), and crystal structures of Ab1303 and Ab1573 (this study). Coordinates for the two Fab-BG505

structures and *N*-linked glycans were manually refined and built in Coot<sup>55</sup>. Iterations of whole-complex refinements using phenix.real\_space\_refine<sup>53,54</sup> and manual refinements were performed to correct for interatomic bonds and angles, clashes, residue side chain rotamers, and residue Ramachandran outliers.

### **Structural analyses**

CDR lengths were derived based on IMGT definitions<sup>61</sup>. Structural figures were made using PyMOL v2.3 (Schrödinger, LLC) or ChimeraX v0.9<sup>62</sup>. Buried surface areas were calculated using PDBePISA<sup>63</sup> and a 1.4 Å probe. Potential hydrogen bonds were assigned using the geometry criteria with separation distance of <3.5 Å and A-D-H angle of >90°. The maximum distance allowed for a potential van der Waals interaction was 4.0 Å. Protein surface electrostatic potentials were calculated in PyMOL v2.3 (Schrödinger LLC). Briefly, hydrogens were added to proteins using PDB2PQR<sup>64</sup>, and an electrostatic potential map was calculated using APBS<sup>65</sup>. Epitopes for antibodies in Fig. 3 were identified as gp120 residues containing an atom within 4 Å of an antibody as calculated in PyMOL v2.3 (Schrödinger, LLC).

### **SOSIP V1 Spin Labeling and Pulsed DEER Spectroscopy**

SOSIP spin labeling and pulsed DEER spectroscopy were performed similarly to methods described previously<sup>38</sup>. Briefly, purified BG505 S174C SOSIP protein was concentrated to ~100 µM in TBS (pH 7.4) and reduced with tris(2-carboxyethyl)phosphine (TCEP) buffer such that the final concentration of TCEP was in a 2x molar excess relative to the target cysteine residue for one hour. TCEP was removed using a desalting column (Zeba, 89883) and the reduced protein was then incubated with 5-molar excess of the V1 nitroxide spin label (bis(2,2,5,5-tetramethyl-3-imidazoline-1-oxyl-4-yl)-disulfide) for 5 hours at room temperature then at 4°C overnight. A size-exclusion chromatography column (Superose 6 Increase 10/300 GL) was used to remove excess V1 spin label. V1-labeled SOSIP was then buffer exchanged into deuterated solvent containing 20% glycerol. Unliganded V1-labeled SOSIP and V1-labeled SOSIP incubated with a 3-molar excess of Ab1303 Fab or Ab1573 Fab were placed at 37°C for 3 hours immediately prior to flash freezing.

For DEER spectroscopy, approximately 60  $\mu\text{L}$  samples of  $\sim 150 \mu\text{M}$  spin-labeled protein complexes were flash frozen within a 2.0/2.4 mm borosilicate capillary (Vitrocom, Mountain Lakes, NJ) in liquid nitrogen. Sample temperature was maintained at 50 K during data collection by a recirculating/closed-loop helium cryocooler and compressor system (Cold Edge Technologies, Allentown, PA). Four-pulse DEER spectroscopy data were collected on a Q-band Bruker ELEXSYS 580 spectrometer using a 150 W TWT amplifier (Applied Engineering Systems, Fort Worth, TX) and an E5106400 cavity resonator (Bruker Biospin). Pulse lengths were optimized via nutation experiment but ranged from 21 to 22 ns ( $\pi/2$ ) and 42 to 44 ns ( $\pi$ ); Observer frequency was set to a spectral position 2 G downfield of the low and central resonance intersection minimum in the absorption spectrum, and the pump envelope frequency was a 50 MHz half-width square-chirp pulse (generated by a Bruker arbitrary waveform generator) set 70 MHz downfield from the observer frequency. Dipolar data were analyzed using LongDistances v.932, a custom program written by Christian Altenbach in LabVIEW (National Instruments); software available online (<http://www.biochemistry.ucla.edu/biochem/Faculty/Hubbell/>) and described elsewhere<sup>66</sup>. As demonstrated previously, control experiments in which mock-labeled native SOSIPs without an introduced unpaired cysteine did not exhibit DEER signals above background<sup>38</sup>.

### **Data Availability**

The atomic models generated in this study have been deposited in the Protein Data Bank (PDB) under accession codes 7RYU [<https://doi.org/10.2210/pdb7RYU/pdb>] and 7RYV [<https://doi.org/10.2210/pdb7RYV/pdb>] for Ab1303 Fab and Ab1573 Fab X-ray crystal structures, respectively. The cryo-EM maps and atomic coordinates have been deposited in the Electron Microscopy Data Bank (EMDB) and Protein Data Bank with accession codes EMD-25877 and PDB 7TFN [<https://doi.org/10.2210/pdb7TFN/pdb>] for Ab1303-BG505 complex, and EMD-25878 and PDB 7TFO [<https://doi.org/10.2210/pdb7TFO/pdb>] for Ab1573-BG505 complex. Source data are provided with this paper.

## Figures and Tables

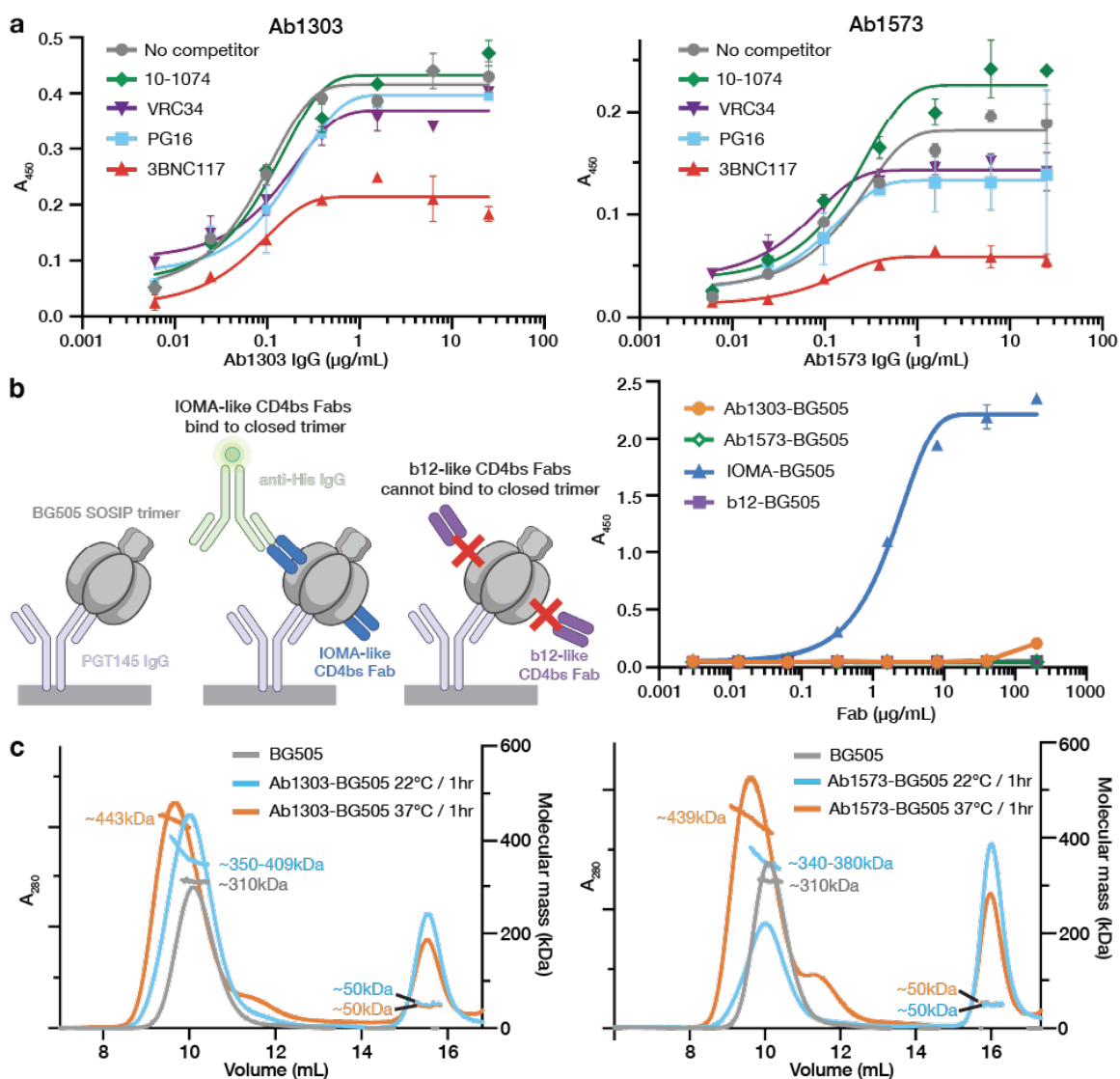


**Figure 1. Ab1303 and Ab1573 are CD4bs NAb that bind an Env conformation other than the closed, prefusion state.** **a**, Competition ELISA to map the binding sites of Ab1303 (left) and Ab1573 (right) on BG505 SOSIP. Randomly biotinylated BG505 SOSIP trimer was immobilized on a streptavidin plate and then incubated with a Fab from a bNAb that recognizes the V3 loop (10-1074), the fusion peptide (VRC34), the V1V2 loop (PG16), or the CD4bs (3BNC117). Increasing concentrations of Ab1303 or Ab1573 IgG were added to the Fab-BG505 complex, resulting in competition in both cases with the CD4bs bNAb 3BNC117. Data represents mean  $\pm$ s.d. from  $n=2$  biologically independent samples. **b**,

ELISA to assess binding of Ab1303 and Ab1573 to closed, prefusion conformation of BG505 trimer. Left: schematic of the experiment: PGT145 IgG, which constrains BG505 to a closed prefusion conformation, was immobilized and captured BG505. Binding of His-tagged Fab to BG505 was detected using a labeled anti-His-tag antibody. Right: Ab1303, Ab1573, and b12 do not bind to BG505 captured by PGT145, but IOMA binds to BG505 captured by PGT145. Data represents mean  $\pm$ s.d. from n=2 biologically independent samples. Cartoon representation is made with BioRender.com. **c**, SEC-MALS of Ab1303-BG505 (left) and Ab1573-BG505 (right) complexes incubated at different temperatures. SEC traces were monitored by absorption at 280 nm. Traces and calculated molecular mass distributions for unliganded BG505 (gray) and for Ab1303 Fab or Ab1573 Fab incubated with BG505 SOSIP trimer at 37°C (orange) or 22°C (blue) for 1 hour are shown.

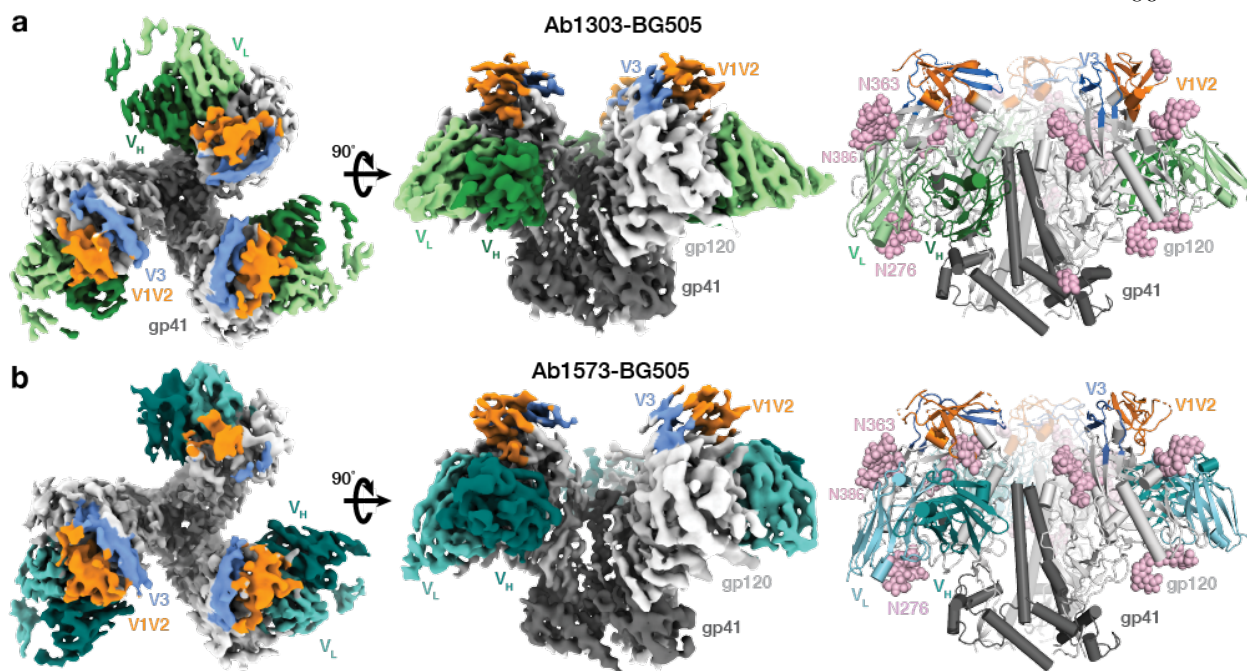


**Figure 2. Cryo-EM maps and atomic models of Ab1303-BG505 and Ab1573-BG505 complexes.** a-b, Cryo-EM density maps of Ab1303-BG505 (a) and Ab1573-BG505 (b) complexes shown from the top (left) and side (middle). Right: cartoon diagrams of the structures with N-linked glycans shown as pink spheres. Highlighted in colours include: gp120 subunits (light gray), gp41 (dark gray), Ab1303 VH (dark green) and VL (pale green) domains and Ab1573 VH (dark teal) and VL (light teal) domains. The gp120 V1V2 and V3 regions are shown in orange and blue, respectively.

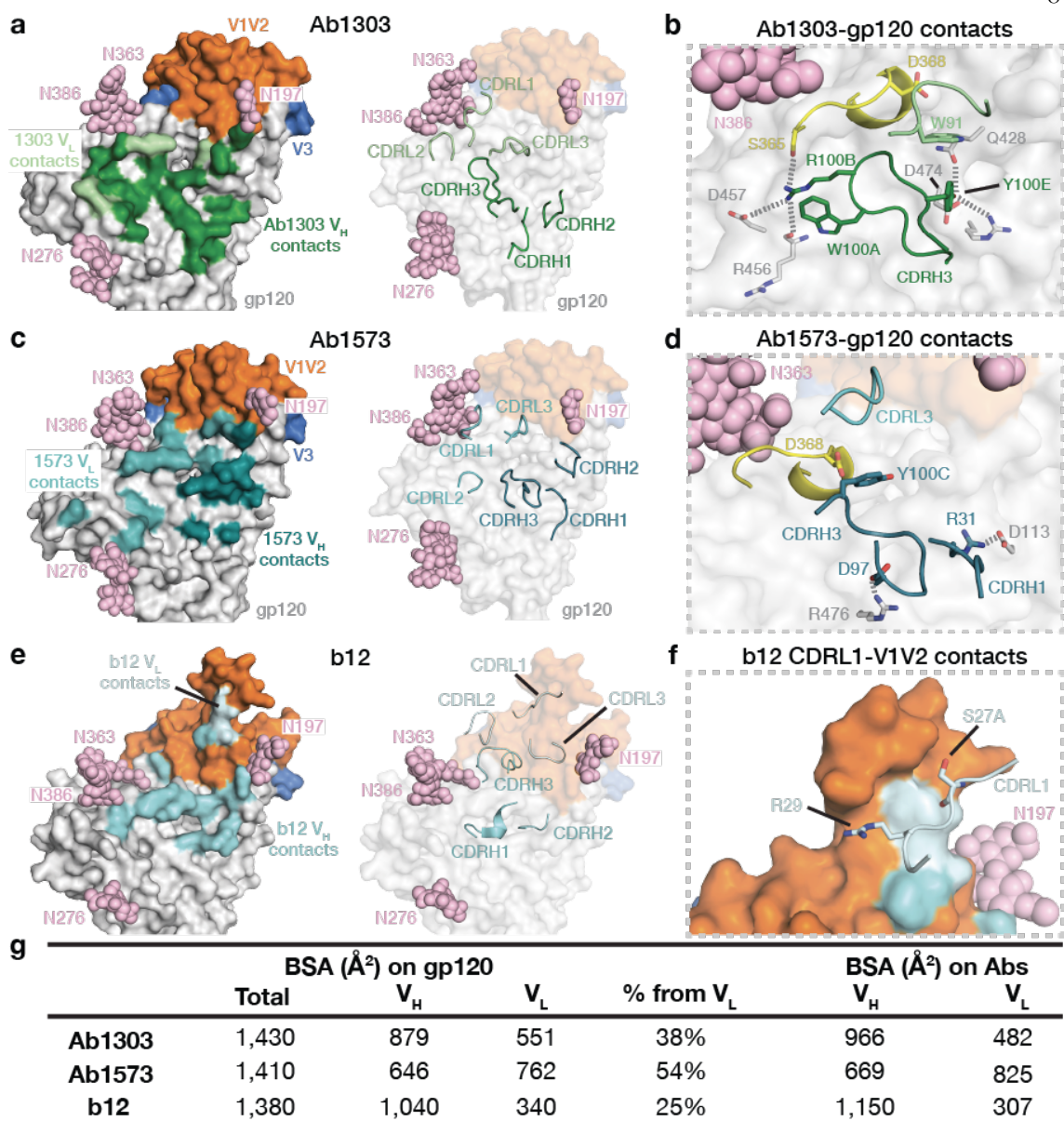


**Figure 3. Ab1303 and Ab1573 recognize the CD4bs of BG505 Env trimer.** **a**, Left: epitope of Ab1303 on gp120 surface with contacts made by antibody heavy and light chains colored in dark and light green, respectively. Right: CDR loops of Ab1303 mapped onto the gp120 surface. **b**, Highlighted interactions between gp120 residues and the Ab1303 CDRH3. The gp120 CD4 binding loop is shown in yellow with D368<sub>gp120</sub> residue highlighted in stick representation. **c**, Left: epitope of Ab1573 on gp120 surface with contacts made by antibody heavy and light chains colored in dark and light teal, respectively. Right: CDR loops of Ab1573 mapped onto the gp120 surface. **d**, Highlighted

interactions between gp120 residues and the Ab1573 CDRH1 and CDRH3. CD4 binding loop of gp120 is shown in yellow with D368 residue shown in stick. **e**, Left: epitope of b12 on gp120 surface with contacts made by antibody heavy and light chains colored in dark and light cyan, respectively. Right: CDR loops of b12 mapped onto the gp120 surface. **f**, Highlighted interactions between gp120 V1V2 and the b12 V<sub>L</sub>. **g**, Table of buried surface areas (BSAs).

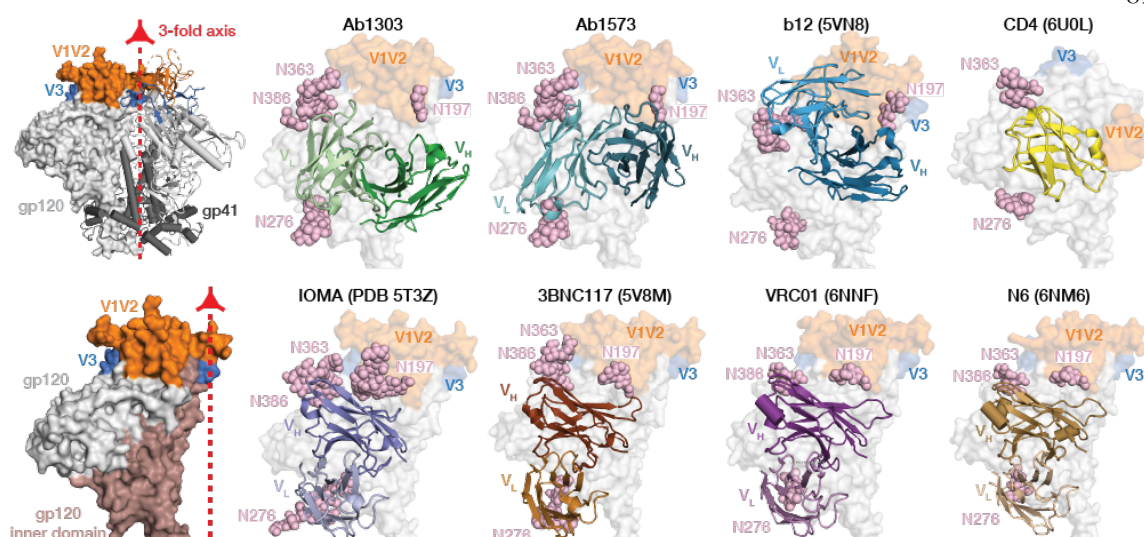


**Figure 4. Differences in antibody-binding poses for CD4bs bNAbs compared with CD4.** Upper and lower left: surface representation of HIV-1 Env trimer (top) and gp120 monomer (bottom) showing locations of the 3-fold axis relating Env protomers (red arrow), the gp120 inner domain, V1V2, V3, and gp41. Remaining panels: Cartoon diagrams of V<sub>H</sub>-V<sub>L</sub> domains of the indicated bNAbs bound to HIV-1 gp120 (gray surface, pink spheres for N-linked glycans, V1V2 in orange, V3 in blue). PDB codes: Ab1303 and Ab1573 (this study), b12 (5VN8), CD4 (6U0L), IOMA (5T3Z), 3BNC117 (5V8M), a VRC01 derivative (6NNF), and an N6 derivative (6NM6). The V1V2 and V3 regions were largely disordered in the CD4-bound Env structure (PDB 6U0L).

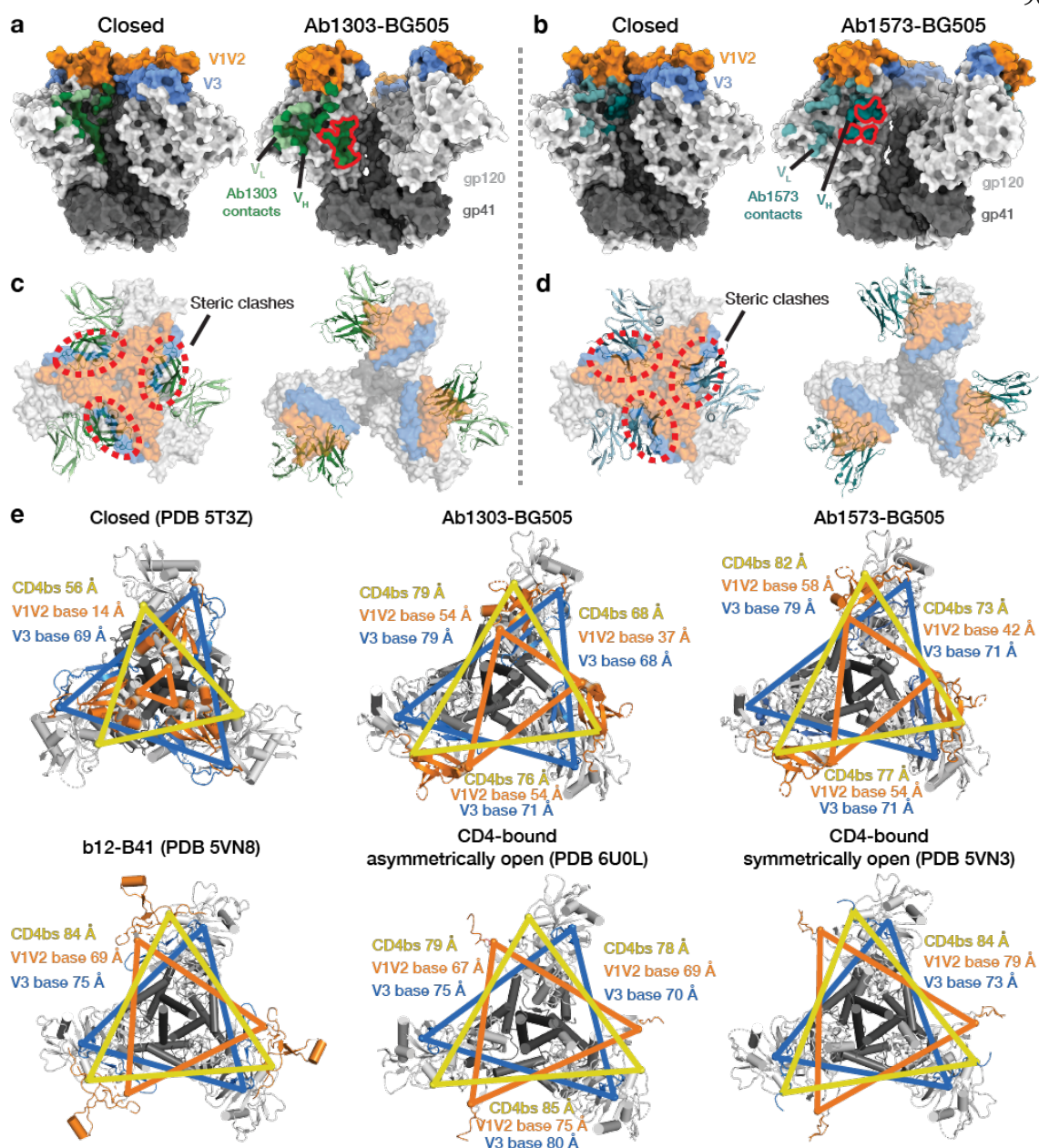


**Figure 5. Ab1303 and Ab1573 bind an Env trimeric state distinct from the closed and CD4-bound open trimer conformations**

**a-b**, Ab1303 (a) or Ab1573 (b) contacts mapped onto a side-view surface representation of a closed BG505 trimer (PDB code 5CEZ) (left) and the occluded-open trimer to which each mAb binds (right). Regions of the antibody epitope that are buried in the closed state but accessible in the Ab1303- or Ab1573-bound state are outlined in red on the occluded-open Env trimer structures. **c-d**, Cartoon representations of Ab1303 (c) or Ab1573 (d)

interacting with closed (left) or occluded-open (right) Env trimers (seen from the top). Regions with steric clashes between the Fab and the closed trimer indicated by dashed, red ovals. **e**, Comparison of inter-protomer distances of C $\alpha$  atoms from selected residues at the CD4bs (yellow), the V1V2 base (orange), and the V3 base (blue) in a closed Env trimer (PDB 5T3Z), Ab1303-bound BG505 trimer, Ab1573-bound BG505 trimer, b12-bound B41 trimer (PDB 5VN8), a CD4-bound asymmetrically-open BG505 trimer (PDB 6U0L), and a sCD4-bound symmetrically-open B41 trimer (PDB 5VN3).

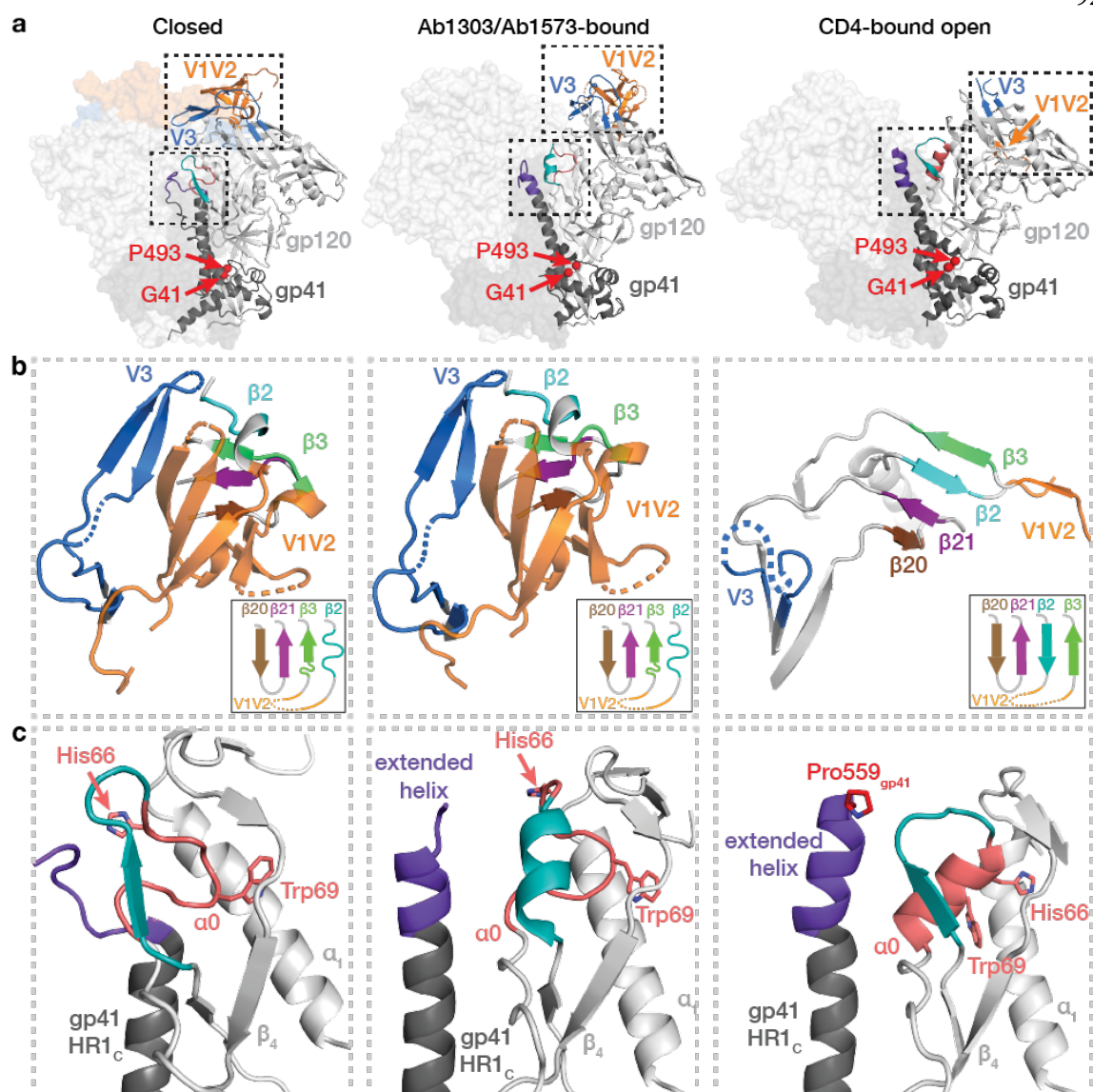


**Figure 6. Structural changes between Env trimer states.** **a**, Conformations of gp120/gp41 protomers in closed (left), Ab1303/Ab1573-bound (middle), and CD4-bound (right) states. The gp120 V1V2-V3 regions and gp120  $\alpha$ 0/gp41 HR1C regions are highlighted in dashed boxes. Positions of Gly41<sub>gp120</sub> and Pro493<sub>gp120</sub> are shown as red spheres. **b**, Structural rearrangements of gp120 V1V2 and V3 regions in closed (left), Ab1303/Ab1573-bound (middle), and CD4-bound (right) states. Secondary structures and relative locations of the 3-stranded sheet (left and middle) and rearranged 4-stranded bridging sheet (right) are highlighted, and respective topology models are shown in insets. Dotted lines represent disordered regions. **c**, Comparison of gp120  $\alpha$ 0 and neighboring

region in closed (left), Ab1303/Ab1573-bound (middle), and CD4-bound (right) structures. Residues Asp57<sub>gp120</sub> - Glu62<sub>gp120</sub> are teal,  $\alpha$ 0 residues (Lys65<sub>gp120</sub> - Ala73<sub>gp120</sub>) are salmon, with the His66<sub>gp120</sub> and Trp69<sub>gp120</sub> side chains shown. The N-terminal segment of gp41 HR1<sub>C</sub> is dark purple.

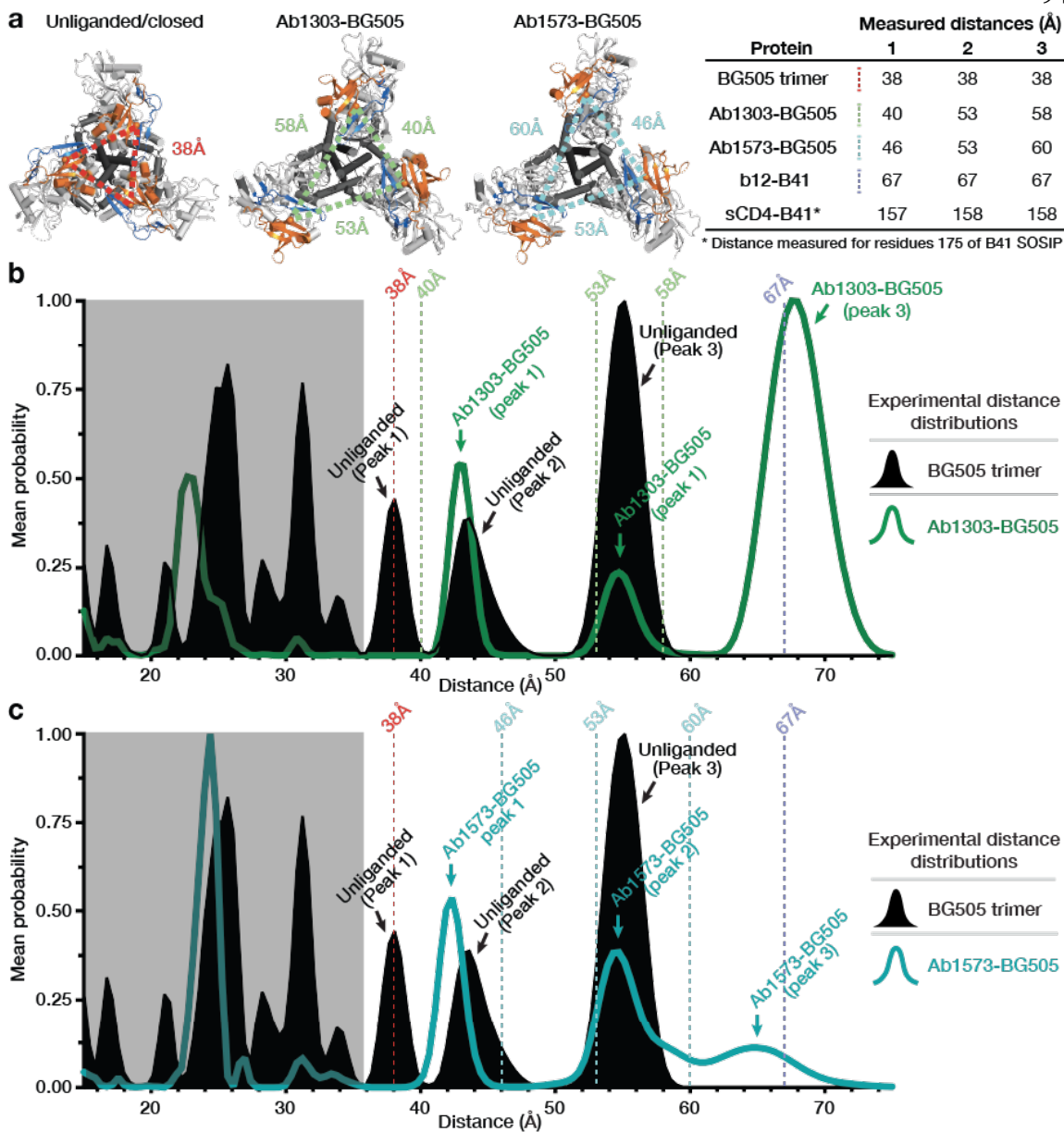
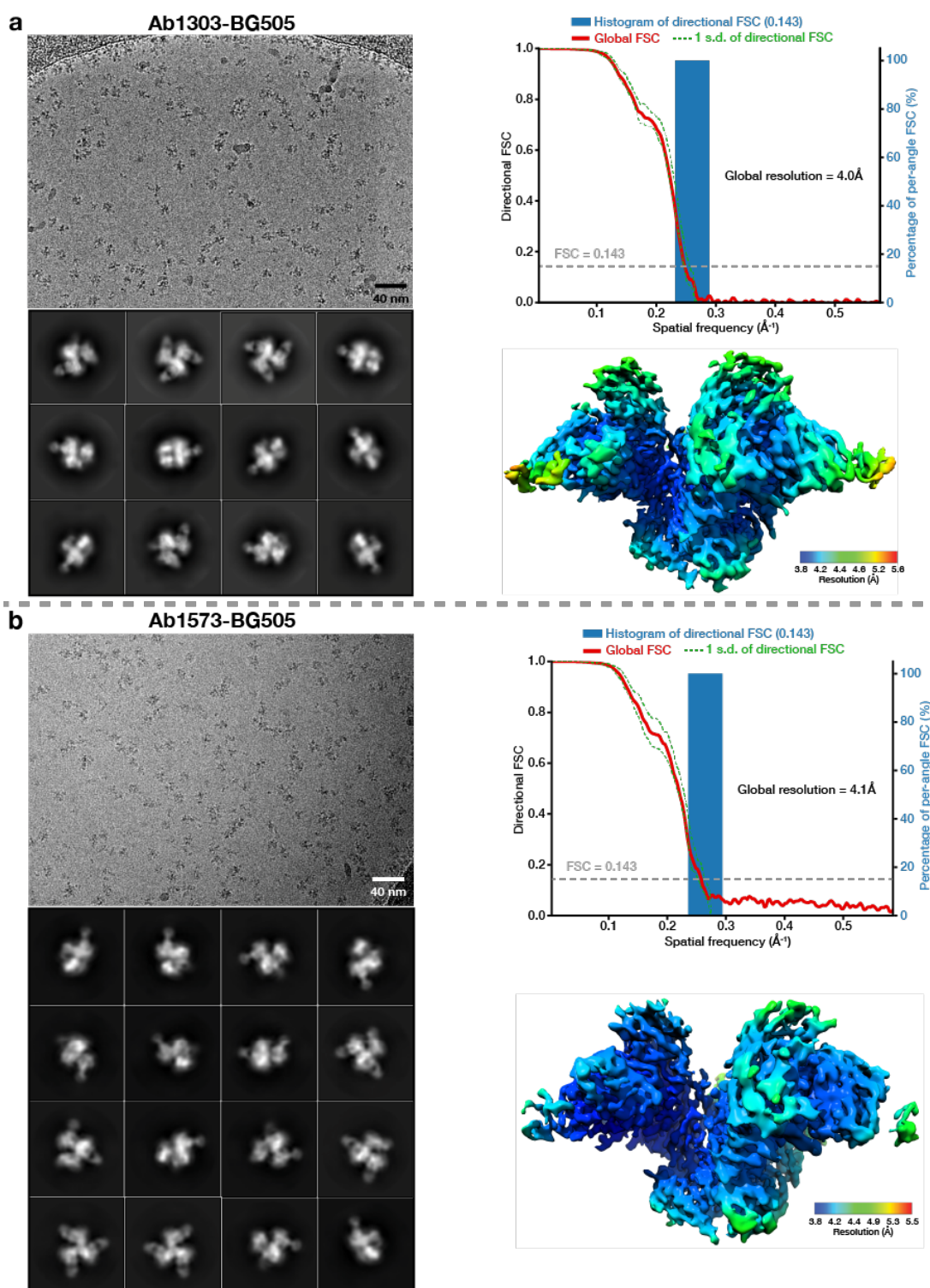


**Figure 7. DEER spectra of unliganded BG505 trimer compared to Ab1303-bound and Ab1573-bound BG505 trimer. a**, Left: Triangles showing distances between residue 174 Ca atoms on cartoon representations of Env trimers seen from the top. Right: Interprotomer distances between Ca atoms for V1V2 residue 174 in different Env conformational states measured using coordinates from the indicated structures (BG505 trimer: PDB 5T3Z; Ab1303-BG505 and Ab-1573-BG505: this study; b12-B41: PDB 5VN8; CD4-B41: PDB 5VN3). **b-c**, Left: Distance distributions for spin labels attached to V1V2 residue 174 in unliganded BG505 Env (solid black), Ab1303-bound BG505 (green trace in

b), and Ab1573-bound BG505 (teal trace in c). Vertical dashed lines indicate the inter-subunit distances measured from coordinates (panel a) for each site in structures of closed, unliganded Env (red line), Ab1303-bound Env (green dashed lines in b), Ab-1573-bound Env (teal dashed lines in c), and b12-bound Env (purple dashed line). Right: Legend for DEER spectra. The distance distributions smaller than 38Å were boxed in light gray shades.



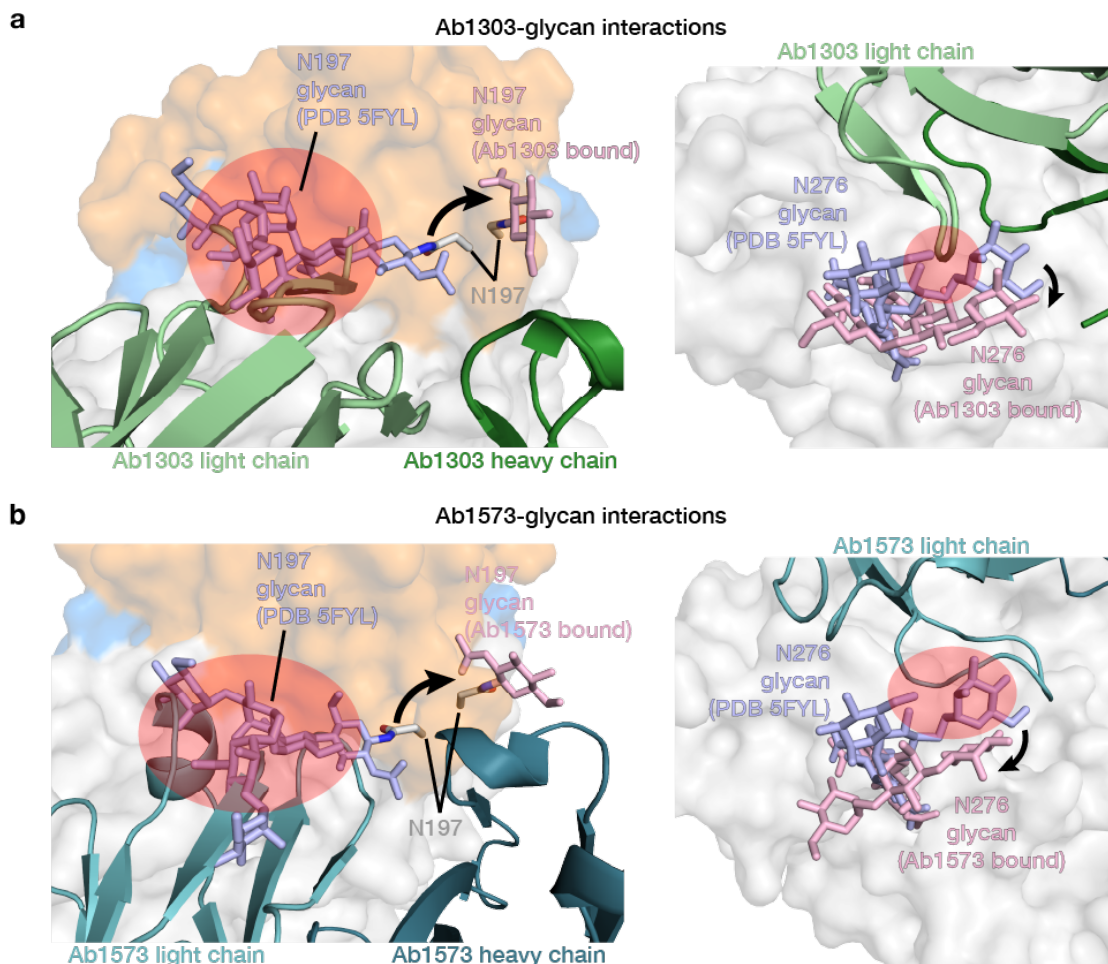
made with BioRender.com. **b**, Sequence alignments of Ab1303 and Ab1573  $V_H$  and  $V_L$  domains with their germline  $V$  gene precursors. **c**, Crystal structures of unliganded Ab1303 and Ab1573 Fabs. CDRs of the two antibodies were highlighted in various colors. **d**, Superimposition of structures of bound (from Fab-Env cryo-EM structures) and free (from Fab crystal structures)  $V_H$ - $V_L$  domains.



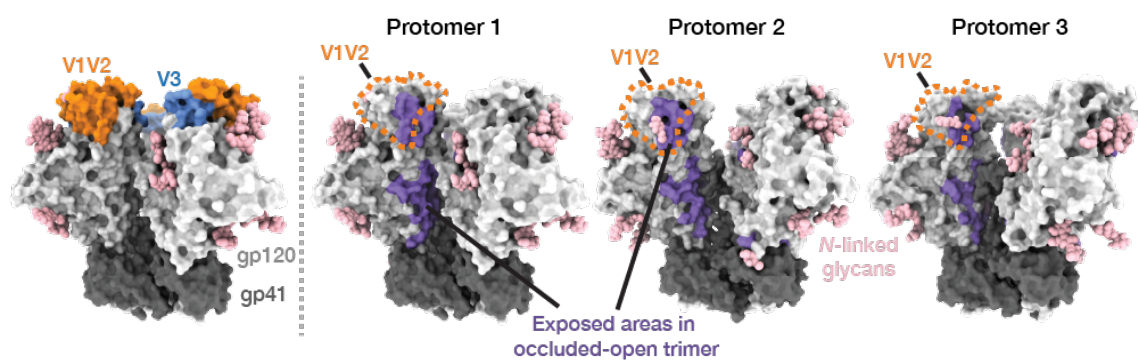
**Supplementary Figure 2. Cryo-EM processing, validation and reconstructions.**

**a-b,** Left: Example micrographs and 2D class averages of Ab1303-BG505 (a) and Ab1573-BG505 (b) complexes. Upper right: Plots of global half-map FSCs (solid red line), directional

resolution values  $\pm 1\sigma$  from the mean (left axis, green dashed lines), and histogram distributions sampled over 3D FSC (right axis, blue bars) for Ab1303-BG505 (a) and Ab1573-BG505 (b). Bottom right: local resolution maps of Ab1303-BG505 (a) and Ab1573-BG505 (b).



**Supplementary Figure 3. gp120 N-glycans were displaced to adapt for antibody binding.** Locations of Asn197<sub>gp120</sub> and Asn276<sub>gp120</sub> glycans (pink) in (a) Ab1303- and (b) Ab1573-bound Env structures were compared with an Env structure that does not have an antibody bound in the vicinity of this region (PDB 5FYL, glycans colored in light blue). Spatially close or clashing regions between the Fabs and glycans in a CD4bs Ab-free trimer are highlighted in red shades. Directions of glycan shifting are indicated with black arrows.



**Supplementary Figure 4. gp120 surface area exposed in occluded-open versus closed Env trimers.** Left: Occluded-open Env trimer showing V1V2 and V3 regions as colored highlights. Right: Env trimers showing surface areas (purple) that are exposed in occluded-open trimers but buried in closed trimers. Orange dashed shape indicates V1V2 region.

**Supplementary table 1. X-ray data collection and refinement statistics (molecular replacement)**

	Ab1303 Fab (PDB 7RYU)	Ab1573 Fab (PDB 7RYV)
<b>Data collection</b>		
Space group	P2 <sub>1</sub> 2 <sub>1</sub> 2 <sub>1</sub>	P2 <sub>1</sub>
Cell dimensions		
<i>a</i> , <i>b</i> , <i>c</i> (Å)	63.85, 66.97, 136.59	81.50 138.40 83.73
$\alpha$ , $\beta$ , $\gamma$ (°)	90, 90, 90	90 95.71 90
Resolution (Å)	38.27 - 1.51 (1.53 - 1.51) *	38.91 - 2.50 (2.78-2.50) *
<i>R</i> <sub>merge</sub> (%)	8.4 (124)	17.4 (98.1)
<i>R</i> <sub>pim</sub> (%)	2.4 (37.8)	10.8 (62.2)
CC <sub>1/2</sub> (%)	99.9 (80.2)	99.4 (85.8)
<i>I</i> / $\sigma$ <i>I</i>	16.5 (1.2)	8.8 (2.8)
Completeness (%)	99.9 (98.2)	98.3 (95.9)
Multiplicity	13.3 (11.4)	3.6 (3.6)
<b>Refinement</b>		
Resolution (Å)	1.51	2.50
No. reflections	92,598 (9,145)	63,132 (6,140)
<i>R</i> <sub>free</sub> / <i>R</i> <sub>work</sub> (%)	20.0 / 18.0	25.7 / 22.4
No. atoms		
Protein	3,330	12,931
Ligand/ion	0	0
Water	680	880
R.m.s. deviations		
Bond lengths (Å)	0.008	0.006
Bond angles (°)	0.86	1.15
Rotamer outliers (%)	0	0.34
Ramachandran plot		
Favored (%)	99.3	97.3
Allowed (%)	0.7	2.7
Disallowed	0	0
Average <i>B</i> -factor	27.0	30.2

\*Values in parentheses are for highest-resolution shell.

**Supplementary table 2. Cryo-EM data collection, refinement, and validation statistics**

	Ab1303-BG505 (PDB 7TFN) (EMDB-25877)	Ab1573-BG505 (PDB 7TFO) (EMDB-25878)
<b>Data collection and processing</b>		
Magnification *	105,000x	105,000x
Voltage (kV)	200	300
Electron exposure (e-/Å <sup>2</sup> )	60	60
Defocus range (µm)	1.4-3.0	1.4-3.0
Pixel size (Å)	0.4345	0.4275
Recording mode	Super resolution	Super resolution
Symmetry imposed	C1	C1
Initial particle images (no.)	1,095,744	842,259
Final particle images (no.)	386,825	443,817
Overall map resolution (Å) ** (masked/unmasked)	4.0 (4.4)	4.1 (4.4)
<b>Refinement</b>		
Initial model used (PDB code)	5CEZ ***	5CEZ ***
Map and model CC	0.77	0.73
Map sharpening <i>B</i> factor (Å <sup>2</sup> )	79.3	112
Model composition		
Protein residues	2344	2283
Carbohydrate residues	57	21
Validation		
MolProbity score	2.06	2.23
Clashscore	14.1	16.4
Poor rotamers (%)	0	0
Ramachandran plot		
Favored (%)	93.9	91.1
Allowed (%)	6.1	8.9
Disallowed (%)	0	0
RMS deviations		
Length (Å)	0.003	0.005
Angles (°)	0.63	0.70

\* Nominal magnification; \*\* FSC threshold 0.143; \*\*\* Partial structure composed of trimeric gp120/gp41

## References

1. Robertson, D.L., Hahn, B.H. & Sharp, P.M. Recombination in AIDS Viruses. *Journal of Molecular Evolution* **40**, 249-259 (1995).
2. Escolano, A., Dosenovic, P. & Nussenzweig, M.C. Progress Toward Active or Passive HIV-1 Vaccination. *J Exp Med* **214**, 3-16 (2017).
3. Andrabi, R., Bhiman, J.N. & Burton, D.R. Strategies for a Multi-stage Neutralizing Antibody-based HIV Vaccine. *Current Opinion in Immunology* **53**, 143-151 (2018).
4. West, A.P., Jr. et al. Structural Insights on the Role of Antibodies in HIV-1 Vaccine and Therapy. *Cell* **156**, 633-648 (2014).
5. McCoy, L.E. & Burton, D.R. Identification and Specificity of Broadly Neutralizing Antibodies Against HIV. *Immunol. Rev.* **275**, 11-20 (2017).
6. Harrison, S.C. Viral Membrane Fusion. *Virology* **479-480**, 498-507 (2015).
7. Choe, H. et al. The Beta-chemokine Receptors CCR3 and CCR5 Facilitate Infection by Primary HIV-1 Isolates. *Cell* **85**, 1135-48 (1996).
8. Feng, Y., Broder, C.C., Kennedy, P.E. & Berger, E.A. HIV-1 Entry Cofactor: Functional cDNA Cloning of a Seven-transmembrane, G protein-coupled Receptor. *Science* **272**, 872-7 (1996).
9. Sanders, R.W. et al. A Next-generation Cleaved, Soluble HIV-1 Env Trimer, BG505 SOSIP.664 gp140, Expresses Multiple Epitopes for Broadly Neutralizing but not Non-neutralizing Antibodies. *PLoS Pathog.* **9**, e1003618 (2013).
10. Ward, A.B. & Wilson, I.A. The HIV-1 Envelope Glycoprotein Structure: Nailing Down a Moving Target. *Immunol. Rev.* **275**, 21-32 (2017).
11. Ozorowski, G. et al. Open and Closed Structures Reveal Allostery and Flexibility in the HIV-1 Envelope Spike. *Nature* **547**, 360-363 (2017).
12. Wang, H., Barnes, C.O., Yang, Z., Nussenzweig, M.C. & Bjorkman, P.J. Partially Open HIV-1 Envelope Structures Exhibit Conformational Changes Relevant for Coreceptor Binding and Fusion. *Cell Host & Microbe* **24**, 579-592 e4 (2018).
13. Wang, H. et al. Cryo-EM Structure of a CD4-bound Open HIV-1 Envelope Trimer Reveals Structural Rearrangements of the gp120 V1V2 Loop. *Proc. Natl. Acad. Sci.* **113**, E7151-E7158 (2016).

14. Yang, Z., Wang, H., Liu, A.Z., Gristick, H.B. & Bjorkman, P.J. Asymmetric Opening of HIV-1 Env Bound to CD4 and a Coreceptor-mimicking Antibody. *Nat. Struct. Mol. Biol.* **26**, 1167-1175 (2019).
15. Burton, D.R. et al. A Large Array of Human Monoclonal Antibodies to Type 1 Human Immunodeficiency Virus from Combinatorial Libraries of Asymptomatic Seropositive Individuals. *Proc. Natl. Acad. Sci.* **88**, 10134-10137 (1991).
16. Scheid, J.F. et al. Sequence and Structural Convergence of Broad and Potent HIV Antibodies That Mimic CD4 Binding. *Science* **333**, 1633-1637 (2011).
17. Wu, X. et al. Rational Design of Envelope Identifies Broadly Neutralizing Human Monoclonal Antibodies to HIV-1. *Science* **329**, 856-61 (2010).
18. Zhou, T. et al. Structural Definition of a Conserved Neutralization Epitope on HIV-1 gp120. *Nature* **445**, 732-7 (2007).
19. Escolano, A. et al. Sequential Immunization of Macaques Elicits Heterologous Neutralizing Antibodies Targeting the V3-glycan Patch of HIV-1 Env. *Science Translational Medicine* **13** (2021).
20. Steichen, J.M. et al. HIV Vaccine Design to Target Germline Precursors of Glycan-Dependent Broadly Neutralizing Antibodies. *Immunity* **45**, 483-96 (2016).
21. Escolano, A. et al. Immunization Expands B Cells Specific to HIV-1 V3 Glycan in Mice and Macaques. *Nature* **570**, 468-473 (2019).
22. McCoy, L.E. et al. Holes in the Glycan Shield of the Native HIV Envelope Are a Target of Trimer-Elicited Neutralizing Antibodies. *Cell Rep.* **16**, 2327-38 (2016).
23. Duan, H. et al. Glycan Masking Focuses Immune Responses to the HIV-1 CD4-Binding Site and Enhances Elicitation of VRC01-Class Precursor Antibodies. *Immunity* **49**, 301-311 e5 (2018).
24. Klasse, P.J. et al. Epitopes for Neutralizing Antibodies Induced by HIV-1 Envelope Glycoprotein BG505 SOSIP Trimers in Rabbits and Macaques. *PLoS Pathog.* **14**, e1006913 (2018).
25. Brune, K.D. et al. Plug-and-Display: Decoration of Virus-Like Particles via Isopeptide Bonds for Modular Immunization. *Sci. Rep.* **6**, 19234 (2016).
26. Zakeri, B. et al. Peptide Tag Forming a Rapid Covalent Bond to a Protein, Through Engineering a Bacterial Adhesin. *Proc. Natl. Acad. Sci.* **109**, E690-7 (2012).

27. Wang, Z. et al. Isolation of single HIV-1 Envelope Specific B Cells and Antibody Cloning from Immunized Rhesus Macaques. *J. Immunol. Methods* **478**, 112734 (2020).
28. deCamp, A. et al. Global panel of HIV-1 Env Reference Strains for Standardized Assessments of Vaccine-elicited Neutralizing Antibodies. *J. Virol.* **88**, 2489-507 (2014).
29. Mouquet, H. et al. Complex-type N-glycan Recognition by Potent Broadly Neutralizing HIV Antibodies. *Proc. Natl. Acad. Sci.* **109**, E3268-77 (2012).
30. Walker, L.M. et al. Broad and Potent Neutralizing Antibodies from an African Donor Reveal a New HIV-1 Vaccine Target. *Science* **326**, 285-289 (2009).
31. Kong, R. et al. Fusion Peptide of HIV-1 as a Site of Vulnerability to Neutralizing Antibody. *Science* **352**, 828-33 (2016).
32. Gristick, H.B. et al. Natively glycosylated HIV-1 Env Structure Reveals New Mode for Antibody Recognition of the CD4-binding Site. *Nat. Struct. Mol. Biol.* **23**, 906-915 (2016).
33. Lee, J.H. et al. A Broadly Neutralizing Antibody Targets the Dynamic HIV Envelope Trimer Apex via a Long, Rigidified, and Anionic beta-Hairpin Structure. *Immunity* **46**, 690-702 (2017).
34. Henderson, R. et al. Disruption of the HIV-1 Envelope Allosteric Network Blocks CD4-induced Rearrangements. *Nat. Commun.* **11**(2020).
35. Jette, C.A. et al. Cryo-EM structures of HIV-1 Trimer Bound to CD4-mimetics BNM-III-170 and M48U1 Adopt a CD4-bound Open Conformation. *Nat. Commun.* **12**, 1950 (2021).
36. West, A.P., Jr., Diskin, R., Nussenzweig, M.C. & Bjorkman, P.J. Structural Basis for Germline Gene Usage of a Potent Class of Antibodies Targeting the CD4 Binding Site of HIV-1 gp120. *Proc. Natl. Acad. Sci.* **109**, E2083-90 (2012).
37. Jeschke, G. DEER Distance Measurements on Proteins. *Annu. Rev. Phys. Chem.* **63**, 419-46 (2012).
38. Stadtmueller, B.M. et al. DEER Spectroscopy Measurements Reveal Multiple Conformations of HIV-1 SOSIP Envelopes that Show Similarities with Envelopes on Native Virions. *Immunity* (2018).
39. Hubbell, W.L., Lopez, C.J., Altenbach, C. & Yang, Z. Technological Advances in Site-directed Spin Labeling of Proteins. *Curr. Opin. Struct. Biol.* **23**, 725-33 (2013).

40. Khramtsov, V.V. et al. Quantitative Determination of SH Groups in Low- and High-molecular-weight Compounds by an Electron Spin Resonance Method. *Anal. Biochem.* **182**, 58-63 (1989).
41. Hubbell, W.L., Cafiso, D.S. & Altenbach, C. Identifying Conformational Changes with Site-directed Spin Labeling. *Nat. Struct. Biol.* **7**, 735-739 (2000).
42. Toledo Warshaviak, D., Khramtsov, V.V., Cascio, D., Altenbach, C. & Hubbell, W.L. Structure and Dynamics of an Imidazoline Nitroxide Side Chain with Strongly Hindered Internal Motion in Proteins. *J. Magn. Reson.* **232**, 53-61 (2013).
43. Haynes, B.F. & Mascola, J.R. The Quest for an Antibody-based HIV Vaccine. *Immunological Reviews* **275**, 5-10 (2017).
44. Kwong, P.D. et al. Structure of an HIV gp120 Envelope Glycoprotein in Complex with the CD4 Receptor and a Neutralizing Human Antibody. *Nature* **393**, 648-59 (1998).
45. Pancera, M. et al. Crystal Structures of Trimeric HIV Envelope with Entry Inhibitors BMS-378806 and BMS-626529. *Nat. Chem. Biol.* **13**, 1115-1122 (2017).
46. Huang, J. et al. Identification of a CD4-Binding-Site Antibody to HIV that Evolved Near-Pan Neutralization Breadth. *Immunity* **45**, 1108-1121 (2016).
47. Liu, Q. et al. Improvement of Antibody Functionality by Structure-guided Paratope Engraftment. *Nat. Commun.* **10**, 721 (2019).
48. Scharf, L. et al. Broadly Neutralizing Antibody 8ANC195 Recognizes Closed and Open States of HIV-1 Env. *Cell* **162**, 1379-90 (2015).
49. Kabsch, W. Integration, Scaling, Space-group Assignment and Post-refinement. *Acta Crystallogr. D Biol. Crystallogr.* **66**, 133-44 (2010).
50. Kabsch, W. XDS. *Acta Crystallogr. D Biol. Crystallogr.* **66**, 125-32 (2010).
51. Winn, M.D. et al. Overview of the CCP4 Suite and Current Developments. *Acta Crystallogr. D Biol. Crystallogr.* **67**, 235-42 (2011).
52. McCoy, A.J. et al. Phaser Crystallographic Software. *J. Appl. Crystallogr.* **40**, 658-674 (2007).
53. Adams, P.D. et al. PHENIX: A Comprehensive Python-based System for Macromolecular Structure Solution. *Acta Crystallogr. D Biol. Crystallogr.* **66**, 213-21 (2010).
54. Afonine, P.V. et al. Real-space Refinement in PHENIX for Cryo-EM and Crystallography. *Acta Crystallogr. D Struct. Biol.* **74**, 531-544 (2018).

55. Emsley, P., Lohkamp, B., Scott, W.G. & Cowtan, K. Features and Development of Coot. *Acta Crystallogr. D Biol. Crystallogr.* **66**, 486-501 (2010).
56. Zheng, S.Q. et al. MotionCor2: Anisotropic Correction of Beam-induced Motion for Improved Cryo-electron Microscopy. *Nat. Methods* **14**, 331-332 (2017).
57. Rohou, A. & Grigorieff, N. CTFFIND4: Fast and Accurate Defocus Estimation from Electron Micrographs. *J. Struct. Biol.* **192**, 216-21 (2015).
58. Zivanov, J. et al. New Tools for Automated High-resolution Cryo-EM Structure Determination in RELION-3. *Elife* **7**(2018).
59. Scheres, S.H. RELION: Implementation of a Bayesian Approach to Cryo-EM Structure Determination. *J. Struct. Biol.* **180**, 519-30 (2012).
60. Tan, Y.Z. et al. Addressing Preferred Specimen Orientation in Single-particle Cryo-EM through Tilting. *Nat. Methods* **14**, 793-796 (2017).
61. Lefranc, M.P. et al. IMG(T), the International ImMunoGeneTics Information System(R) 25 years on. *Nucleic Acids Res.* **43**, D413-22 (2015).
62. Goddard, T.D. et al. UCSF ChimeraX: Meeting Modern Challenges in Visualization and Analysis. *Protein Sci.* **27**, 14-25 (2018).
63. Krissinel, E. & Henrick, K. Inference of Macromolecular Assemblies from Crystalline State. *J. Mol. Biol.* **372**, 774-97 (2007).
64. Dolinsky, T.J. et al. PDB2PQR: Expanding and Upgrading Automated Preparation of Biomolecular Structures for Molecular Simulations. *Nucleic Acids Res.* **35**, W522-W525 (2007).
65. Baker, H.M., Mason, A.B., He, Q.Y., MacGillivray, R.T. & Baker, E.N. Ligand Variation in the Transferrin Family: the Crystal Structure of the H249Q Mutant of the Human Transferrin N-lobe as a Model for Iron Binding in Insect Transferrins. *Biochemistry* **40**, 11670-5 (2001).
66. Fleissner, M.R. et al. Site-directed Spin Labeling of a Genetically Encoded Unnatural Amino Acid. *Proc. Natl. Acad. Sci. U S A* **106**, 21637-42 (2009).